1993

Study of melting and freezing processes of water for application to ice thermal energy storage system

Liang Yong
Iowa State University

Order Number 9414040

Study of melting and freezing processes of water for application to ice thermal energy storage system

Yong, Liang, Ph.D.

Iowa State University, 1993

U·M·I
300 N. Zeeb Rd.
Ann Arbor, MI 48106

Study of melting and freezing processes of water for application to ice thermal energy storage system

by

Liang Yong

A Dissertation Submitted to the

Graduate Faculty in Partial Fulfillment of the

Requirements for the Degree of

DOCTOR OF PHILOSOPHY

Department: Mechanical Engineering
Major: Mechanical Engineering

Approved:

Signature was redacted for privacy.

In Charge of Major Work

Signature was redacted for privacy.

For the Major Department

Signature was redacted for privacy.

For the Graduate College

Iowa State University
Ames, Iowa
1993

TABLE OF CONTENTS

INTRODUCTION

Objective of the Dissertation

The study of the heat transfer characteristics of melting and solidification processes has been one of the most active areas in contemporary heat transfer research. Extensive reviews of the literature on this subject are presented by Viskanta (1985), as well as Yao and Prusa (1989).

An importance of this study is the application of solid-liquid phase-change processes in thermal energy storage systems. These systems used in the air-conditioning industry have the potential of saving building owners substantial dollars in initial equipment cost as well as the operating cost of air-conditioning systems for commercial and industrial buildings. The basic principle of a thermal energy storage system for air conditioning is to store cool thermal energy produced during off-peak electric periods for use during on-peak electric periods when the building is occupied. These systems provide the means for reducing building energy costs by taking advantage of the lower utility rates during the off-peak hours to produce a cold reservoir for daytime building air conditioning. In addition to savings in operating costs, the use of thermal energy storage systems can reduce the overall initial equipment costs by allowing the refrigeration equipment to be downsized because of reserve capacity in

the storage systems.

Several designs have been considered for cool thermal energy storage systems. These include chilled water tanks, ice storage, and other phase-change material storages. Of these, ice storage systems offer the greatest potential for cost savings. There are many kinds of ice storage systems used in commercial and industrial air-conditioning systems. Among them, the encapsulated ice storage system has the advantage of high volume usage.

One problem faced by air-conditioning industries is the lack of performance testing and evaluations for encapsulated ice storage systems. The objective of this study was to conduct research on heat transfer in a specific ice storage system which utilizes rectangular ice containers and to develop computer models which can be used to simulate and evaluate the performance of the thermal energy storage system.

Explanation of the Dissertation Organization

In this dissertation, the study of melting and freezing of encapsulated ice for use in thermal energy storage system is divided into four independent papers. Each paper is written using a technical paper format in preparation for submission to related technical journals. The test apparatus section preceding Paper I will be included in Paper II and Paper III when submitted to the journal.

Paper I presents the experimental investigation of ice melting in a rectangular enclosure. The temperature distribution and solid-liquid interface position under different conditions were measured experimentally. The sensible heat change, latent heat change, Nusselt number, and Rayleigh number were evaluated. A natural convection heat transfer correlation for ice-water phase change process in a horizontal

rectangular enclosure was obtained based on the experiments.

In Paper II, analytical models were developed to predict freezing and melting processes separately. The effects of conduction, convection, subcooling, and superheating were discussed. The predictions made satisfactory agreement with the experiments results.

Paper III deals with the melting of unfixed ice in the rectangular enclosure. The analytical model is based on fundamental physical principles incorporating energy balance and force balance. The interface position and melting rates were determined by the model and compared with the experimental results.

In Paper IV, a model was developed to simulate the overall performance of melting in a cool thermal energy storage system which utilizes rectangular ice containers. Both integral and finite difference methods were employed in the model development. Engineering analysis was performed to determine the effects of initial temperature, inlet temperature, geometric factors, etc, on the system performance.

A general conclusion is summarized at the end of this dissertation. References cited in the general introduction follow the general conclusions.

PAPER I.

AN EXPERIMENTAL INVESTIGATION OF ICE MELTING IN A HORIZONTAL RECTANGULAR ENCLOSURE

ABSTRACT

The present work is to investigate melting processes in an encapsulated ice thermal energy storage system. Melting of ice in a horizontal rectangular enclosure, heated isothermally from below, was studied experimentally. It was determined that natural convection heat transfer dominates the melting process. The temperature distribution within the enclosure as well as the ice-water interface position were measured for different wall temperatures. Sensible and latent heat changes, the Nusselt number, and the Rayleigh number were calculated. A correlation between the Nusselt number and the Rayleigh number for the phase-change process was obtained and compared with other correlations found in the literatures for the single phase situation.

NOMENCLATURE

A, area;

c_p, specific heat;

h, heat transfer coefficient;

H, Height;

h_f, latent heat of fusion;

k, thermal conductivity;

Nu, Nusselt number, hs/k_l;

Pr, Prandtl number, $\mu_l c_{p_l}/k_l$;

Ra, Rayleigh number, $g_l\beta(T_w - T_f)s^3/\nu\alpha$;

s, thickness of water layer below ice;

t, time;

T, temperature;

y, coordinate.

Greek Symbols

α, thermal diffusivity, $k/\rho c$;

β, thermal expansion coefficient;

ν, kinematic viscosity;

μ, viscosity;

ρ, density.

Superscripts

$'$, refers to previous step.

Subscripts

f, refers to fusion;

i, refers to number of element;

j, refers to number of ruler scale;

l, refers to liquid;

lat, refers to latent heat;

s, refers to solid;

sen, refers to sensible heat;

w, refers to wall.

INTRODUCTION

The effect of natural convection heat transfer for water has been studied experimentally and analytically. Dlobe and Droplin (1959) obtained a natural convection correlation for liquids confined between two horizontal plates. O'Tool and Silveston (1960) experimentally developed a correlation of heat transfer through a horizontal layer confined by two parallel plates for different regions of Rayleigh number. Chu and Goldstein (1973) developed a correlation equation of convection in a horizontal layer of water for higher Rayleigh number region. The onset of free convection has been studied experimentally by Yen (1968), Heitz and Westwater (1971), Seki et al. (1977), and Boger and Westwater (1967). The Rayleigh number is the important factor which determines the heat transfer mode. Before the Rayleigh number reaches the critical point, heat transfer occurs by a pure conduction mechanism; after the Rayleigh number reaches or exceeds the critical value, the natural convection heat transfer plays a dominant role. It was found that the critical Rayleigh number Ra_c for natural convection is about 1700.

Many experimental studies have also been performed for the solid-liquid phase-change problem. For example: Experiments for melting around horizontal cylinders have been performed by Sparrow et al. (1978), Bathelt et al. (1979), Abdel-Wahed et al. (1979), and Bathelt et al. (1980). Experiments for melting around vertical

cylinders have been studied by Ramsey et al. (1978), Vanburen et al. (1980), Kemiink et al. (1981), Ho et al. (1984). The results from these investigations have conclusively established that the correlations for classical free convection heat transfer results are not applicable to the case of the natural convection in the presence of a phase change. Average heat transfer coefficients for melting in the vertical rectangular cavity have been obtained by Marshall (1978), Ho and Viskanta (1982).

Horizontal rectangular containers are widely used in many applications. Hale and Viskanta (1979) investigated melting and freezing of n-octadecane in horizontal plate geometries, and the convection correlation for the single liquid region was used in their analytical prediction. Experimental and analytical results have shown that natural convection effects are of great importance for melting.

Natural convection in the case of phase change in the horizontal rectangular geometry is still not fully understood. The current work deals with the melting of ice inside a horizontal rectangular enclosure. Distilled water was used. Temperatures and the solid-liquid interface position inside the cavity were recorded during the tests. Latent and sensible heat changes, heat transfer rate on the heated wall and heat transfer rate on the interface, Nusselt numbers Nu and Rayleigh number Ra were calculated. A relationship between the Nusselt number and Rayleigh number has been obtained and compared with the correlations in the previous publications for the natural convection occurring in the horizontal liquid layers. The new correlation may be used to predict melting of ice in the geometry considered.

EXPERIMENT

Test Apparatus

The experimental apparatus consists of a test cell, a chiller unit, an in-line electric heater, a thermal reservoir, and associated piping system. The schematic diagram is shown in Fig. 1.

The test cell, shown in Fig. 2, is a rectangular enclosure constructed from two parallel 3.1 mm thick aluminum plates and four side walls of 12.7 mm thick plexiglas. The plexiglas side walls permitted visual observation of the phase-change process inside the enclosure. The inside dimensions of the test cell are 304 mm long, 304 mm wide, and 54 mm high. The large ratio of the length (or width) to the height reduced the edge effects so the heat transfer was only in one dimension. Two 8 mm diameter holes are located at the middle of one plexiglas sidewall and are fitted with two rubber tubes. The tubes were used to fill the test cell with water and to allow for overflow due to the expansion of the water as it froze. The aluminum plates with high thermal conductivity were used as two heat transfer walls for the test cell. Two aluminum cover plates were bolted to the heat transfer walls. These cover plates had slots machined in them which channeled the heat transfer fluid along the heat transfer walls. Piping manifolds were connected to each cover to provide inlet and

outlet connection for the heat transfer fluid. The entire test cell was covered by 50 mm - thick styrofoam insulation which could be removed in order to observe and photograph the solid-liquid interface position.

A 30% ethylene glycol-water solution was used as the heat transfer fluid in the test system. The solution could be stored in the thermal reservoir. The thermal reservoir was used as a constant temperature source to the test cell. The thermal reservoir was also insulated.

Fifty copper-constantan thermocouples were used to measure temperatures. The thermocouples were connected to a digital voltmeter and a switch unit. The accuracy of the thermocouples is $0.025°C$. The output of the voltmeter was read by a computer which converted the voltage information into temperature and stored the values. The equation used for converting voltage to temperature allows an error of $\pm 0.5°C$. Six thermocouples were used to measure the outside surface temperature of the test cell. Shallow holes were drilled into the outside surface of the aluminum plates, and the thermocouple beads were mounted in the holes using thermocouple cement at the different holes. Forty-two thermocouples were arranged inside the test enclosure to measure temperature distribution on one cross-section. A plexiglas frame was used to hold the thermocouples. The uncertainty on the position of the thermocouple beads with the desired point was within 0.5 mm. Two thermocouples were located at the inlet and outlet of the heat exchangers, and two thermocouples were inserted in the thermal reservoir to check the stability of heating liquid temperature. The arrangement of thermocouples is shown in Fig. 3. During the experimental process, the measurements were taken in each time interval (three or five minutes).

In order to measure the interface position, six ruler scales were attached to one of

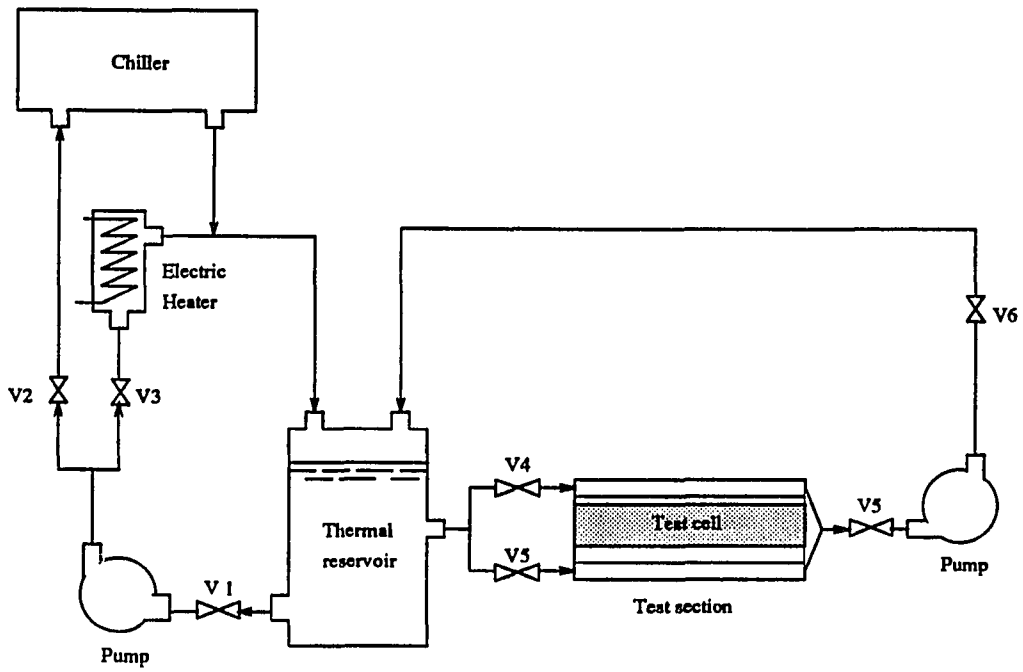

Figure 1: Schematic diagram of experimental apparatus

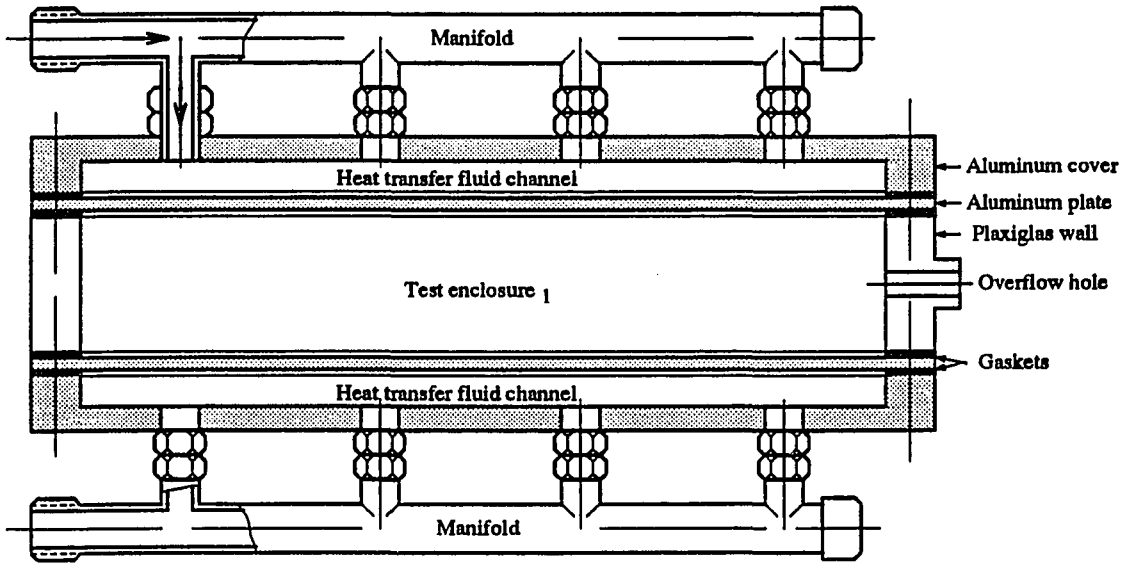

Figure 2: End view of test cell

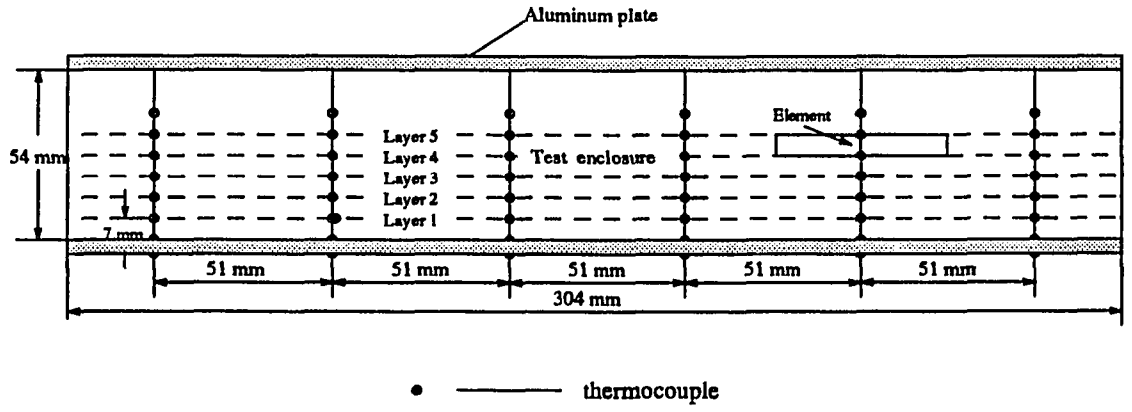

Figure 3: Arrangement of thermocouples in the test cell

the sidewalls. The location of the interface position was manually recorded through visual observation, and some photographs were taken.

Test Procedure

The test cell was fully filled with pure distilled water, and precautions were taken to remove any air bubbles in the water out of the test cell through the overflow tubes. The test cell was then placed horizontally on a supporting frame.

The ethylene glycol-water solution was circulated through the chiller, the electric heater and the the thermal reservoir to reach a desired temperature before the beginning of the experiment. The temperature of the ethylene glycol-water solution could be controlled within $\pm 0.2^{o}C$ by adjusting the flow rates through the heater and chiller. To begin the experiment the solution was circulated in the loop including the test cell. The flow rate of the solution passing through the test cell was kept large enough to minimize the temperature difference between the inlet and the outlet of the test cell.

At the beginning of the freezing process, the ethylene glycol-water solution was circulated through the loop which includes the test section and the storage bath to make the test cell a nearly constant temperature. The uniform temperature of the test cell could be either superheating or equal to the fusion temperature T_f. Then valves 4 and 5 were closed; the ethylene glycol-water solution was cooled by the chiller to a desired steady cooling temperature and circulated to cool the test cell until all of the water inside the test cell became ice.

Once the water in the test cell became ice, the valves 4 and 5 were closed. The ethylene glycol-water solution was heated by the electric in-line heater to a

temperature close to $0°C$. It then was circulated through the test cell to reduce the subcooling degree of the ice and make the temperature of the ice more uniform. This process would take from thirty minutes to one hour depending on the initial temperature of the ice. Then the glycol-water solution was heated as quickly as possible to the desired temperature for the melting experiment. The warm solution was circulated to heat the lower side of test cell and was maintained at that level until the experiment was finished.

At regular intervals during the experiments, an insulation was removed from one side of the test cell to allow visual observations or photographs to record the position of the solid-liquid interface. These actions were done as quickly as possible so that insulation could be replaced to minimize heat loss from the test cell.

RESULTS AND DISCUSSION

A series of experiments were performed for the melting processes. The experimental conditions for different runs are listed in Table 1.

Fig. 4 shows the variation of the average temperature on different layers with time for two selected runs. It is observed that the temperature of the heating fluid was nearly constant. But the average temperature on the wall did not reach the desired value at the beginning of melting, because part of the heat energy in the glycol-water solution was used to eliminate the sensible heat existing in the materials of the test system. The average wall temperature in the run with lower flow temperature was slower to reach a desired steady temperature than that in the run with higher flow temperature. These could cause some discrepancy between experimental data and prediction results which assumed a constant wall temperature.

The variation of interface position with time is presented in Fig. 5. After the beginning of the melting, in which heat conduction played a dominant role [6-9], the solid-liquid interface increases at a nearly linear rate due to convection heat transfer. The surface of the solid-liquid interface was observed to be smooth at the early time of the experiments, then semispherical-capped cells formed on the interface surface because of convection effect of the flow. But the overall shape of the interface was still kept quite planar; the differences among the locations of the ruler scale were

Table 1: Conditions of experiments

No. of run	Average flow temperature ^oC	Average wall temperature ^oC	Range of Ra
1	7.4	5.4	0 - 73,140
2	7.5	5.7	0 - 133,914
3	7.7	6.1	0 - 249,963
4	9.5	6.7	0 - 142,235
5	12.1	8.8	0 - 574,959
6	14.4	10.2	0 - 591,047
7	16.8	11.9	0 - 1,625,181
8	19.8	13.2	0 - 1,726,265
9	22.7	15.1	0 - 4,285,943
10	24.2	16.0	0 - 3,201,686
11	25.0	16.8	0 - 4,953,353
12	23.0	15.4	0 - 5,727,797
13	22.3	15.0	0 - 6,883,875

within ± 1 mm. According to the above observations, an assumption can be made that heat transfer only occurs in one dimensional direction.

Heat transfer for the solid-liquid phase changing process in the test cell includes two parts, sensible heat change and latent heat change. The sensible heat change rate can be evaluated by following equation

$$Q_{sen} = \sum_{i=1}^{m} \rho_i c_{p_i} A_i \frac{T_i - T_i'}{\Delta t}, \tag{1}$$

where i represents the number of a element; m the total number of the elements, A_i the cross-section area of the element, and Δt the time step for data measurement.

The latent heat can be presented by

$$Q_{lat} = \sum_{j=1}^{n} \rho_s h_f W_i \frac{\Delta s_j}{\Delta t}, \tag{2}$$

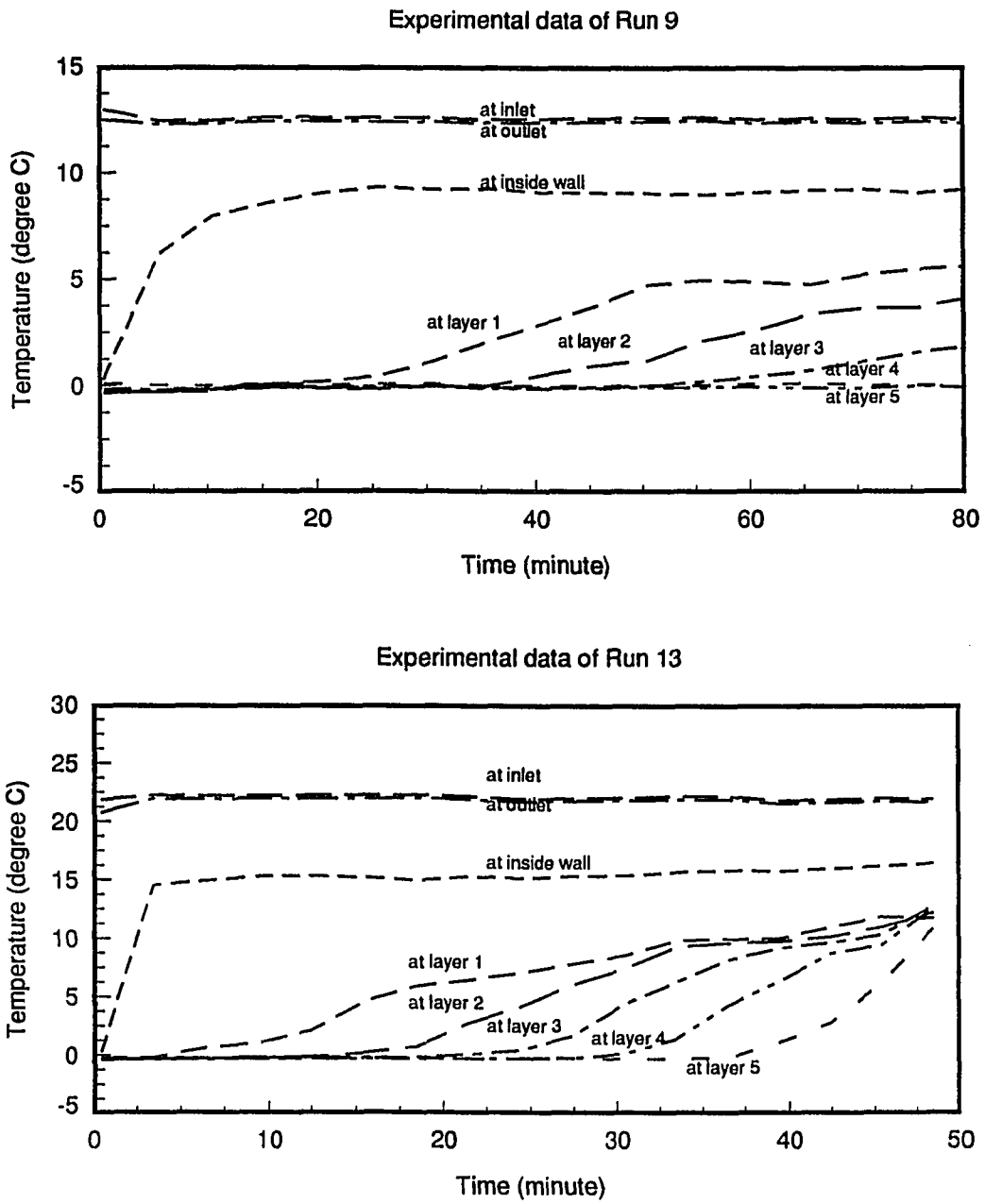

Figure 4: Variation of average temperature at different layers with time during melting

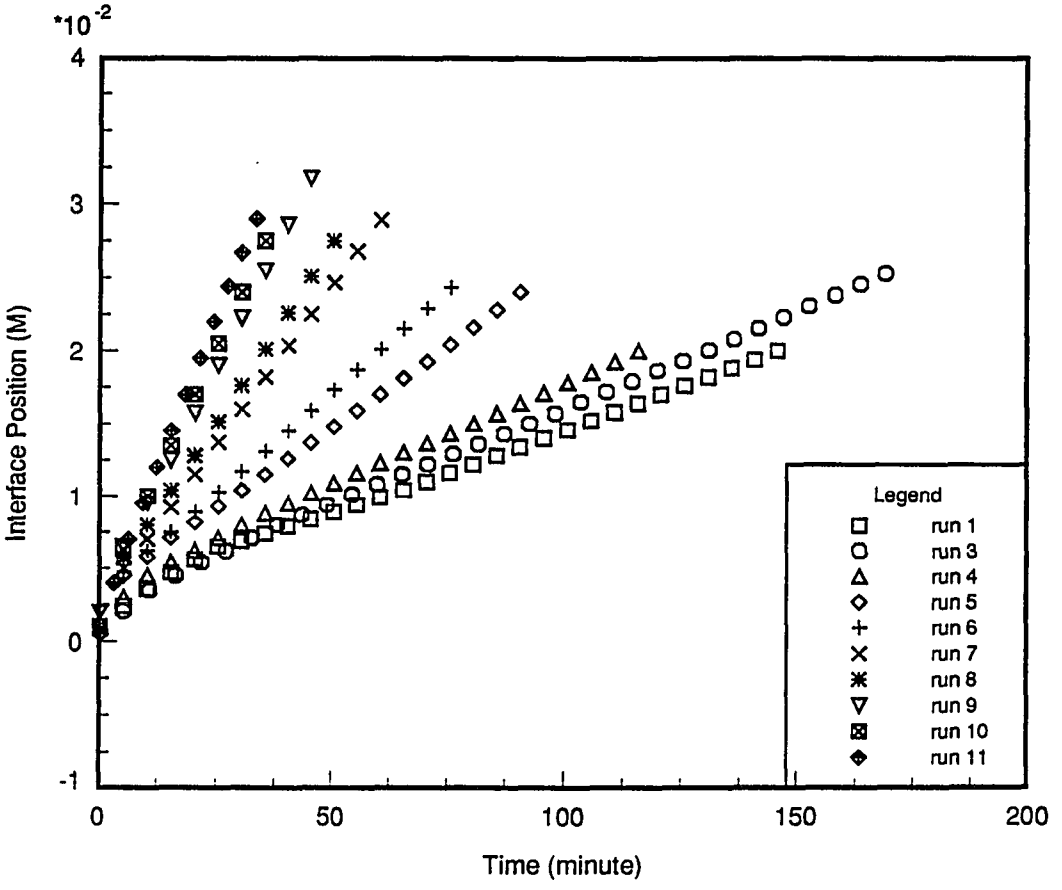

Figure 5: Variation of the solid-liquid interface position with time during melting

where j represents the number of the ruler scales, W_i the width of the element, Δs_j interface position change at location j for each time step Δt.

The total heat transfer rate on the heated wall is

$$q = \frac{Q_{sen} + Q_{lat}}{W}, \tag{3}$$

where W is the width of the test cell.

Fig. 6 shows heat change rates inside the test cell for different test runs. It was observed that the latent heat change was higher at an early time due to close-contact conduction heat transfer. After a short transition time, it dropped down, and then was kept at a nearly constant level. The sensible heat change was always much lower than the latent heat change. It only took 5% – 15% of the total heat change, but it increased as time and interface grew. For the process under higher heating temperature (or higher heated wall temperature), the latent heat change rate decreased during the later time because more heat was used to increase sensible heat, for example, in run 8 to run 10.

The heat transfer coefficient on the heated wall is expressed as

$$h_{wall} = \frac{q}{T_w - T_f}. \tag{4}$$

On the interface, the energy equation is given by

$$\rho_s h_l \frac{\Delta \bar{s}}{\Delta t} = K_s \frac{\partial T_s}{\partial y} + h_{int}(T_w - T_f), \tag{5}$$

where $\Delta \bar{s}$ represents the average interface increase in the time step Δt.

In the present experimental condition, the temperature in the solid region was close to 0 ^oC. The first term in the right side of Eq. (5) could be neglected. Thus,

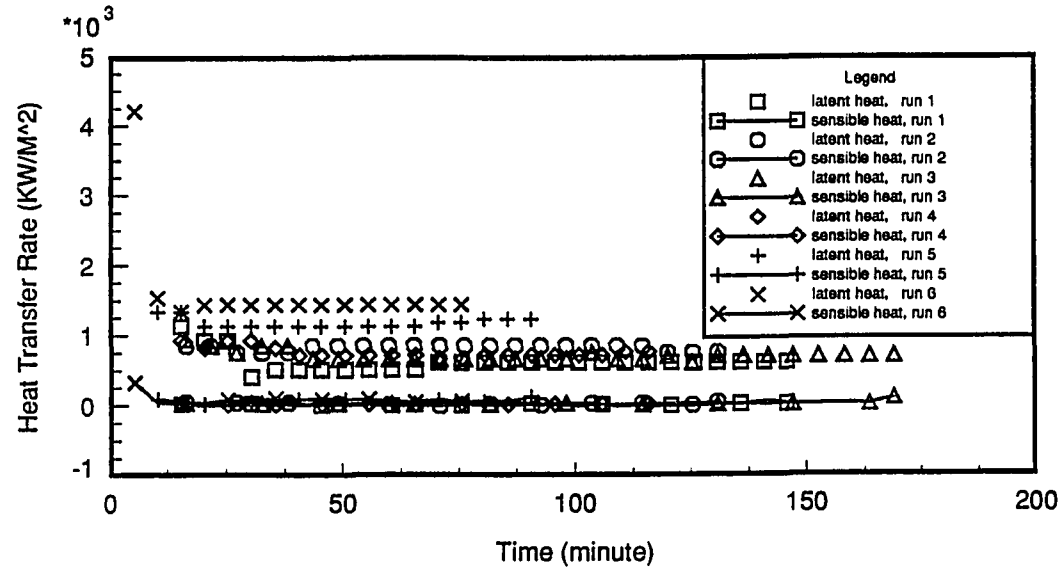

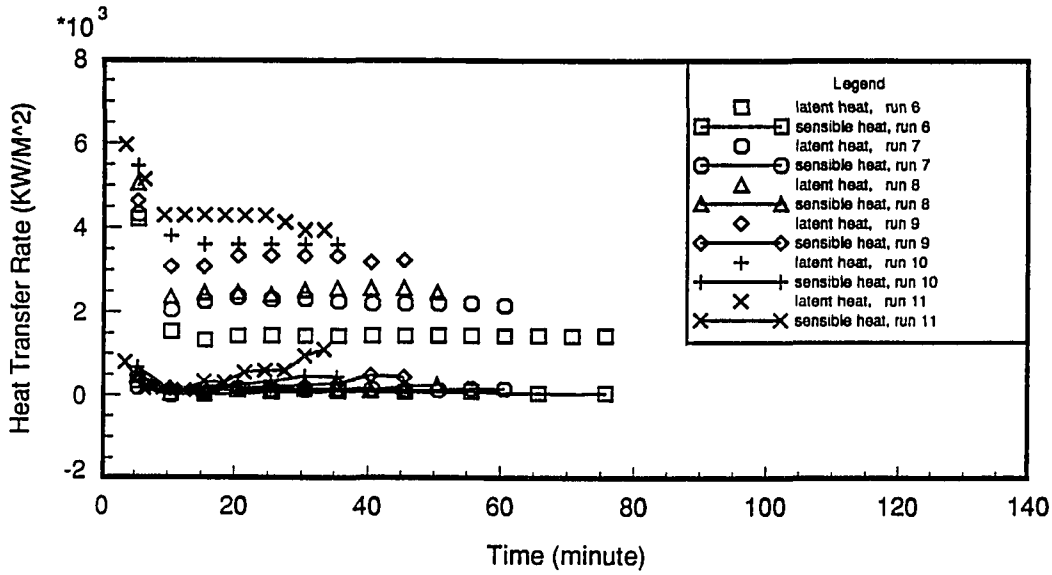

Figure 6: Comparison of sensible heat and latent heat inside the test enclosure

heat transfer coefficient on the interface is

$$h_{int} = \rho_s h_l \frac{\Delta \bar{s}}{\Delta t}/(T_w - T_f). \tag{6}$$

The Nusselt number is defined as

$$N_u = hs/k_l, \tag{7}$$

and the Rayleigh number is given as:

$$Ra = g\beta(T_w - T_f)s^3/\alpha\nu. \tag{8}$$

A relationship between the Rayleigh number and time is shown in Fig. 7. The Rayleigh number has a higher value corresponding to a higher wall temperature and a thicker liquid below the ice.

For the natural convection heat transfer, a general correlation has the following form

$$Nu = CRa^a Pr^b. \tag{9}$$

Several correlations have been developed for the single phase layer confined by two horizontal plates, such as in (Dlobe et al., 1959), (Chu et al., 1960) and (O'tool et al., 1960). Fig. 8 shows comparison of the Nusselt number versus the Rayleigh number at the heated wall between the present work and the results by the previous correlations, and Fig. 9 shows that at the interface. The Logarithmic scales are used in the figures. From these results, it is found that the correlations used for single phase processes are not perfect to the phase-change cases. The Nusselt numbers for the phase-change on the heated wall are about $5-15\%$ less than those by the previous correlations for single phase. The Nusselt numbers at the heated walls close to the

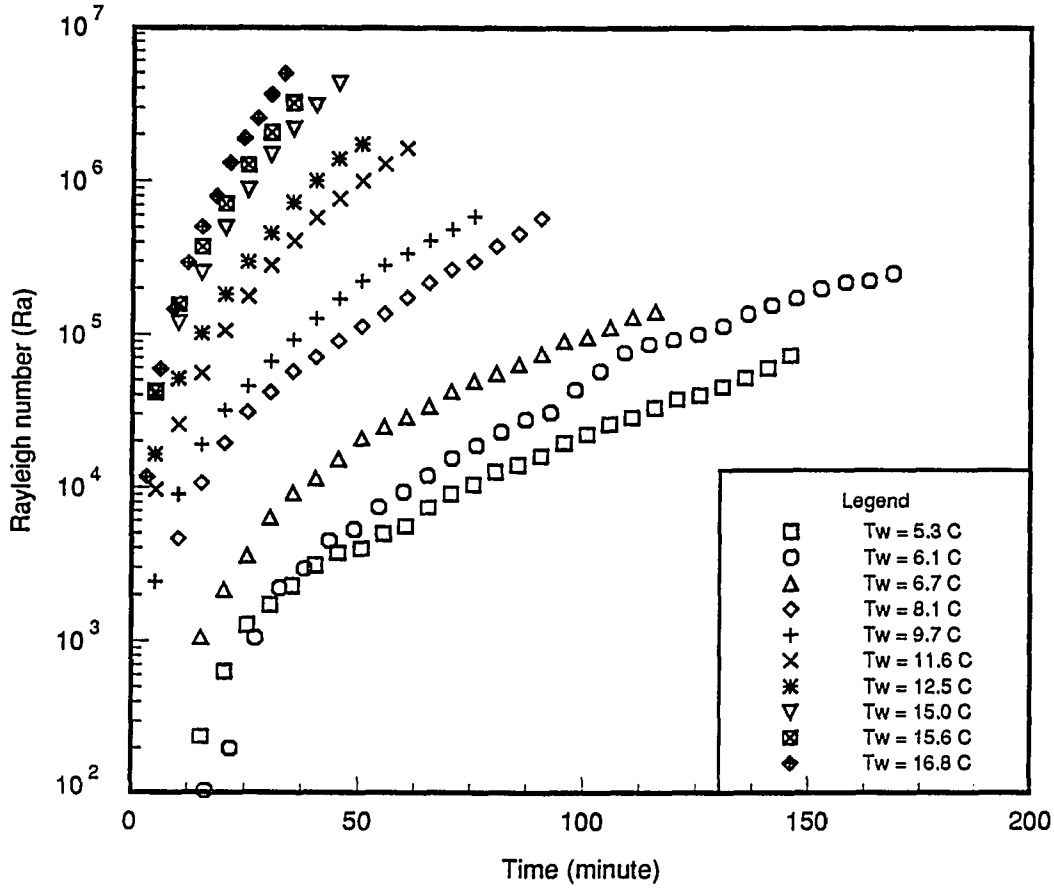

Figure 7: Variation of Rayleigh number with time

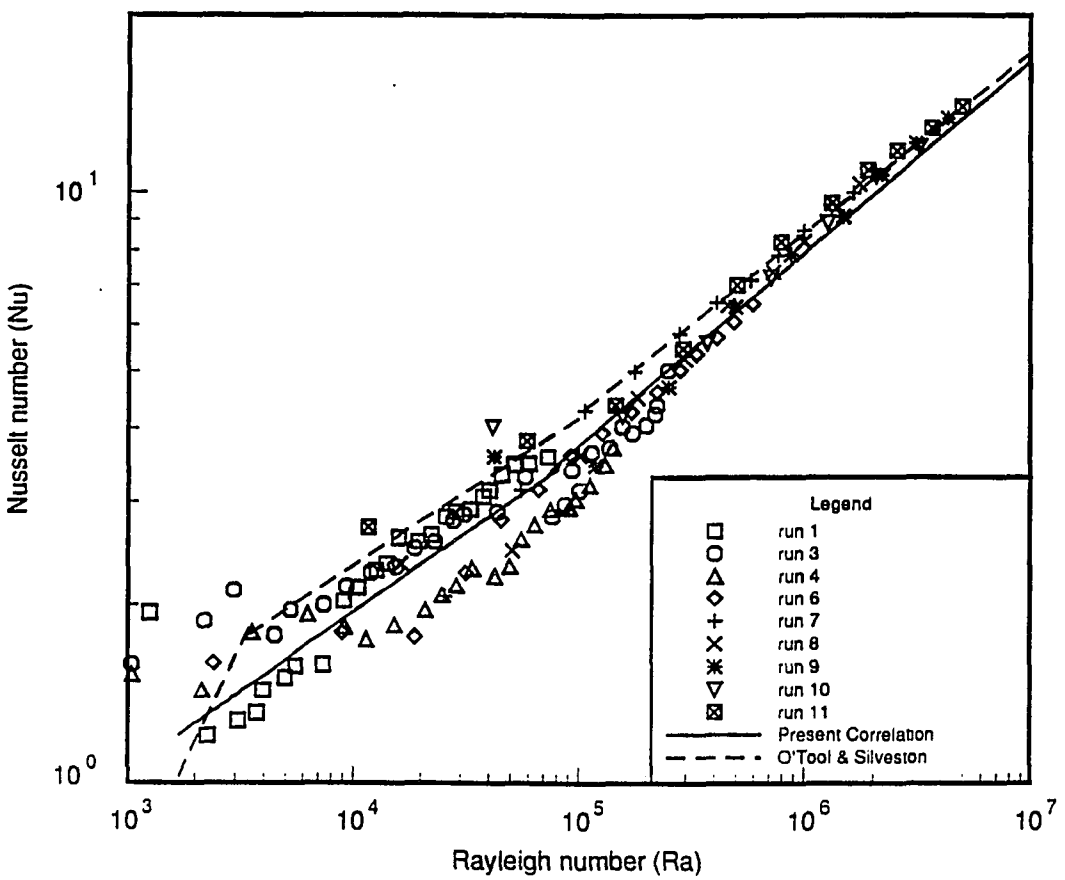

Figure 8: Relation of the Nusselt number with the Rayleigh number at the heated wall

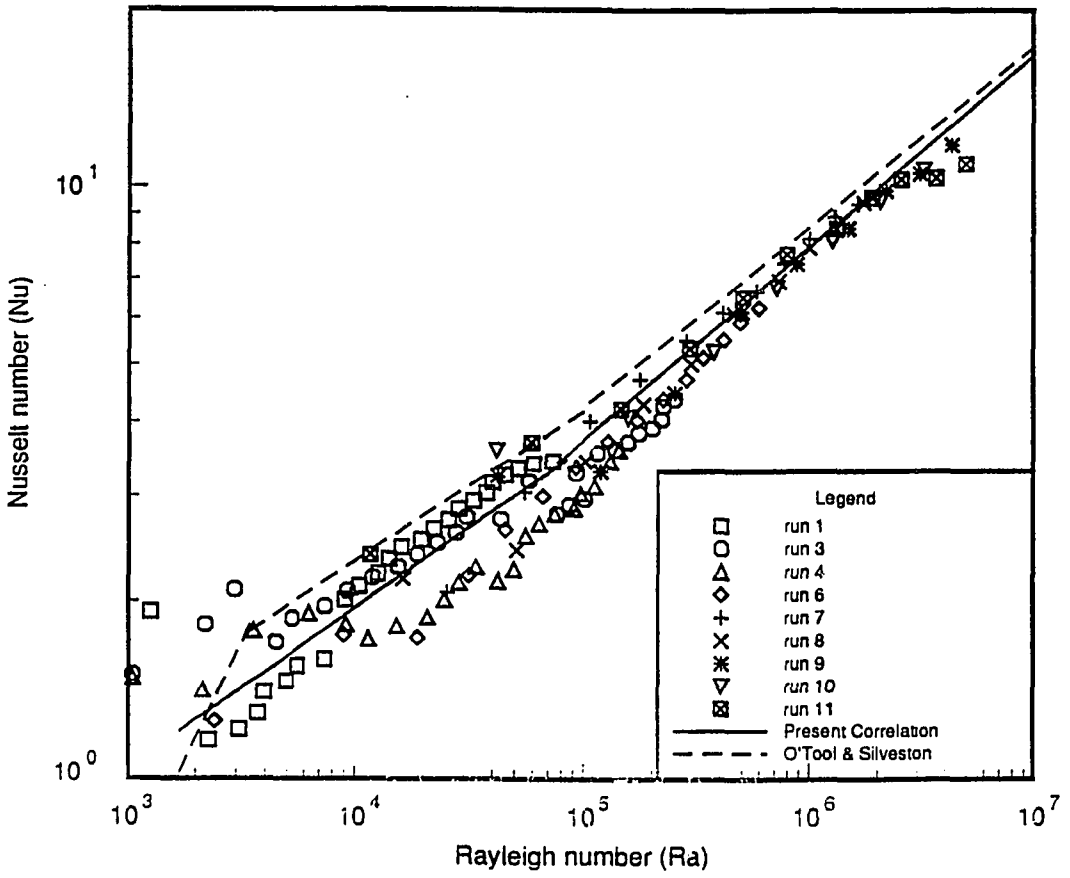

Figure 9: Relation of the Nusselt number with the Rayleigh number at the interface

the Nusselt number at the interface in the range of lower Rayleigh number (below 10^5) since the sensible heat change is very small in this range. In higher Rayleigh number range (above 10^5), the Nusselt number on the heated wall is close to those by the previous correlations; however the Nusselt number on the interface is still about $5 - 10\%$ less. The modified equations based on current experiments are listed in Table 2. More agreeable comparison could be obtained for the phase-change problem in water by using them.

Table 2: Equation of convection heat transfer in ice-water phase change Process

Range of Ra	Correlation equation	Estimate of error
$1,700 - 10^5$	$Nu = 0.165Ra^{0.268}$	$+12.2\%, \ -14.3\%$
$10^5 - 10^7$	$Nu = 0.072Ra^{0.325}Pr^{0.084}$	$+5.4\%, \ -6.1\%$

The errors caused by temperature measurements and conversions were within $\pm 1.0°C$, and the observation error for the interface position were within $\pm 1.0mm$. These errors influenced the values of the Ra and Nu which were obtained by the experimental data. The relative errors to the Ra are from 1.6% to 7.2%, and the relative errors to the Nu are from 0.7% to 2.1% in the range of the current experiments. The relative errors of the Nusselt number are higher in the range of the lower Rayleigh number than in the range of the higher Rayleigh number because of the absolute errors in temperature measurements and interface observations. The results by the modified correlations are also shown in Fig. 8 and Fig. 9 and compared with the present experimental data.

CONCLUSION

Experiments of ice melting in a horizontal rectangular enclosure were performed under different conditions. The interface and temperature changes were recorded and illustrated. The heat transfer rates, the heat transfer coefficients, the Rayleigh number and the Nusselt number were evaluated.

Based on the observations and experimental data, it was reasonable to treat the present model as one-dimensional heat transfer problem. It was found that the sensible heat change was the minor part, and that the most heat energy was used to change the latent heat in the phase-change process. The heat transfer rate on the heated wall was higher than that on the solid-liquid interface. The difference is due to part heat energy was used to increase sensible heat in the liquid. The total heat transfer rate dropped down at the beginning time, then stayed at a closed-constant level.

A relationship between the Nusselt number and the Rayleigh number was obtained by analyzing the experimental data. It was observed that the Nusselt numbers by the current study were less than those by the correlations for single phase, especially in the range of the lower Rayleigh number. The average difference is about $\pm 7.5\%$ for the Nu on the heated wall, and is -13% for the Nu on the interface comparing with those by the correlations applied to the single phase.

REFERENCES

Abdel-Wahed, R. M., Ramsey, J. W., and Sparrow, E. M., "Photographic Study of Melting about an Embedded Horizontal heating Cylinder," *International Journal of Heat and Mass Transfer*, Vol. 22, 1979, pp. 171-173.

Bathelt, A. G., and Viskanta, R. "An Experimental Investigation of Natural Convection in the Melted Region around a Heated Horizontal Cylinder," *Journal of Fluid Mechanics*, Vol. 90, 1979, pp. 227-239.

Bathelt, A. G., and Viskanta, R., "Heat Transfer at the Solid-Liquid Interface During Melting from Horizontal Cylinder," *International Journal of Heat and Mass Transfer*, Vol. 23, 1980, pp. 1403-1443.

Boger, D. V. and Westwater, J. W., "Effect of Buoyancy on the Melting and Freezing Process," *Journal of Heat Transfer*, Vol. , 1967, pp. 81-89

Chu, T. and Goldstein, R., "Turbulent convection in a Horizontal layer of water," *Journal of Fluid Mechanics*, Vol. 60, 1973, pp. 141-159

Dlobe, S. and Dropkin, D., "Natural Convection Heat Transfer in Liquids Confined Between Two Horizontal plates," *Journal of Heat Transfer*, Vol. 81c, 1959, pp. 24-30

Hale, N. and Viskanta, R., "Solid-Liquid Phase-Change Heat Transfer and Interface Motion in Materials Cooled or heated from Above or Below," *International Journal of Heat and Mass Transfer*, Vol. 23, 1979, pp. 283-292

Heitz,W. L. and Westwater, J. W., "Critical Rayleigh Numbers for Natural Convection of water Confined in Square Cells with L/D from 0.5 to 8," *Journal of Heat Transfer*,Vol. 93 , 1971, pp. 188-196

Ho, J. C., and Viskanta, R., "Experimental Study of Melting in a Rectangular Cavity," In *Heat Transfer - 1982*, eds. U. Griqull et al., Vol. 2, pp. 369-374, Hemisphere Publishing Corporation, Washington D. C., 1982

Ho, J. C., and Viskanta, R., "Heat transfer During Melting From an Isothermal Vertical Wall", *Journal of Heat Transfer*, Vol. 106, 1984, pp. 12-19

Kemink, R. G., and Sparrow, E. M., "Heat Transfer Coefficients for Melting about a Vertical Cylinder with or without Subcooling and for Open or Closed Containment," *International Journal of Heat and Mass transfer*, Vol. 25, 1981, pp. 1699-1710

Marshall, R. H., "Natural Convection Effects in Rectangular Enclosures Containing a Phase Change Materials," in *Thermal Storage and Heat Transfer in Solar Energy Systems*, eds. F. Kreith et al., pp. 61-69, ASME, New York, 1978

O'Tool, J and Silveston, P., " Correlations of convection Heat transfer confined in Horizontal Layers," *HEAT TRANSFER - BUFFALO, AICHE Chemical Progress Symposium series*, Vol. 32, 1960, pp. 81-86

Ramsey, J. W., and Sparrow, E. M., "Melting and Natural Convection due to a Vertical Embedded Heater," *Journal of Heat transfer*, Vol. 100, 1978, pp. 368-370

Seki, N., Fukusako, S. and Sugawara, M., "A Criterion of Onset of Free convection in a Horizontal Melted Water Layer with Free Surface," *Journal of Heat Transfer*, Vol. 99, 1977, pp. 92-98

Sparrow, E. M., Schmidt, R., and Ramsey, J. W., "Experimental Investigation of Natural Convection in the Melting of Solids," *Journal of Heat Transfer*, Vol. 100, 1978, pp. 11-16

Vanburen, P. D., and Viskanta, R., "Interferometric Measurement of Heat Transfer During Melting from a Vertical Surface," *International Journal of Heat and Mass Transfer*, Vol. 23, 1980, pp. 568-571

Yen, Y., "Onset of Convection in a Layer of Water Formed by Melting Ice from Below," *The Physics of Fluids*, Vol. 11, 1968, pp. 1263-1270

PAPER II.

FREEZING AND MELTING OF ICE IN A HORIZONTAL RECTANGULAR ENCLOSURE COOLED OR HEATED ISOTHERMALLY

ABSTRACT

The present work is to investigate freezing and melting of ice in a horizontal rectangular enclosure. Constant surface temperature boundary conditions were applied to the top and bottom surfaces of the enclosure while adiabatic conditions were maintained on the edges of the enclosure. The location of the solid (ice)-liquid interface along with temperatures were recorded for various test conditions.

During the freezing process, the rates of ice formation on the upper and lower surfaces were found to be nearly the same, and the principle mode of heat transfer was by conduction. For the melting process, heat transfer was dominated by natural convection.

Experimental results were compared to solutions obtained from an analysis of both the freezing and melting problems. The comparison shows good agreement between the two.

NOMENCLATURE

c_p, specific heat;

h, heat transfer coefficient;

h_f, latent heat of fusion;

H, thickness of test enclosure;

H_{ice}, thickness of ice slab;

k, thermal conductivity;

Nu, Nusselt number, hs/k_l;

Pr, Prandtl number, $\mu_l c_{p_l}/k_l$;

Ra, Rayleigh number, $g_l\beta(T_w - T_f)s^3/\nu\alpha$;

s, distance of solid-liquid interface to the boundary;

Sbc, subcooling number, $(T_i - T_f)/(T_w - T_f)$;

Sph, superheating number, $(T_i - T_f)/(T_f - T_m)$;

Ste, Stefan number, $c_p(T_w - T_f)/h_f$;

t, time;

T, temperature;

y, coordinate.

Greek Symbols

α, thermal diffusivity, $k/\rho c$;

β, thermal expansion coefficient;

Θ_k, dimensionless temperature, $(T_k - T_f)/(T_w - T_f)$;

ν, kinematic viscosity;

μ, viscosity;

ρ, density.

Superscripts

$*$, refers to dimensionless;

$'$, refers to previous step.

Subscripts

f, refers to fusion;

i, refers to initial;

k, refers to various symbols, f, or i, or l, or s, or t, or w;

l, refers to liquid;

s, refers to solid;

t, refers to thermal penetration layer;

w, refers to wall.

INTRODUCTION

Heat conduction problems involving phase change are described in the literature. Good solutions were obtained by the integral method for the freezing process. For example in (Cho et al., 1969; Heitz et al., 1970; Menning et al., 1984; and Frederick et al., 1985). the effect of natural convection heat transfer for single phase has been studied both experimentally and analytically. Dlobe and Droplin (1959) obtained a natural convection correlation for single phase of liquids confined between two horizontal plates. O'Tool and Silveston (1960) experimentally developed the correlations for heat transfer through a horizontal layer confined by two parallel plates under the different regions of Rayleigh number. Chu and Goldstein (1973) developed a convection correlation in a horizontal layer of water for higher Rayleigh number region. The onset of free convection has been studied experimentally (Yen et al., 1968; Seki et al., 1977). It was found that the critical Rayleigh number for natural convection was about 1700. Before the Rayleigh number reaches the critical point, heat transfer occurs in a pure conduction mechanism. After this transfer, the Rayleigh number reaches or exceeds the critical value and the convection heat transfer plays a dominant role. Also, the effect of natural convection on phase change processes were studied. Boger and Westwater (1967) discussed the effect of buoyancy on the melting and freezing process. Hale and Viskanta (1979) also investigated melting and

freezing of n-octadecane in horizontal plate geometries. Their studies showed that natural convection effects are of great importance for melting.

One importance of phase change materials is its potential use in thermal energy storage systems(Garg et al., 1985). Water is the most common substance and rectangular is a widely used geometry in thermal energy storage systems. The focus of our work was to study the freezing and melting that occurs inside a horizontal rectangular enclosure. Water was used as the test substance. The ice-water interface positions and the temperature changes inside the enclosure during the tests were recorded. The analytical formulations of the problems were developed based on an integral method and were solved numerically. The problem was treated as pure conduction before Ra reached the critical point. After the critical point, some convection heat transfer correlations obtained from experiments in analysis were applied in my analysis. Effects of subcooling in solid and superheating in liquid were also considered in the analysis.

EXPERIMENT

The arrangement of thermocouples is shown in Fig. 1. The test cell (the rectangular enclosure) was fully filled with pure distilled water. Bubbles in the water were removed through the overflow tubes by vibrating the test cell. The test cell was then placed on a supporting frame horizontally.

The ethylene glycol-water solution was circulated through the chiller or heater and then the thermal reservoir to reach a required steady temperature in the beginning period of the experiment. The temperature of the ethylene glycol-water solution could be controlled to within $\pm 0.2^{o}C$ by adjusting the flow rates through the heater and chiller, respectively. Then the solution was circulated in the loop which included the test cell and bath. The flow rate of the solution that passed the heat exchangers was kept high enough to minimize the temperature difference between the inlet and outlet of the heat exchangers.

At the beginning of the freezing process, the ethylene glycol-water solution was circulated through the test-section storage-bath loop to make the test cell a nearly constant temperature. The temperature of the test cell could be above or equal to T_f. Then the valves 4 and 5 were closed. The ethylene glycol-water solution was cooled by the chiller to a desired steady cooling temperature and was circulated to cool the test cell until all of the water inside the test cell became ice.

After the rectangular enclosure was fully occupied by ice through the freezing process, the valves, which were installed between the heat exchangers and the constant thermal reservoir, were closed. The ethylene glycol-water solution was heated to a desired steady temperature by the electric in-line heater and the temperature reached uniform throughout the entire ice slab. This period usually took twenty to thirty minutes, depending how high temperature that was desired. The glycol-water solution with nearly steady higher temperature was then circulated through the thermal reservoir and the test cell to reach a desired temperature. The solution was maintained at that level until all ice was melted. During the experiments, visual observations or photographs were taken at regular intervals. These actions had to be done as quickly as possible to minimize heat loss from the rectangular enclosure. The enclosure could be cooled or heated from above and below, or from either side separately. The data collected for different situations were compared with the solutions of analytical models.

Since fifty thermocouples were arranged inside the enclosure, the ice was fixed by the thermocouples and support frame.

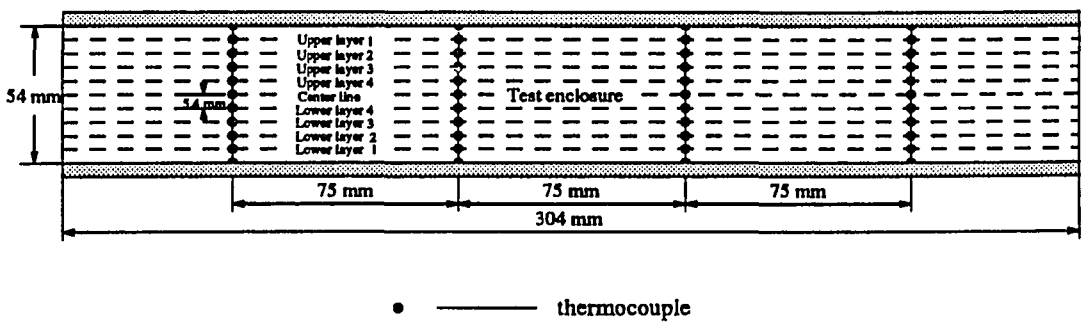

Figure 1: Arrangement of thermocouple in the test cell

ANALYSIS

Fig. 2 shows the geometry used to describe the problem. The rectangular enclosure is originally filled with water or ice at a uniform initial temperature T_i, which might be either above or below the fusion temperature T_f. When the wall temperature suddenly reaches a temperature T_w, the freezing or melting process begins. The wall temperature is maintained nearly constant. Heat transfer occurs due to the difference between the wall temperature and the temperature inside the rectangular enclosure. At the interfaces, the solid and liquid temperatures embrace at the melting point T_f. The entire ice doesn't move because it is fixed by the frame installed inside the test cell. The analysis is based on the following assumptions.

- Temperature distribution is symmetric about the center horizontal line of the ice mass. Therefore, the center line is adiabatic.
- No heat transfer occurs through the sides of the enclosure. Heat transfer only take place in a one dimensional direction (the y direction).
- The solid-liquid interfaces are sufficiently straight and horizontal.
- One-dimensional heat transfer.

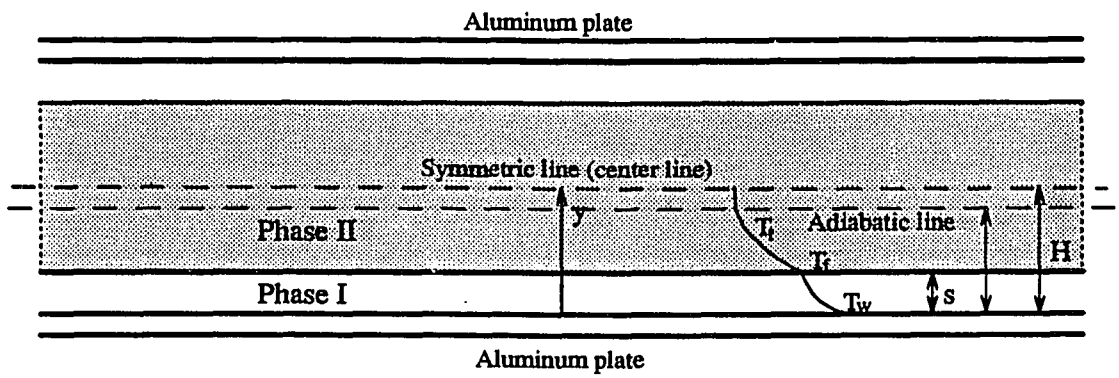

Figure 2: Schematic representation of geometric model

Freezing process

No closed-form exact solution exists for the freezing or melting of a slab with finite thickness. In this paper, the integral technique is used. First, consider a water region which is initially at temperature T_i. T_i can be superheating or equal to the fusion temperature T_f. The wall temperature T_w, is below T_f and remains constant. As time passes, the solid-liquid interface increases in temperature and the temperature in the liquid phase decreases until it reaches T_f.

Considering the freezing process to be pure conduction, the energy equations for the solid and liquid regions are:

$$\frac{\partial T_s}{\partial t} = \alpha_s \frac{\partial^2 T_s}{\partial y^2}, \qquad 0 \leq y \leq s, \tag{1}$$

and

$$\frac{\partial T_l}{\partial t} = \alpha_l \frac{\partial^2 T_l}{\partial y^2}, \qquad s \leq y \leq H. \tag{2}$$

The rate at which the solid-liquid interface moves is determined from an energy balance at the interface. The energy balance equation is expressed as

$$\rho_s h_f \frac{ds}{dt} = k_s \frac{\partial T_s}{\partial y} - k_l \frac{\partial T_l}{\partial y}, \qquad at \;\; y = s. \tag{3}$$

The initial conditions are

$$T_s = T_l = T_i \quad for \quad t \leq 0, \tag{4}$$

and the boundary conditions are

$$T_s = T_w, \quad at \;\; y = 0 \quad for \;\; t > 0, \tag{5}$$

$$T_s = T_l = T_f, \quad at \;\; y = s, \tag{6}$$

$$T_l = T_t, \quad \frac{\partial T_l}{\partial y} = 0, \quad at \ \ y = H_t, \tag{7}$$

where H_t represents the thermal penetration layer, and T_t the temperature at H_t, which varies with time.

The dimensionless variables are defined as

$$y^* = \frac{y}{H}; \quad s^* = \frac{s}{H}; \quad H_t^* = \frac{H_t}{H} \tag{8}$$

$$t_l^* = \frac{\alpha_l t}{H^2}; \quad t_s^* = \frac{\alpha_s t}{H^2}, \tag{9}$$

$$\Theta_k = \frac{T_k - T_f}{T_w - T_f}, \quad k = f, \ or \ i, \ or \ l, \ or \ s, \ or \ t, \ or \ w. \tag{10}$$

The dimensionless forms of the above equations are respectively

$$\frac{\partial \Theta_s}{\partial t_s^*} = \frac{\partial^2 \Theta_s}{\partial y^{*2}}, \quad 0 \le y^* \le s^*, \tag{11}$$

$$\frac{\partial \Theta_l}{\partial t_l^*} = \frac{\partial^2 \Theta_l}{\partial y^{*2}}, \quad s^* \le y^* \le 1, \tag{12}$$

$$\frac{ds^*}{dt_s^*} = Ste(\frac{\partial \Theta_s}{\partial y^*} - \frac{k_l}{k_s}\frac{\partial \Theta_l}{\partial y}), \quad at \quad y^* = s*, \tag{13}$$

The temperature profiles in the solid and liquid regions can be assumed, which must satisfy the initial and boundary conditions. The temperature distribution in the solid region is given by Özisik (1980):

$$\Theta_s = \Theta_w[1 - \frac{erf(x/2\sqrt{t_s^*})}{erf(s/2\sqrt{t_s^*})}], \tag{14}$$

and the temperature distribution in the liquid region is given by Incropera and De Witt (1990):

$$\Theta_l = \Theta_t[1 - (\frac{H_t^* - y^*}{H_t^* - s^*})^2]. \tag{15}$$

The initial condition is

$$\Theta_l = \Theta_i, \quad t^* \le 0. \tag{16}$$

The boundary conditions are

$$\Theta_s = \Theta_w = 1, \qquad at \;\; y^* = 0, \qquad t^* > 0, \tag{17}$$

$$\Theta_s = \Theta_l = \Theta_f = 0, \qquad at \;\; y^* = s^* \qquad t^* > 0, \tag{18}$$

and

$$\Theta_l = \Theta_t, \qquad \frac{\partial \Theta_l}{\partial y^*} = 0, \quad at \;\; y^* = H_t^*. \tag{19}$$

Substituting Eq. (14), Eq. (15), and Eq. (18) into Eq. (13) results

$$\frac{ds^*}{dt_s^*} = 2Ste[\frac{\Theta_w e^{-s/2\sqrt{t_s^*}}}{\sqrt{\pi t_s^*} erf(s/2\sqrt{t_s^*})} - \frac{k_l}{k_s}\frac{\Theta_t}{(H_t^* - s^*)}]. \tag{20}$$

Integrating Eq. (12) with respect to y^* from s^* to H_t^* yields

$$\int_{s^*}^{H_t^*} \frac{\partial \Theta_l}{\partial t_l^*} dy^* = \int_{s^*}^{H_t^*} \frac{\partial^2 \Theta_l}{\partial y^{*2}} dy^* \tag{21}$$

or

$$\frac{d}{dt_l^*}\int_{s^*}^{H_t^*} \Theta_l dy^* - (\Theta \mid_{H_t^*} \frac{dH_t^*}{dt_l^*} - \Theta_l \mid_{s^*} \frac{ds_b^*}{dt_l^*}) = \frac{\partial \Theta_l}{\partial y^*} \mid_{H_t^*} - \frac{\partial \Theta_l}{\partial y^*} \mid_{s^*} . \tag{22}$$

Substituting the boundary conditions Eq. (18) and Eq. (19) into Eq. (22) and rearranging results .

$$[1 - s^* - \frac{1}{3}(H_t^* - s^*)]\frac{d\Theta_t}{dt_l^*} - \frac{\Theta_t}{3}\frac{dH_t^*}{dt_l^*} + \frac{2\Theta_t}{H_t^*} = 0. \tag{23}$$

In Eq. (20) and Eq. (23), s^*, H_t^*, and Θ_t are variables. H_t^* increases as time. For the thin container, H_t^* can be treated as 1, since it reaches the center line in a short time. So one variable is omitted. Thus, Eq. (20) and Eq. (23) can be solved simultaneously for s^* and Θ_t by the first order finite difference method. In the first step, Θ_t is same as Θ_i, and s^* is solved by the Neumann method described in Cho and

Sunderland (1969). Then, the forward finite difference forms of $d\Theta_l/dt^*$ and ds^*/dt^* can be expressed as:

$$\frac{d\Theta_l}{dt^*} \doteq \frac{\Theta_l - \Theta_l'}{\triangle t^*}, \tag{24}$$

$$\frac{ds^*}{dt^*} \doteq \frac{(s^*) - s^{*\prime}}{\triangle t^*}, \tag{25}$$

where superscript "′" means the value at the previous step, and $\triangle t^*$ means the time grid for each step. If the values of s^* and Θ_t in the other terms of Eq. (20) and Eq. (23) are used as the values in the previous step, the problem is explicit and can be solved directly. Otherwise, the values of s^* and Θ_t in the other terms are treated as the values in the advanced step, the problem is implicit, and Eq. (20) is in a transcendental form. This transcendental equation can be solved numerically by the Newton-Raphson method. The iterations are necessary to obtain accurate results in each step of the solution procedure. In current work, the problems are solved implicitly.

In the above analysis, heat transfer was considered as pure conduction . This generally in case of Ra for the liquid less than 1,700. For the Ra greater than 1,700, convection heat transfer occurs in the liquid.

The energy balance equation at the solid-liquid interface can be expressed as

$$\rho_s h_f \frac{ds}{dt} = k_s \frac{\partial T_s}{\partial y} - h(T_t - T_f), \quad at \quad y = s, \quad t > 0, \tag{26}$$

where h is the convection heat transfer coefficient. Values for h are obtained from the Nusselt number correlation (Yong and Maxwell, 1993).

$$Nu = 0.165 Ra^{0.268} \qquad 1,700 < Ra < 100,000. \tag{27}$$

The dimensionless forms of the governing equations are

$$\frac{\partial \Theta_s}{\partial t_s^*} = \frac{\partial^2 \Theta_s}{\partial y^{*2}}, \qquad 0 \le y^* \le s^*, \quad t_s^* > 0, \tag{28}$$

$$\frac{ds^*}{dt_s^*} = Ste(\frac{\partial \Theta_s}{\partial y^*} - \frac{h}{k_s}\Theta_t H), \qquad at \quad y^* = s^* \quad t_l^* > 0. \tag{29}$$

The definition of each dimensionless term, the initial condition, and the boundary conditions are the same as those given for the pure conduction model.

An approximate temperature distribution in the solid region that satisfies the boundary conditions in the is given in Goodman (1964):

$$\Theta_s = \phi\frac{y^*}{s^*} + (1-\phi)(\frac{y^*}{s^*})^2, \tag{30}$$

where ϕ is a function of time. This function can be determined in the following way.

Differentiating equation (18) with respect to t^* results in

$$\frac{\partial \Theta_s}{\partial y^*}\frac{ds_s^*}{dt^*} + \frac{\partial \Theta_s}{\partial t_s^*} = 0, \tag{31}$$

where it has been assumed that Θ_s does not change with time. Then ds^*/dt^* can be eliminated by combining Eq. (28), Eq. (29), and Eq. (31) to yield

$$\frac{\partial \Theta_s}{\partial y^*}Ste(\frac{\partial \Theta_s}{\partial y^*} - \frac{h}{k_s}\Theta_t H) + \frac{\partial^2 \Theta_s}{\partial y^{*2}} = 0 \qquad at \quad y^* = s^*. \tag{32}$$

Substitution of equation (30) into the equation (32) results in

$$\phi = 2 - [\frac{h}{k_s}\Theta_t H s^* - \frac{2}{Ste} + \sqrt{(\frac{h}{k_s}\Theta_t H s^* - \frac{2}{Ste})^2 + \frac{8}{Ste}}/2]. \tag{33}$$

Now the energy balance at the solid-liquid interface can be written as

$$\frac{ds^*}{dt^*} = \frac{2-\phi}{s^*} - \frac{h}{k_s}\Theta_t H. \tag{34}$$

The temperature distribution in the liquid region is also assumed to have a form described by Eq. (15). The same result as Eq. (23) can be obtained.

Similarly, s^* and Θ_t can be obtained by solving Eq. (23) and Eq. (34) simultaneously.

Melting Process

Let's consider the melting process now. Before the melting process begins ($t < 0$), it is assumed that the ice in the enclosure is initially at a uniform temperature, T_i, which is less than or equal to the fusion temperature, T_f. For time $t > 0$, heat is transferred into the ice from the boundary surface ($y = 0$), which is at a constant temperature, T_w. Before Ra reaches the critical value ($Ra = 1,700$), heat transfer is considered as pure conduction mechanism, and the temperature distribution and interface position can be predicted by the Neumann analysis.. After it reaches the critical point, the convection heat transfer is dominant in the liquid region. and the natural convection correlation is used in the evaluation. The dimensionless governing equations can be expressed as

$$\frac{\partial \Theta_s}{\partial t_s^*} = \frac{\partial^2 \Theta_s}{\partial y^{*2}}, \quad s^* < y^* < 1, \tag{35}$$

$$\frac{ds^*}{dt_l^*} = Ste\left(\frac{k_s}{k_l}\frac{\partial \Theta_s}{\partial y^*} + \frac{Nu}{s^*}\right), \quad at \quad y^* = s^*, \tag{36}$$

where Nu can be selected in (Yong and Maxwell, 1993) for the natural convection heat transfer of a phase-change process in a horizontal enclosure.

The definitions of the dimensionless terms are the same as those used in the freezing process. The initial condition and the boundary conditions are given as

$$\Theta_s = \Theta_i, \quad t^* < 0, \tag{37}$$

$$\Theta_l = \Theta_w = 1, \quad at \quad y^* = 0 \quad t^* > 0, \tag{38}$$

$$\Theta_l = \Theta_l = \Theta_f = 0, \quad at \quad y^* = s^* \quad t^* > 0, \tag{39}$$

$$\Theta_s = \Theta_t, \quad \frac{\partial \Theta_s}{\partial y^*} = 0, \quad at \quad y^* \geq H_t^*. \tag{40}$$

The distribution of temperature in the solid region is assumed as

$$\Theta_s = \Theta_t[1 - (\frac{1_t - y^*}{1_t - s^*})^2]. \tag{41}$$

Substitution of equation (41) into equation (36) results in

$$\frac{ds^*}{dt_l^*} = Ste(\frac{\Theta_t}{1 - s^*} + \frac{Nu}{s^*}), \quad at \quad y^* = s^*. \tag{42}$$

Similarly, the integral method is used to obtain the relation between the temperature at H_t^* and time t^* in the solid region :

$$\frac{2}{3}(1 - s^*)\frac{d\Theta_t}{dt_l^*} - \frac{\Theta_t}{3}\frac{ds^*}{dt_l^*} + 2\frac{\Theta_t}{1 - s^*} = 0. \tag{43}$$

In Eq. (42) and Eq. (43), only s^* and Θ_t are unknowns. Theses two unknowns can be solved by the method used in the freezing process.

RESULTS AND DISCUSSION

A series of freezing and melting experiments (four tests for freezing and four for melting) was conducted in order to obtain data which could be compared to the analytical models.

Fig. 3 shows the variation histories of the average temperature at different layers for the freezing, and Fig. 4 for melting respectively. Observations can be obtained that the average temperature at a layer with a certain distance to the top boundary has a value close to that of a layer with the same distance to the bottom boundary during the freezing and melting. This means that the temperature distribution in the enclosure is approximately symmetric to the horizontal center line.

In the experiments, the wall temperatures did not reach the desired value at the beginning of freezing and melting because part of the energy of the glycol-water solution was consumed to eliminate the sensible heat existing in materials of the test system. This could cause some discrepancy between experimental data and analytical results.

For the process in which the enclosure was cooled from above and below, ice formed on both the upper and lower surfaces at nearly the same rate. The variation of interface position with time is presented in Fig. 5. The solid-liquid interface were found to be quite planar during the experiments. This phenomenon is in agreement

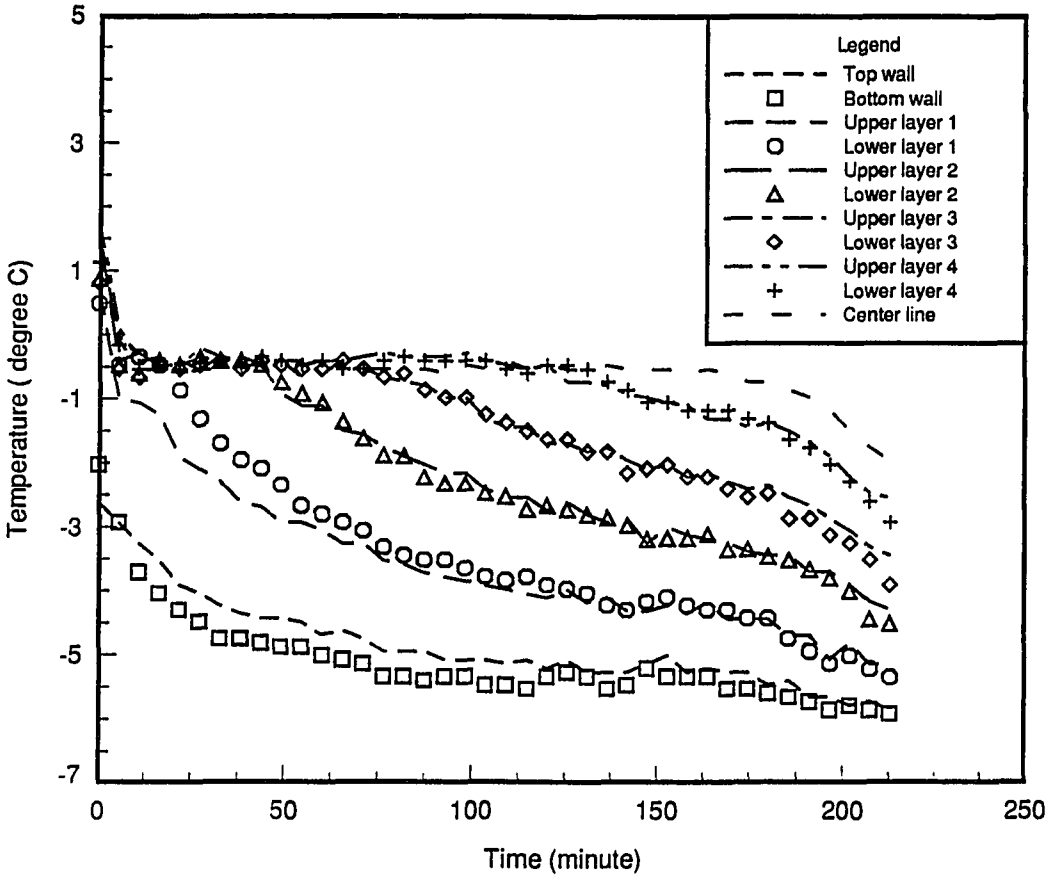

Figure 3: Variation of average temperature at different layers with time during freezing experiment

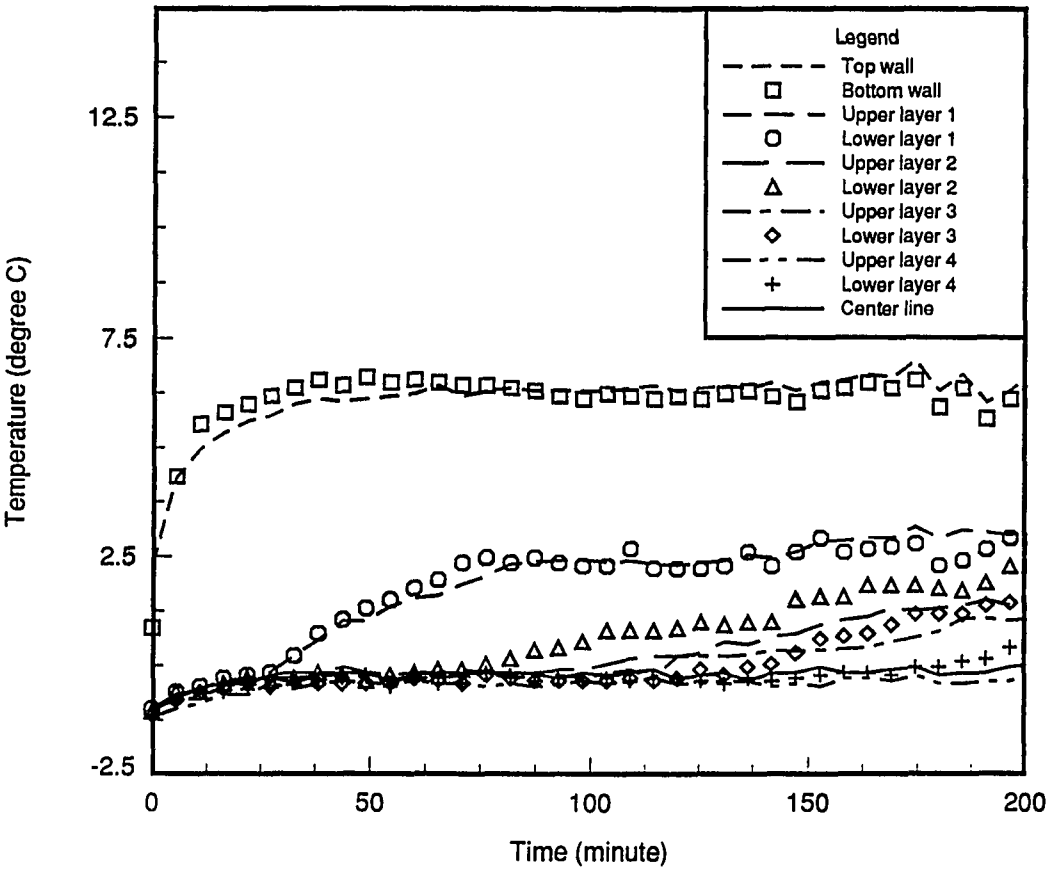

Figure 4: Variation of average temperature at different layers with time during melting experiment

with the assumptions that heat transfer occurs in a one-dimensional direction and is symmetric to the horizontal center line.

Another phenomenon observed is that no clear solid-liquid interface could be seen, but the liquid temperature reached the subcooling level when a very thin ice layer formed after a short time of the freezing. At these times, the temperature difference between the interface and the cold boundary was smaller, for example, 3.3 ^oC ($Ste = 0.029$). This behavior might be interpreted by the nucleating theory by Garg et al. (1985). This phenomenon is not included in the present study.

Fig. 6 shows a comparison of the experimental data with the analytical solutions for interface positions for a selected wall temperature of $-5,4^oC$. The experimental data generally match those obtained by both the pure conduction model and the model that considers natural convection effect in overall process. But it is found the experiments data are little less than those by analytical models at the beginning of freezing. This is attributed to the part of heat energy transferred from glycol solution was used for the sensible heat existed in the system and the wall temperature was not reached the desired T_w. Also, the experiments data were higher than those by the models as time passed. The reason for this is that the actual wall temperature was lower than the average temperature used in the models in that period. From Fig. 3, it can be seen that temperature in the liquid region reached the fusion temperature quickly (took only about $5-10\%$ of the test period). Once the liquid region reached T_f, the convection effect disappeared, and only conduction heat transfer took place in the solid region. So that, conduction heat transfer plays a dominant role in the overall freezing process.

The ice-water interface positions were measured at different times and at different

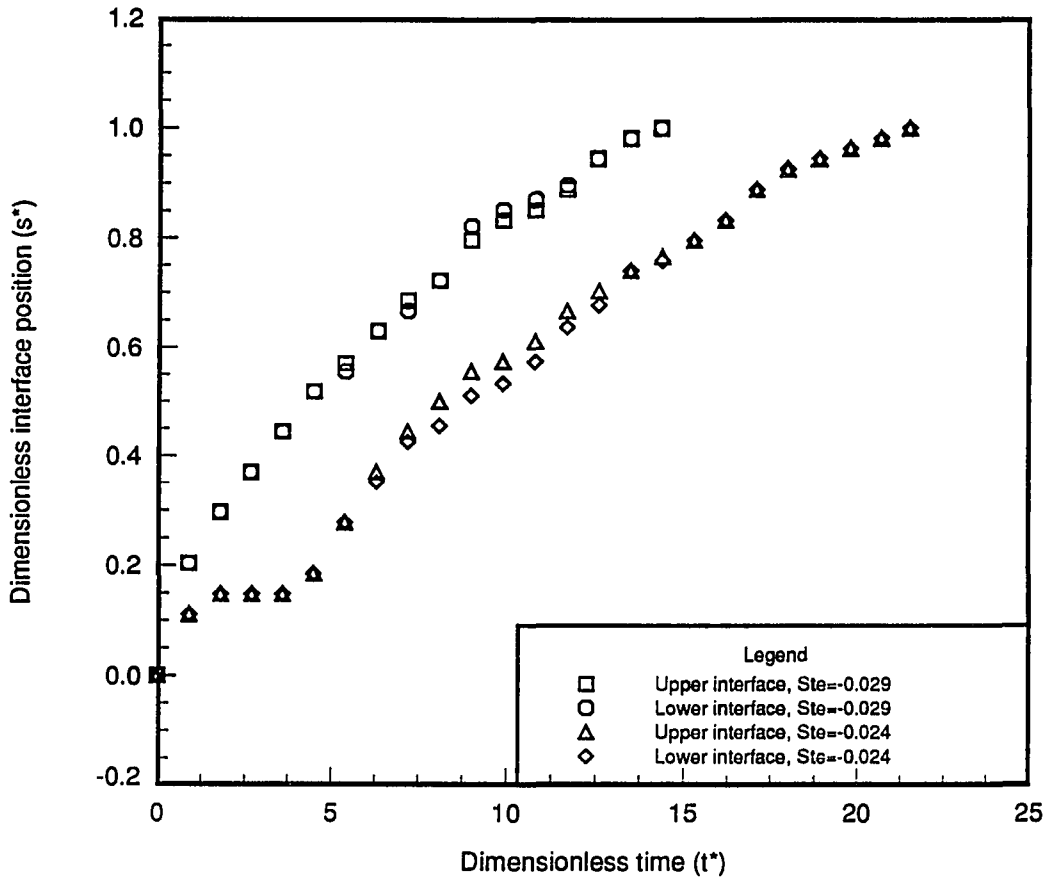

Figure 5: Variation of solid-liquid interface position with time during freezing from above and below

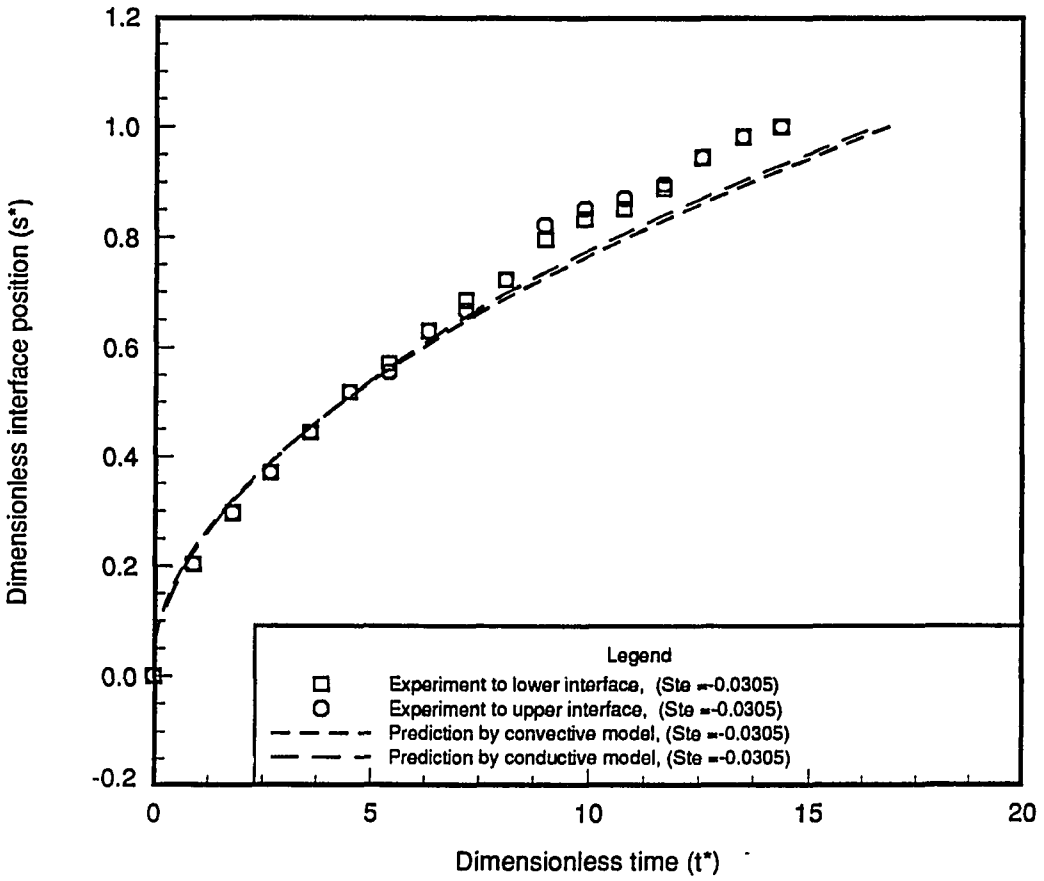

Figure 6: Comparison of measured and predicted interface position during freezing

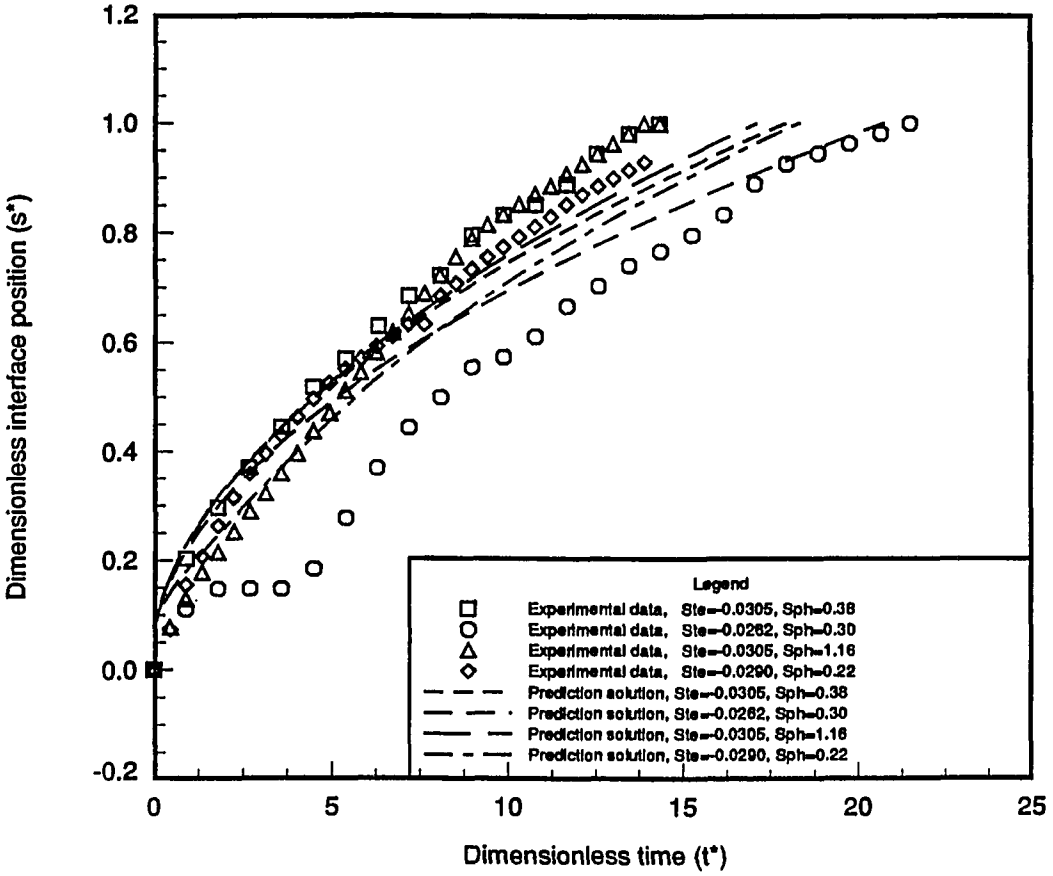

Figure 7: Comparison of measured and predicted interface position during freezing for different wall temperatures

boundary temperatures then compared with the analytical results. Fig. 7 shows the variation of the interface position with respect to time both as measured from the experiments and as predicted by the model which considers the effect of the natural convection. The predicted solution has quite good agreement with the experimental data.

The history of interface position in the melting heated from above and below is illustrated in Fig. 8. It is found that the lower interface increased faster than the upper one during the later period of the test. The difference is due to higher convection heat transfer on the lower interface than that on the upper. But the overall difference between the two interface is within 15%. This allows to treat the both the upside and downside as approximately symmetric to the center line.

The comparison of the experimental data with the predicted solutions from the convection model and the pure conduction model in melting is presented in Fig. 9. It is obvious that the solution by the model that considers the natural convection heat transfer is much close to the experimental data than the solution that considers the pure conductive heat transfer. In addition, the temperature in the solid region reached T_f quickly. These results indicate that natural convection effect is more important in the melting process.

The variation of the interface position with time during the melting processes at different wall temperatures is illustrated in Fig. 10. These variations indicate that the ice-water interface almost linearly increases with time. The results from the prediction method matched the data measured in the experiments quite well.

Fig. 11 and Fig. 12 show the variation with time of temperature at the horizontal center line for freezing and melting respectively. During freezing, the temperature

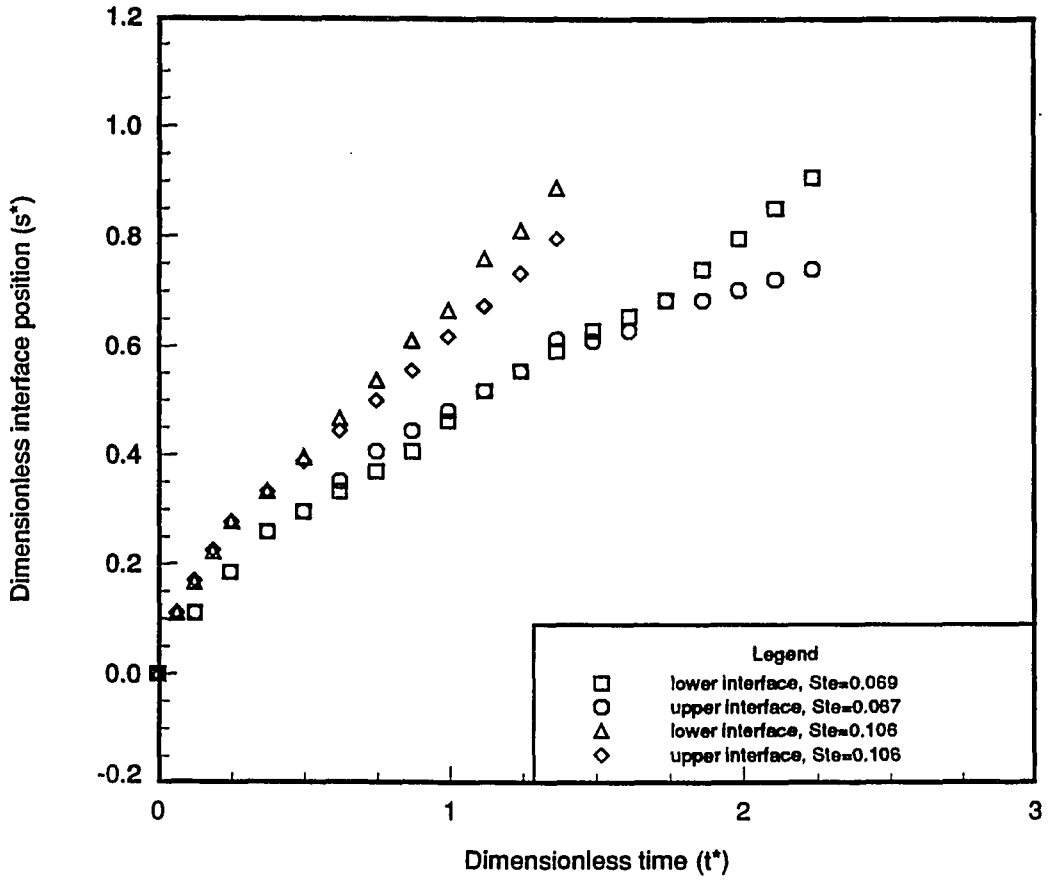

Figure 8: Variation of solid-liquid interface position with time during melting from above and below

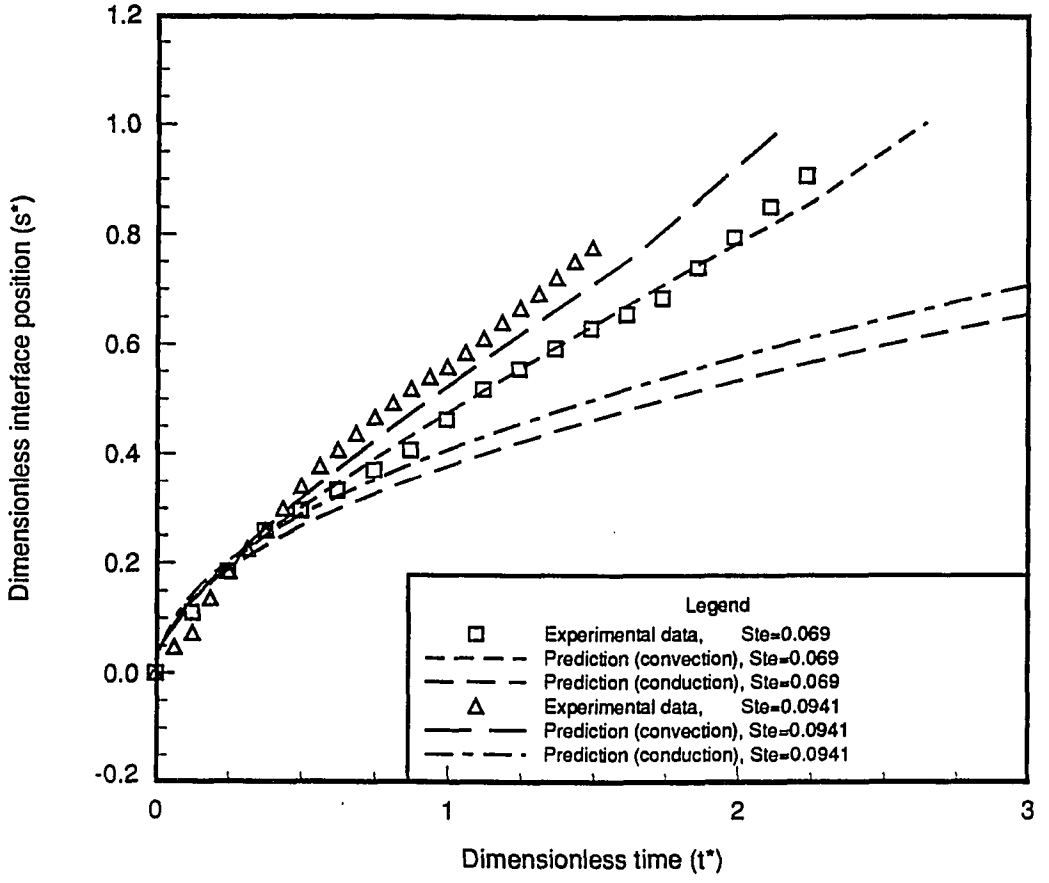

Figure 9: Comparison of measured and predicted interface position during melting from above and below

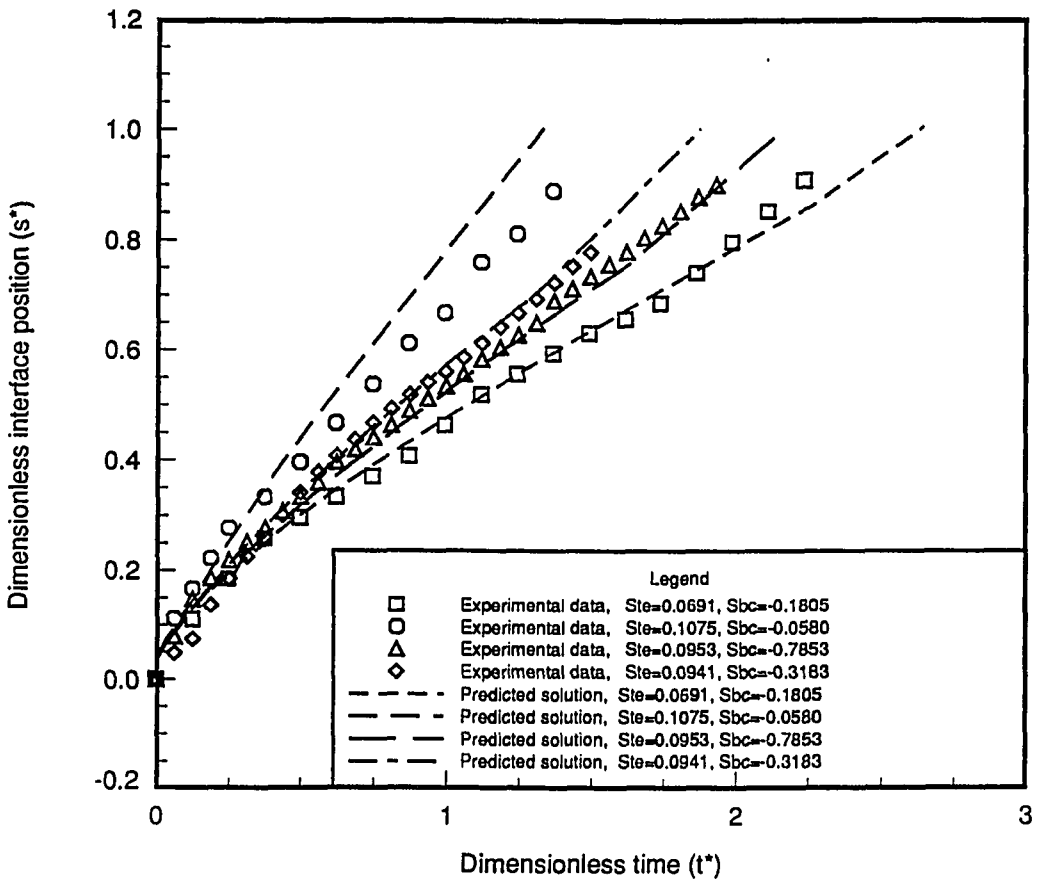

Figure 10: Comparison of measured and predicted interface position during melting for different wall temperatures

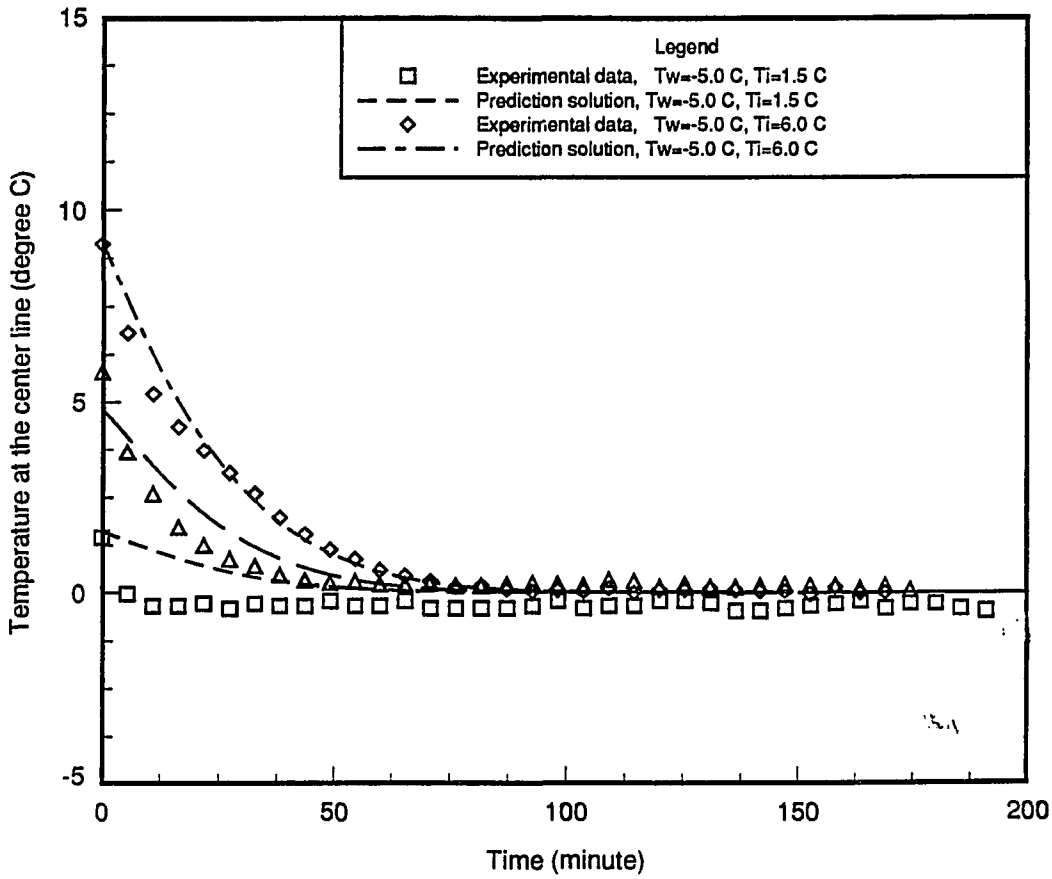

Figure 11: Variation of temperature at horizontal center line with time during freezing

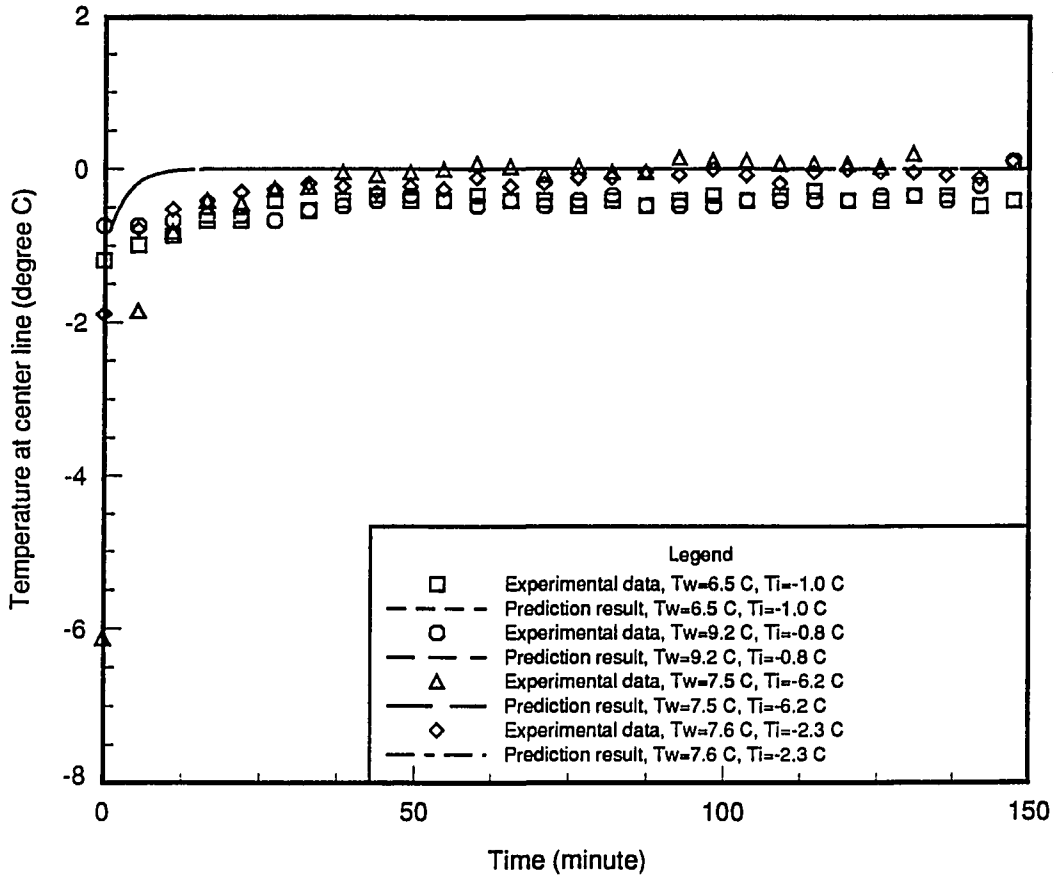

Figure 12: Variation of temperature at horizontal center line with time during melting

at the symmetric line quickly reached a stable level, which is close to the fusion temperature from a super-heating level. Otherwise, the temperature at the symmetric line reached the fusion temperature from a subcooling level in a melting process. It can be seen that the temperature in the liquid phase decreased more slowly during freezing than the temperature in the solid phase increased during melting. This is because the thermal diffusivity of the water is less than that of the ice. The discrepancy between the predicted and experimental may come from two reasons: first, the assumptions of temperature profiles used in the analysis may not be accurate enough; second, measurement errors during the experiments may have occurred.

CONCLUSION

The experiments with ice formation and melting in a horizontal rectangular enclosure were performed under different conditions. The analytically predicted solutions based on the close integral method were developed to determine the interface position and the temperature change in the phase-change materials for both freezing and melting. The results obtained by the analytical method have acceptable agreement with the experimental data.

From the observations and experimental results, it is reasonable to treat the present model as symmetric to the horizontal center line of the test cell in the case where the test cell is heated or cooled from above and below. This allows us to consider only half of region in the analysis.

It was found that the natural convection heat transfer occurred only in the early stage. In the later stage, the conductive heat transfer controlled the freezing process. But the natural convection heat transfer played a more important role in the overall melting process. The sensible heat was only a minor part in the phase-change process.

REFERENCES

Boger, D. and Westwater, J., "Effect of Buoyancy on The Melting and freezing Process," *Journal of Heat Transfer*, Vol. 89, 1967, pp. 81-89

Cho, S. and Sunderland, J., "Heat Conduction Problems with Melting or Freezing," *Journal of Heat Transfer*, Vol. 91, 1969, pp. 421-426

Chu, T. and Goldstein, R., "Turbulent convection in a Horizontal layer of water," *Journal of Fluid Mechanics*, Vol. 60, 1973, pp. 141-159

Dlobe, S. and Dropkin, D., "Natural Convection Heat Transfer in Liquids Confined Between Two Horizontal plates," *Journal of Heat Transfer*, Vol. 81c,1959, pp. 24-30

Frederick, D. and Greif, R., "A Method for the Solution of Heat Transfer Problems with a Change of Phase," *Journal of Heat Transfer*, Vol. 107, 1985, pp. 520-526

Garg, M., Mullick, S. and Bhargane, A., "Latent Heat or Phase-Change Thermal Energy Storage," *Solar Thermal Energy Storage*, Hingham, Mass., D. Reidael Publishing Company, 1985

Goodman, T., "Application of Integral Methods to Transient Nonlinear Heat Transfer," *Advanced Heat Transfer 1*, 1964, pp. 71

Hale, N. and Viskanta, R., "Solid-Liquid Phase-Change Heat Transfer and Interface Motion in Materials Cooled or heated from Above or Below," *International Journal of Heat and Mass Transfer*, Vol. 23, 1979, pp. 283-292

Heitz, W. and Westwater, J., "Extension of The numerical Method for Melting and Freezing Problems," *Journal of Heat Transfer*,Vol. 93, 1970, pp. 1371-1375

Incropera, F. and De Witt, D., *Introduction to Heat Transfer*, New York, John Wiley & Sons, 1990

Menning, J. and Őzisik, M., "Coupled Integral Equation Approach for Solving Melting or Solidification," *International Journal of Heat and Mass Transfer*, Vol. 28, 1984, pp. 1481-1485

O'Tool, J and Silveston, P., "Correlations of Convective Heat transfer confined in Horizontal Layers," *HEAT TRANSFER - BUFFALO, AICHE Chemical Progress Symposium series*, Vol. 32, 1960, pp. 81-86

Őzisik, M., *Heat Conduction*, New York, John Wiley & Sons, 1980

Seki, N., Fukusako, S. and Sugawara, M., "A Criterion of Onset of Free convection in a Horizontal Melted Water Layer with Free Surface," *Journal of Heat Transfer*, Vol. 99, 1977, pp. 92-98

Yen, Y., "Onset of Convection in a Layer of Water Formed by Melting Ice from Below," *The Physics of Fluids*, Vol. 11, 1968, pp. 1263-1270

Yong, L. and Maxwell, G. M., "An Experimental Investigation of Melting of Ice in a Horizontal Rectangular Enclosure Heated from Below," to be submitted, 1993

PAPER III.

MELTING OF UNFIXED ICE IN A HORIZONTAL RECTANGULAR ENCLOSURE

ABSTRACT

This paper presents the results of an investigation of the melting process that occurs in an encapsulated ice thermal energy storage system. Melting of an unfixed ice slab in a horizontal rectangular enclosure isothermally heated from above and from below is studied experimentally. As a result of buoyancy force, the ice floats to the top of the enclosure during the melting process. This creates a close-contact melting on the upper surface of the the ice slab. Heat transfer in this region is dominated by conduction while melting on the lower surface of the ice slab is dominated by natural convection. The ice-water interface positions at different wall temperatures are recorded and illustrated, and an analytical method is developed to predict the thickness of the fluid film between the top wall of the container and the upper surface of the ice slab, melting rates, and water-ice interface positions. This method demonstrates good agreement with the experimental results.

NOMENCLATURE

c_p, specific heat;

h, heat transfer coefficient;

h_f, latent heat of fusion;

H, height or thickness;

k, thermal conductivity;

L, half width of ice slab;

Nu, Nusselt number, hs_d/k_l;

Pr, Prandtl number, $\mu_l c_{p_l}/k_l$;

Ra, Rayleigh number, $g_l\beta(T_w - T_f)s_d^3/\nu\alpha$;

s, interface position to boundary;

Ste, Stefan number, $c_p(T_w - T_f)/h_f$;

t, time;

T, temperature;

v, flow velocity or melting rate;

V, volume of ice slab;

y, coordinate.

Greek Symbols

α, thermal diffusivity, $k/\rho c$;

β, thermal expansion coefficient;

Θ_k, dimensionless temperature, $(T_k - T_f)/(T_w - T_f)$;

ν, kinematic viscosity;

μ, dynamic viscosity;

ρ, density;

τ, wall shear stress.

Superscripts

$*$, refers to dimensionless;

$'$, refers to previous step.

Subscripts

B, refers to buoyancy;

d, refers to the region below ice;

f, refers to fusion;

F, refers to friction;

i, refers to initial;

ice, refers to ice;

int, refers to interface;

k, refers to various symbols, f, or i, or l, or s, or t, or w;

l, refers to liquid;

s, refers to solid;

t, refers to thermal penetration layer;

u, refers to the region above ice;

w, refers to wall.

INTRODUCTION

In preceding papers, the solid region of the phase-change material was treated as a fixed body which was not allowed to move. If the solid phase is not maintained at a fixed position, it will move through the melted liquid phase due to the different density between the solid and liquid phases. In general, water is the exception since for many substances the solid phase is more dense than the liquid and the solid sinks. This phenomenon happens in many practical applications.

In recent years, study of the melting of an unfixed solid in a solid-liquid phase-change system has attracted more attention. Moor et al. (1982) experimentally investigated the melting of n-octadecane wax within a spherical enclosure, and developed a mathematical model for the interface position and the temperature profiles for various Stefan and Fourier numbers. Bareiss et al. (1984) developed an analytical solution of the heat transfer process during melting of an unfixed solid octadecane mass inside a horizontal tube. Their analysis was based on a force balance between pressure in the thin liquid layer close to the lower tube wall and the gravitational force on the solid phase. Predictions of melting rates and heat transfer coefficients were in good agreement with the experiments. Moallemi et al. (1986) investigated close-contact melting of blocks of solid n-octadecane heated by a horizontal planar heat source. The reducing rate of the solid volume was measured and was reported as

a function of the instantaneous weight of the solid block. A closed-form approximate solution was developed for the motion of the solid, and predictions compared well with the experimental data. Webb et al. (1987) experimentally studied melting of unfixed ice in a horizontal cylinder. The cylinder was heated isothermally and the ice floated up close to the upper wall of the cylinder. The flow structure of the molten liquid region and the morphology of solid-liquid interface were discussed. Similar work also was done by Rivier and Beer (1987). Their investigation showed the influence of the density inversion of the water on the flow regions in the melted zone, and consequently on the shape of the lower ice-water interface. An analytical solution was obtained which was in good agreement with the experiments. Bejan and Tyvand investigated the pressure melting of ice under a body with a flat base (1992). This was related to the contact melting process that occurs when a temperature difference is maintained between the solid body (heat source) and the phase-change material. The differences between the pressure melting of ice and the normal phase-change material were discussed.

In the present work, ice within a horizontal rectangular enclosure is isothermally heated from above and below. This melting process is investigated experimentally and analytically. During the tests, the ice-water interface position and the temperature of the heat transfer walls were recorded and illustrated. An approximately analytical prediction was developed and compared to experimental measurements. The thickness of the thin liquid layer between the top heating wall and the upper interface of the ice slab was determined based on a force balance of buoyancy on the ice slab and the total pressure that exists in the thin liquid layer. Melting occurred on the upper surface of the ice by conduction dominated heat transfer through

the thin water layer. Melting on the lower interface of the ice slab was determined based on the natural convection caused by the temperature difference between the bottom heat source and the ice surface. The mathematical model was developed by an approximate integral method and was solved numerically.

EXPERIMENT

The experimental apparatus and test enclosure are the same as those described in Paper I. But the thickness of the test cell is 27 mm.

Small holes were drilled at certain positions on the aluminum plates which are used as heat transfer wall of the test enclosure. Twelve copper-constantan thermocouples were fixed by thermocouple cement at different positions of outside surface of the aluminum plates. The reason to arrange the thermocouples on the outside of the enclosure is to avoid restricting the free moving of the ice inside the enclosure. The thermal resistance of the aluminum plate can be neglected since the high thermal conductivity of this material. Four thermocouples were located at the inlet and the outlet of the heat exchangers, and two thermocouples were inserted in the constant temperature bath. The temperature readings were recorded and presented by an IEEE-488 inter-bus computer data acquisition system. The thermocouple arrangement is shown in Fig. 1.

The test cell was fully filled with pure distilled water, and the cell wall was vibrated in order to remove air bubbles from the water through the overflow tubes. The test cell was then placed on a supporting frame horizontally.

The ethylene glycol-water solution was circulated through the chiller (or the heater), and the thermal reservoir to reach a desired steady temperature during the

beginning of the experimental processes. The temperature of the ethylene glycol-water solution could be controlled within $0.2°C$ by adjusting the flow rate through the heater and chiller. The solution was then circulated in the loop which includes the test cell and the bath. The flow rate of the solution passing through the heat exchangers was kept high enough to minimize the temperature difference between the inlet and the outlet of the heat exchangers.

After the test cell was fully occupied by ice through a freezing process, the valves, which are installed between the heat exchangers and the thermal reservoir, were closed. The ethylene glycol-water solution was heated to a required steady temperature by the electric in-line heater. Meantime, the temperature of the ice became more uniform. This period usually take twenty to thirty minutes, depending on the temperature levels required. Then the heated glycol-water solution was circulated through the loop which includes the thermal reservoir and the test cell to make the test cell reached a desired temperature. The test cell was maintained at that temperature until the whole ice had melted. During the experiments, visual observations or photographs were taken at regular intervals. These actions had to be done as quickly as possible to minimize heat loss from the test cell. The test cell could be cooled or heated from above, from below, or from both sides separately. The data gathered for different situations could be used to compare with the solutions of different analytical models.

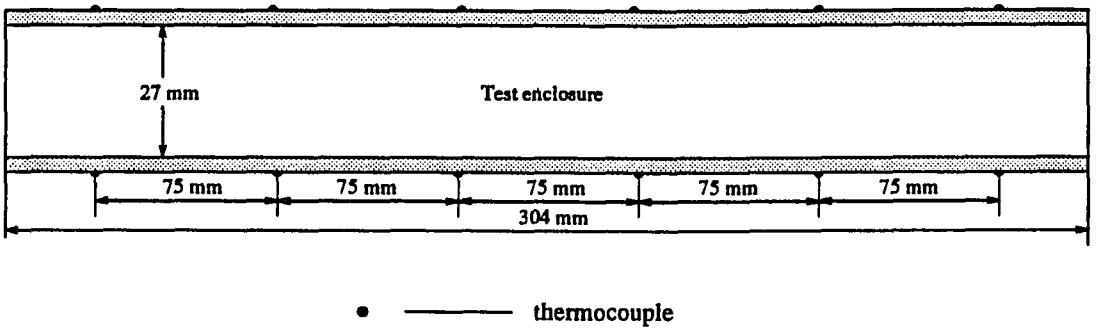

Figure 1: Arrangement of thermocouples on the outside surface of the test cell

ANALYSIS

Fig. 2 shows the geometry used to describe the problem. The rectangular enclosure is originally filled with ice at a uniform initial temperature, T_i, which might be equal to or below the melting temperature, T_f. When the wall temperature suddenly reaches a temperature T_w, which is above the fusion temperature, the melting process begins. The wall temperature is maintained constant. Heat transfer occurs in the liquid region due to the temperature difference between the wall temperature and melting temperature, also occurs in the solid region due to the temperature difference between the melting temperature and solid temperature. The solid and liquid temperatures meet at the interfaces with the fusion point, T_f. The ice slab moves up because of the density difference between the water and the ice. The volume of the ice slab is reduced and the distance of the solid-liquid interface from the bottom increases as time increases. The melting process is modeled based on the following assumptions:

- Heat transfer takes place on the top of the ice slab by one-dimensional conduction crossing the thin water film. Heat transfer takes place on the bottom by natural convection. The forced convection caused by the slow liquid flow is neglected.

- No heat transfer occurs between the sidewalls and the ice.

- The solid-liquid interfaces are sufficiently straight and horizontal.
- The thin liquid layer between the top heated wall and the ice has uniform thickness.
- The horizontal symmetric line of the ice slab is treated as adiabatic.
- The temperature profile in the thin liquid film between the above heated wall and the ice slab is considered to be linear because the thickness of the film is very small.
- The ice is free to float in the enclosure.
- The pressure in the thin liquid layer is assumed constant in the vertical direction because of the small thickness of the liquid layer, and the pressure at the edge of the thin water film is assumed to be equal to the atmospheric pressure, p_o.

In the present work, the melting processes on the upper and lower surfaces of the ice are considered separately. The dimensionless governing equations are given below:

The energy balance equation for the upper solid-liquid interface is given by

$$\frac{ds_u^*}{dt_l^*} = \frac{\rho_l}{\rho_s} Ste\left(\frac{k_s}{k_l}\frac{\partial \Theta_s}{\partial y_u^*} - \frac{\partial \Theta_l}{\partial y_u^*}\right) \quad at \;\; y_u^* = s_u^*, \tag{1}$$

while the energy balance equation on the lower solid-liquid interface is

$$\frac{ds_d^*}{dt^*} = \frac{\rho_l}{\rho_s} Ste\left(\frac{k_s}{k_l}\frac{\partial \Theta_s}{\partial y_d^*} + \frac{Nu}{s_d^*}\right) \quad at \;\; y_d^* = s_d^*. \tag{2}$$

The Nusselt number, Nu, based on previous work (Yong and Maxwell, 1993) for natural convection of a phase-change process in an enclosure confined between two

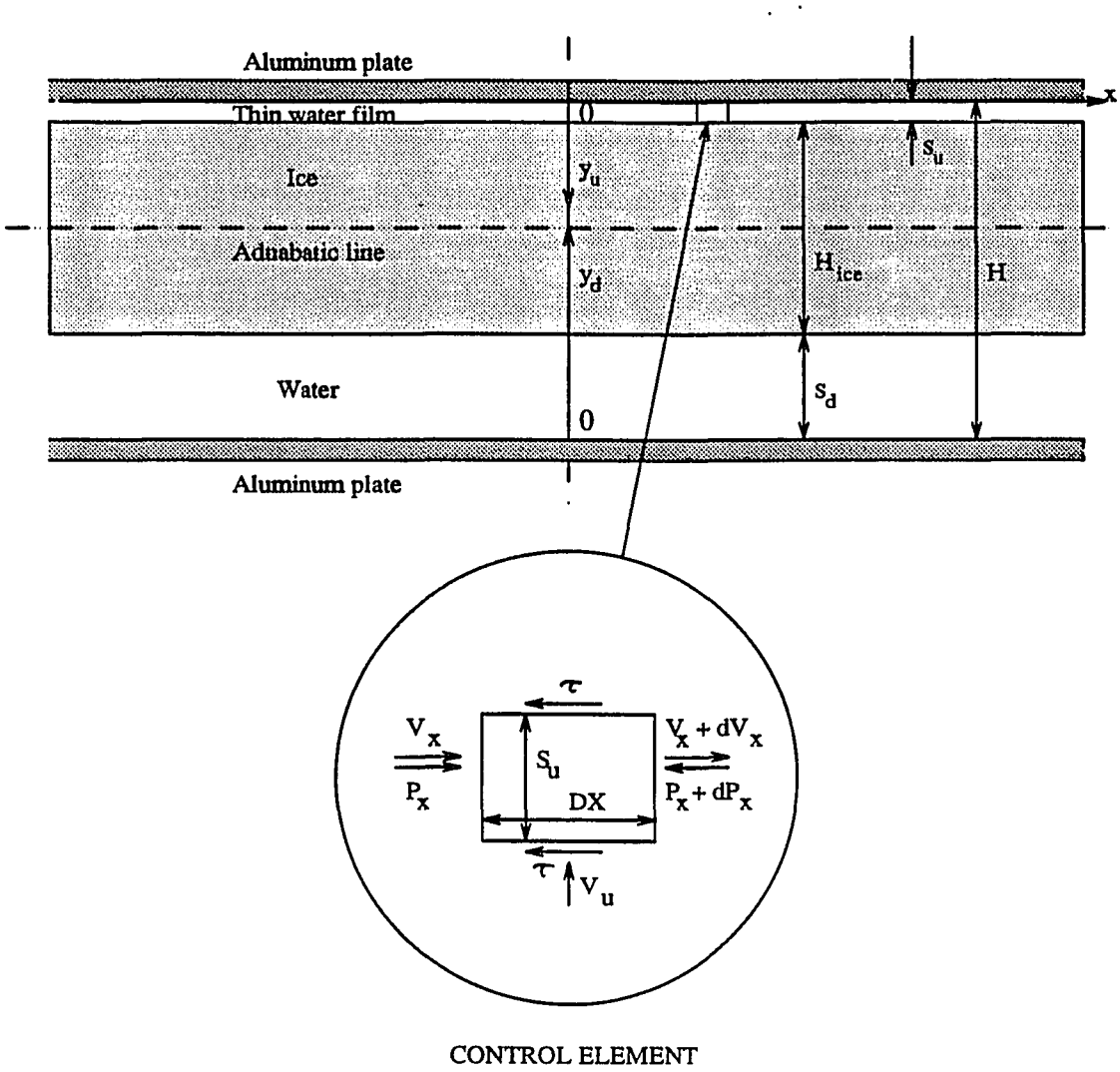

CONTROL ELEMENT

Figure 2: Schematic representation of geometric model

horizontal parallel plates is given by

$$Nu = 0.165 Ra^{0.268}, \qquad 1,700 \leq Ra \leq 10,0000$$
$$Nu = 0.072 Ra^{0.325} Pr^{0.084}, \qquad 100000 < Ra \leq 10,000,000 \tag{3}$$

Since the temperature distribution in the solid region is assumed to be symmetric about the horizontal center line, only the energy equation in the lower half region is considered in the analysis:

$$\frac{\partial \Theta_s}{\partial t^*} = \frac{\alpha_s}{\alpha_l} \frac{\partial^2 \Theta_s}{\partial y_d^{*2}}, \qquad at \;\; s_d^* \leq y_d^* \leq s_d^* + \frac{H_{ice}^*}{2}, \tag{4}$$

where the dimensionless variables are defined as

$$\Theta_k = \frac{T_k - T_f}{T_w - T_f} \qquad k = i, \; or \; l, \; or \; s, \; or \; t, \; or \; w,$$
$$y^* = \frac{y}{H}; \quad s^* = \frac{s}{H}; \quad H_{ice}^* = \frac{H_{ice}}{H}; \quad s_u^* = \frac{s_u}{H};$$
$$t^* = \frac{\alpha_l t}{H^2}.$$

A linear temperature distribution is assumed for the thin liquid layer, and is given by

$$\Theta_{lu} = \Theta_w (1 - \frac{y_u^*}{s_u^*}). \tag{5}$$

For the half solid region, a quadratic temperature distribution is assumed as

$$\Theta_s = \Theta_t [1 - (\frac{H_t^* - y^*}{H_t^* - s_d^*})^2], \tag{6}$$

where H_t^* is defined as the dimensionless thickness of the thermal layer.

The initial condition is

$$\Theta_l = \Theta_i, \quad for \;\; t^* \leq 0. \tag{7}$$

The boundary conditions are

$$\Theta_l = \Theta_w = 1, \quad at \;\; y_u^* = 0 \;\; and \;\; y_d^* = 0, \;\; for \;\; t^* > 0, \tag{8}$$

$$\Theta_s = 0, \quad at \;\; y_d^* = s_d^* \;\; and \;\; y_u^* = s_u^*, \;\; t^* > 0, \tag{9}$$

$$\Theta_s = \Theta_t, \quad at \;\; y_d^* = H_t^* \;\; t^* > 0. \tag{10}$$

Integrate Eq. (4) with respect to to y_d^* from s_d^* to H_t^* to yield

$$\int_{s_d^*}^{H_t^*} \frac{\partial \Theta_s}{\partial t_s^*} dy_d^* = \int_{s_d^*}^{H_t^*} \frac{\partial^2 \Theta_s}{\partial y_d^{*2}} dy_d^*, \tag{11}$$

or

$$\frac{d}{dt_s^*} \int_{s_d^*}^{H_t^*} \Theta_s dy_d^* - \left(\Theta_s \mid_{H_d^*} \frac{ds_d^*}{dt_s^*} - \Theta \mid_{s_t^*} \frac{dH_t^*}{dt_s^*} \right) = \frac{\alpha_s}{\alpha_l} \left(\frac{\partial \Theta_s}{\partial y_d^*} \mid_{H_t^*} - \frac{\partial \Theta_s}{\partial y_d^*} \mid_{s_d^*} \right). \tag{12}$$

Substitute the boundary conditions into the above equation and rearrange it to obtain

$$\frac{2}{3}(H_t^* - s_d^*) \frac{\partial \Theta_t}{\partial t^*} + \frac{\Theta_t}{3} \frac{\partial s_d^*}{\partial t^*} + \frac{2\alpha_s \Theta_t}{\alpha_l (H_t^* - s_d^*)} = 0, \tag{13}$$

where H_t^* might be replaced by H_c^*, the centerline of the ice slab for the thin container. This assumption also satisfies the boundary conditions. H_c^* can be expressed as

$$H_c^* = 0.5(1 - s_d^* - s_u^*). \tag{14}$$

Using v_d^* and v_u^* instead of ds_d^*/dt_L^* and ds_u^*/dt^* respectively, and substituting the boundary conditions into equation (1) and equation (3) results in

$$v_d^* = Ste \frac{\rho_l}{\rho_s} \left(\frac{Nu}{s_d^*} - 2 \frac{k_s}{k_l} \frac{\Theta_t}{H_t^*} \right), \tag{15}$$

$$v_u^* = Ste \frac{\rho_l}{\rho_s} \left(\frac{1}{s_u^*} - 2 \frac{k_s}{k_l} \frac{\Theta_t}{H_t^*} \right). \tag{16}$$

s_u^* is an unknown variable. It can be determined by the balance of the pressure existing in the thin liquid layer between the top heated wall and the upper ice surface and the buoyancy on the ice.

Considering a control element in the thin liquid layer, as shown in the Fig. 3, the related equations are given as follows:

The continuity equation is as

$$\rho_l(v_x^* + \triangle v_x^*)s_u^* = \rho_l(v_x^* s_u^* + v_u^* \triangle x^*), \tag{17}$$

or

$$\triangle v_x^* = v_u^* \triangle x^* / s_u^*. \tag{18}$$

Since at $x^* = 0$, $v_x^* = 0$, there is

$$v_x^* = \frac{v_u^* x^*}{s_u^*}, \qquad for \;\; 0 < x^* < L^*. \tag{19}$$

The momentum equation is

$$\rho_l[(v_x^* + \triangle v_x^*)^2 - v_x^{*2}]s_u^* = [p_x^* - (p_x^* + \triangle p_x^*)]s_u^* - 2\tau^* \triangle x^*, \tag{20}$$

or

$$\triangle p_x^* = -2(v_x^* \triangle v_x^* + \frac{\tau^* \triangle x^*}{s_u^*}), \tag{21}$$

where

$$\tau^* = f\frac{v_x^{*2}}{2}, \tag{22}$$

and where, dimensionless terms are defined as

$$x^* = \frac{x}{H}; \quad \Delta x^* = \frac{\Delta x^*}{H}; \quad L^* = \frac{L}{H}; \quad v_x^* = \frac{v_x H}{\alpha_l};$$

$$p^* = \frac{H_i^2}{\rho_l \alpha_l^2} p; \quad \tau^* = \frac{H_i^2}{\rho_l \alpha_l^2} \tau.$$

For laminar incompressible flow in a channel formed by two parallel plates, f is given as

$$f = \frac{96}{Re}, \tag{23}$$

where Re is defined as

$$Re = \frac{2v_x s_u}{\nu} = \frac{2\alpha_l s_u^* v_x^*}{\nu}. \tag{24}$$

Thus the dimensionless wall shear stress can be written as

$$\tau^* = \frac{24\nu v_u^* x^*}{\alpha_l s_u^{*2}}. \tag{25}$$

Combining Eq. (18), Eq. (19), and Eq. (25) with Eq. (21) yields

$$\triangle p_x^* = -2\left(v_u^{*2} + 24\frac{\nu v_u^*}{\alpha_l s_u^*}\right)\frac{x^*}{s_u^{*2}}\triangle x^* \tag{26}$$

or

$$dp_x^* = -2\left(v_u^{*2} + 24\frac{\nu v_u^*}{\alpha_l s_u^*}\right)\frac{x^*}{s_u^{*2}}dx^*. \tag{27}$$

Eq. (27) can be integrated from $x^* = 0$ to x^* to obtain the local pressure on the upper surface of the ice slab. Integrating Eq. (27) yields

$$p_x^* = -(v_u^{*2} + 24\frac{\nu v_u^*}{\alpha_l s_u^*})\frac{x^{*2}}{s_u^{*2}} + C. \tag{28}$$

Eq. (28) can be integrated from $x^* = 0$ to L^*, then applying the conditions at $x^* = L^*$, $p_x^* = 0$, so C is obtained, and the total pressure on the cross-sectional area of the liquid layer is given by

$$P^* = \frac{2}{3s_u^{*2}}\left(v_u^{*2} + \frac{24\nu}{\alpha_l s_u}v_u^*\right)L^{*3}. \tag{29}$$

The dimensionless buoyancy force acting on the ice is

$$F_B^* = \frac{H_i \rho_l g V_{ice}}{{\alpha_l}^2}(\rho_l - \rho_s) = \frac{g H_i^4 (\rho_l - \rho_s)}{{\alpha_l}^2 \rho_l}(1 - s_u^* - s_d^*)L^*. \tag{30}$$

The force balance on the ice slab can be expressed as

$$P^* = F_B^*. \tag{31}$$

Substitution of Eq. (16), Eq. (29), and Eq. (30) into Eq. (31) results in

$$\frac{g H_i^4 (\rho_l - \rho_s)}{{\alpha_l}^2 \rho_l}(1 - s_u^* - s_d^*)L^* =$$
$$\frac{2}{3}\left\{\left[Ste\frac{\rho_l}{\rho_s}\left(\frac{1}{s_u^*} - 2\frac{k_s}{k_l}\frac{\Theta_t}{H_t^*}\right)\right]^2 + \frac{24\nu}{\alpha_l s_u^*}\left[Ste\frac{\rho_l}{\rho_s}\left(\frac{1}{s_u^*} - 2\frac{k_s}{k_l}\frac{\Theta_t}{H_t^*}\right)\right]\right\}\frac{L^{*3}}{{s_u^*}^2}. \tag{32}$$

The above transcendental equation can be solved numerically by the Newton-Raphson method to obtain the thickness of the thin water layer, s_u^*. The initial value of Θ_t is the same as the initial temperature of the ice, and the initial value of H_{ice}^* is the same as the height of the test cell H^*.

After obtaining s_u^*, Eq. (13), through Eq. (16) are solved simultaneously by applying the first order finite difference method to obtain v_d^*, v_u^*, s_d^*, and Θ_t. The value of s_d^* is determined by applying pure conduction method described in paper (Yong and Maxwell, 1991) for the beginning of the process. In order to gain accurate results, iterations are applied in each time step. The solution proceeds until the value of s_d reaches the height of the test cell.

RESULTS AND DISCUSSION

For the situation in which the test enclosure was heated from above and below, the ice melted from both the top and bottom at almost the same rate and the melting was controlled by heat conduction during the beginning of melting. After a few minutes, a very thin liquid film formed between the Plexiglas sidewalls and the ice due to heat transfer through the side walls. This allowed the ice to float near to the top heated surface. Newly melted water was squeezed out of the thin liquid layer between the top wall and the ice to the liquid pool below the ice. The thickness of the liquid layer was very small and difficult to measure. For the process in which the enclosure was heated only from below, the ice melted and a liquid pool formed only on the lower side. For the process in which the enclosure cell was heated only from above, the ice melted on the top at first. Very thin liquid films then formed on all sides of the ice due to heat transfer through the sidewalls. This also allowed the ice to separate from the walls of the enclosure and float up freely. Subsequently, a liquid pool formed on the lower side, and a thin liquid layer formed between the top heated wall and the upper side of the ice. The lower surface of the ice was found to be quite planar during the experiments. This supports the assumption of one dimensional heat transfer.

The ice-water interface positions to the bottom of the enclosure were measured

at regular time intervals during the melting experiments and compared with the solutions of analytical methods. Fig. 3 shows the variation of the dimensionless interface position versus dimensionless time for several wall temperatures when the enclosure was heated from below. The experimental results agreed well with the analytical solutions. The interface positions during the process of heating from above are presented in Fig. 4. The ice-water interface position increases with a nearly linear profile as time increases. Similar results also can be found in Fig. 5 which is about the melting process by heating from both the above and below. Here, the results of s_d^* from analytical prediction are always higher than the positions measured during the experiments. These results indicate that the actual melting rates are lower than the predicted results. The differences may be attributed to two reasons. One is that the thermal resistance of the aluminum plate was neglected, since the wall temperature used in the model is the same as that measured on the outside surface. Another is that some gas bubbles formed on the top of the container due to air leaks through the gasket and dissolved gases in the water during the melting. These bubbles occupied part of the heat transfer surface and played a role as thermal resistance.

The analytical solutions for melting rates on both sides of the ice are illustrated in Fig. 6. The melting rates increase as Ste (which refers to the wall temperature) increases. As the thickness of the thin water layer, which is required to maintain the balance of the ice, becomes higher as the volume of the ice decreases, the thermal resistance in the thin layer of water becomes larger. This results in that the melting rates on the upper surface of the ice decrease with time. The melting rate on the lower surface increases quickly at the beginning of the melting because of the heat conduction, then quickly decreases to an almost constant rate. The average melting

rate on the upper surface is 4-6 times higher than that on the lower surface of the ice. This means that the close-contact heat transfer on the upper surface plays a dominant role in the melting process of unfixed ice.

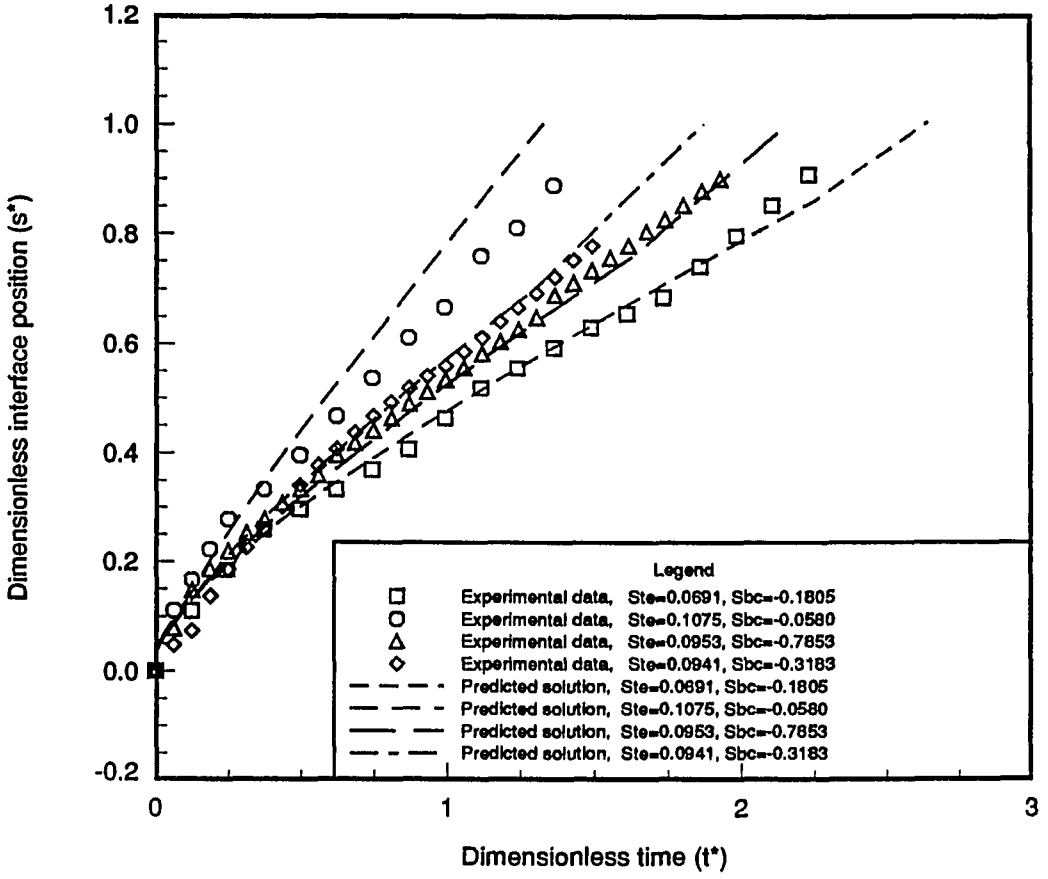

Figure 3: Comparison of measured and predicted ice-water interface positions during melting when heated only from below

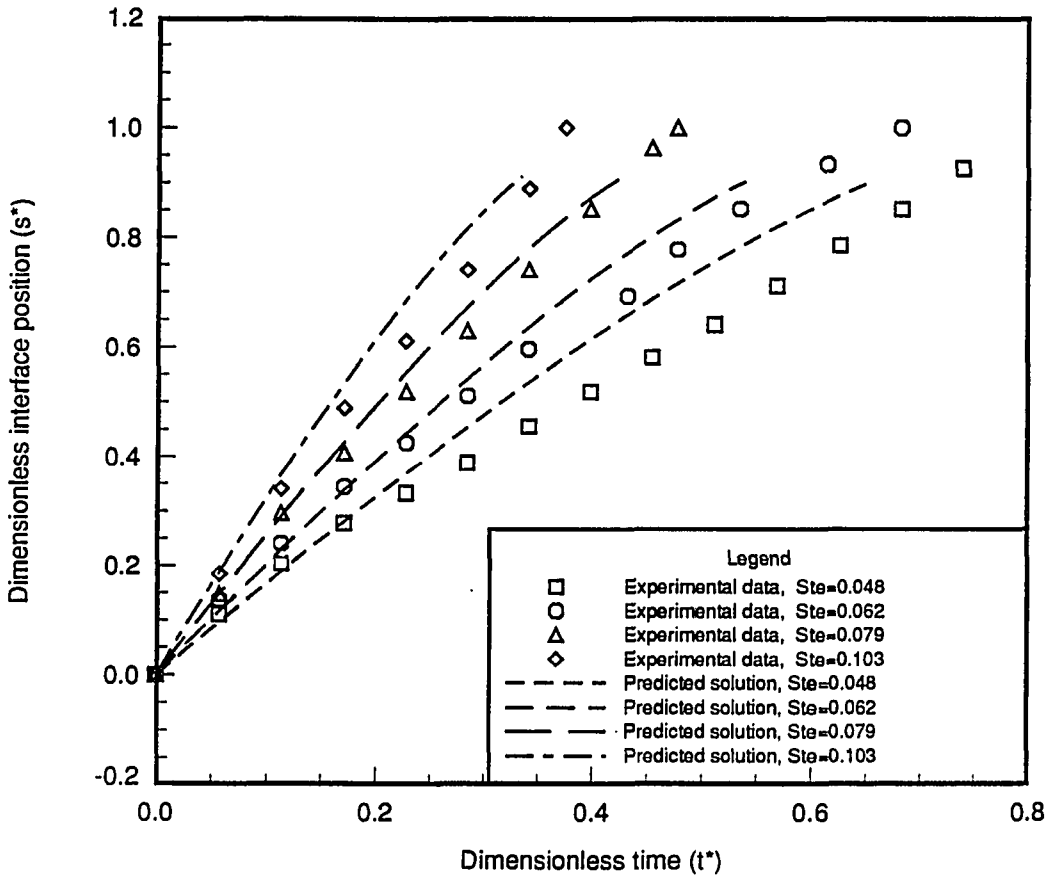

Figure 4: Comparison of measured and predicted ice-water interface positions during melting when heated only from above

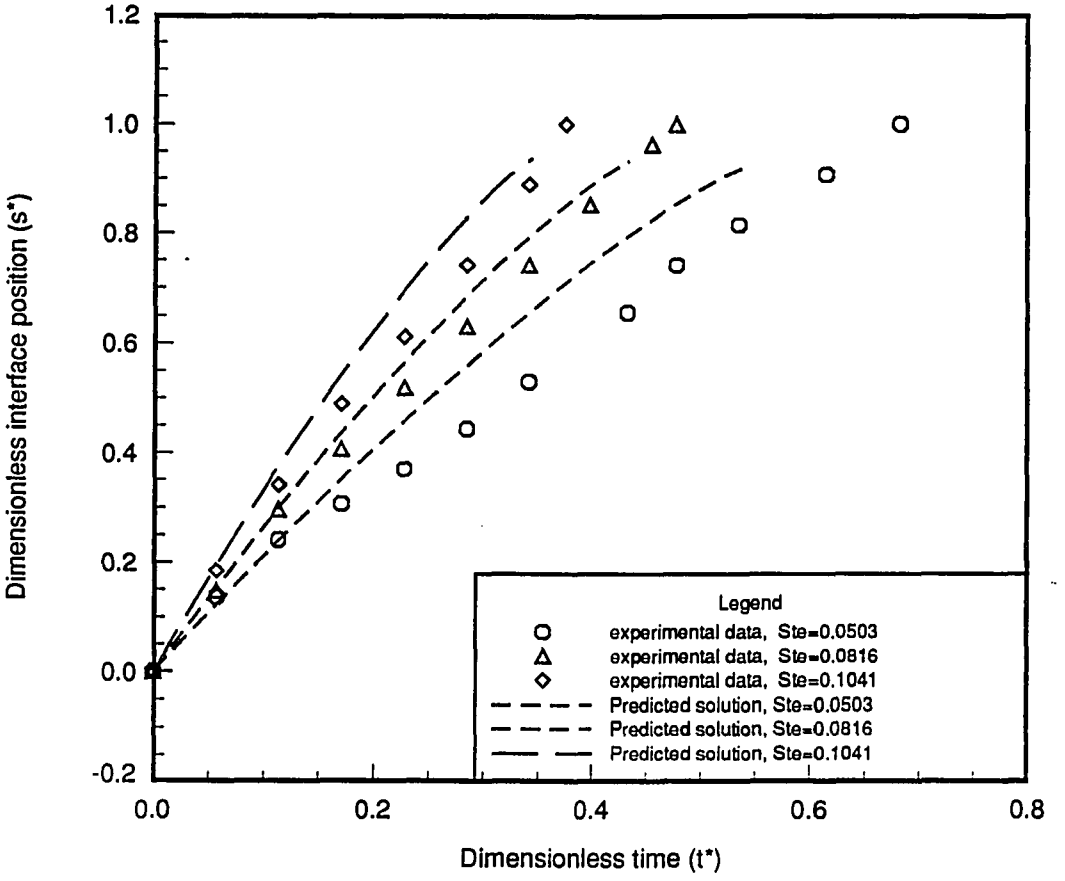

Figure 5: Comparison of measured and predicted ice-water interface positions during melting when heated from above and below

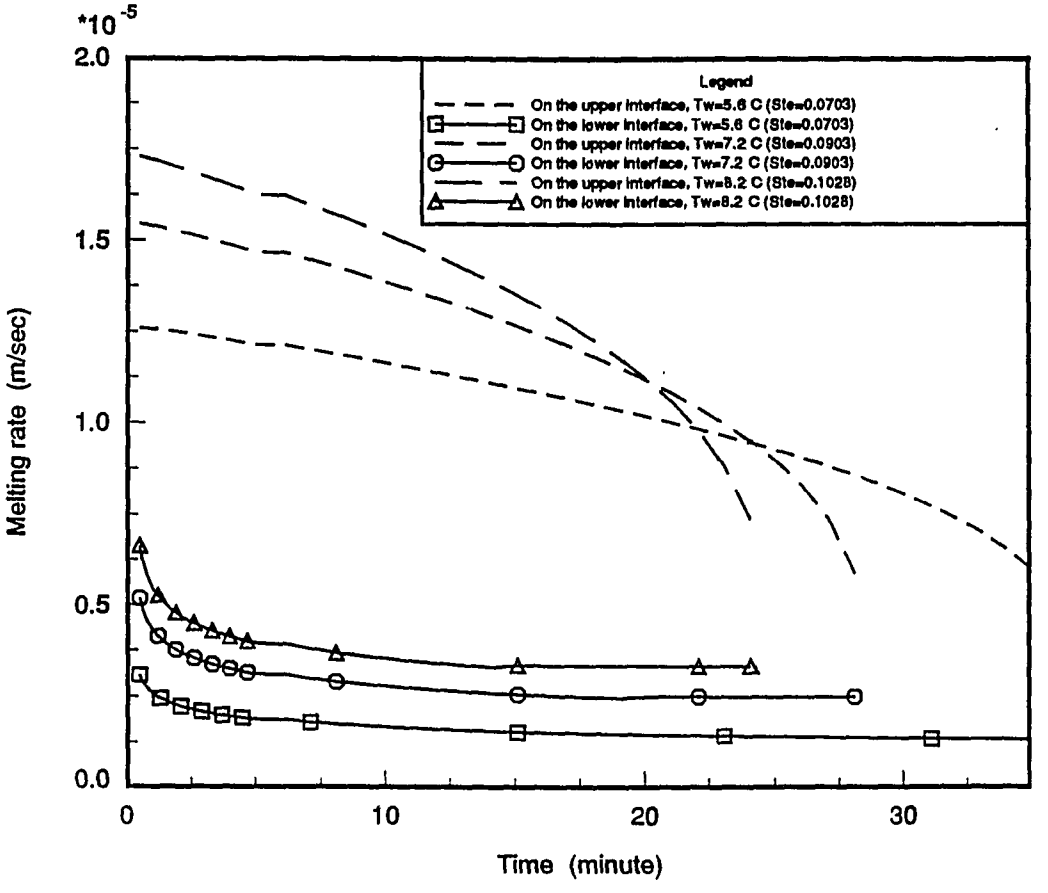

Figure 6: Comparison of melting rates on the upper ice-water interface and melting rates on the lower ice-water interface during melting when heated from above and below

CONCLUSION

Melting experiments with unfixed ice in a horizontal rectangular enclosure were performed under several different test conditions. Measurements were compared to predictions developed from approximate analytical models.

The heat transfer taking place on the upper interface was assumed to be based on pure conduction, and the heat transfer taking place on the lower interface was assumed to be primarily based on natural convection. The thickness of the thin water film above the ice was determined by a force balance on the ice slab. The interface position changed at a nearly constant rate over time. The experimental data were compared with the analytical solutions for the interface positions under different melting conditions.

The predicted solutions for the interface position were found to be 5% – 15% higher than the data measured in the experiments. These differences were due to the assumptions and negligences in the model. The thickness of the thin water layer above the ice was very small and remained nearly constant during the melting process. Thus the thermal resistance across the film was small.. The melting rates on the upper surface of the ice were 4 to 6 times higher than the melting rates on the lower surface. This means that the heat conduction which occurred in the thin liquid layer played a dominant role in the melting of the unfixed ice.

REFERENCES

Bareiss, M. and Beer, H., "An Analytical Solution of The Heat Transfer Process During Melting of An Unfixed Solid phase Change Material Inside a Horizontal Tube," *International Journal of Heat and Mass Transfer*, Vol. 27, No. 5, 1984, pp. 737-746

Bejan, A. and Tyvand, P. A., "The Pressure Melting of Ice Under a Body With Flat Base," ASME *Journal of Heat Transfer*, Vol. 114, 1992, pp. 529-531

Moallemi, M. K., Webb, B. W., and Viskanta, R., " An Experimental and Analytical Study of Close-Contact Melting," ASME *Journal of Heat Transfer*, Vol. 108, 1986, pp. 894-899

Moor, F. E. and Bayazitoglu, Y. "Melting Within a Spherical Enclosure," ASME *Journal of Heat Transfer*, Vol. 104, 1982, pp. 19-23

Riviere, Ph. and Beer, H., "Experimental Investigation of Melting of Unfixed Ice in an Isothermal Horizontal Cylinder," *International Communication of Heat and Mass Transfer*, Vol. 14, 1987, pp. 155-165

Viskanta, R., "Natural Convection Melting and Solidification," *Natural Convection: Fundamental and Applications* (edited by S. Kakac, W. Aung and R. Viskanta), Hemisphere, Washington, D. C.. 1985, pp. 845-877

Webb, B. W., Moallemi, M. K., and Viskanta, R., "Experimental on Melting of Unfixed Ice in a Horizontal Cylindrical Capsule," ASME *Journal of Heat Transfer*, Vol. 109, 1987, pp. 454-459

Yao, L. S. and Prusa, J., "Melting and Freezing," *Advance in Heat Transfer*, Vol. 19, 1989, pp. 1-83

Yong,L., and Maxwell, G. M., "An Experimental Investigation of Ice Melting in Horizontal Rectangular Enclosure," 1993, to be submitted

Yong, L. and Maxwell, G., "An Investigation of The Use of Encapsulated Ice for Thermal Energy Storage Systems," *Twenty-Eighth Annual Power Affiliate Report*, Iowa State University, ISU-ERI-Ames 9120, 1991, pp. 245-260

PAPER IV.

A MODEL OF THE MELTING PROCESS IN A THERMAL ENERGY STORAGE SYSTEM UTILIZING RECTANGULAR ICE CONTAINERS

ABSTRACT

The objective of this paper is to present a model for a thermal energy storage system which utilizes ice confined in rectangular containers. The emphasis is on the phase change process occurring in the containers. The mathematical formulation is based on one-dimensional heat transfer for a cartesian coordinate system. Effects of conduction and convection are included in the analysis, and the asymmetric case due to ice floating during the melting process is incorporated in the model. The effects on the performance of the storage system by different factors, such as inlet temperature of heat transfer fluid, initial temperature, and geometric parameters of the storage system, are evaluated and discussed. The results from this model provide a basis for the design of this type of thermal energy storage systems.

NOMENCLATURE

c_p, specific heat;

h, heat transfer coefficient;

h_f, latent heat of fusion;

H_i, inside thickness of the container;

H_{ice}, thickness of ice slab;

H_o, half thickness of the flow channel;

H_w, thickness of the container wall;

k, thermal conductivity;

Nu, Nusselt number, hs_d/k_l;

P, total pressure acting on the upper surface of ice;

Pr, Prandtl number, $\mu_l c_{p_l}/k_l$;

Ra, Rayleigh number, $g_l\beta(T_w - T_f)s_d^3/\nu\alpha$;

s, interface position to boundary wall;

Ste, Stefan number, $c_p(T_w - T_m)/h_f$;

t, time;

T, temperature;

V, velocity of heat transfer flow;

W, half width of the container;

y, coordinate in transverse direction;

z, coordinate in axial direction;

Z, length of the thermal energy storage system.

Greek Symbols

α, thermal diffusivity, $k/\rho c$;

β, thermal expansion coefficient;

Θ_k, dimensionless temperature, $(T_k - T_m)/(T_{fi} - T_m)$;

ν, kinematic viscosity;

μ, viscosity;

ρ, density.

Superscripts

$*$, refers to dimensionless;

n, refers to time step.

Subscripts

a,	refers to adiabatic line;
d,	refers to region below ice;
f,	refers to heat transfer fluid;
fi,	refers to inlet flow;
fo,	refers to outlet flow;
i,	refers to initial;
ice,	refers to ice;
j,	refers to node number;
k,	refers to various symbols, d, or f, or i, or l, or m, or s, or t, or u, or w;
l,	refers to liquid;
m,	refers to melting point;
s,	refers to solid;
t,	refers to thermal penetration layer;
u,	refers to upside;
w,	refers to wall;
$w1$,	refers to outside surface of the container wall;
$w2$,	refers to inside surface of the container wall.

INTRODUCTION

Some results of testing and evaluation of the overall performance of latent thermal energy storage systems with contained phase-change materials have been published in the literature.

Saitoh and Hiros (1984) presented a simple lumped model for latent thermal energy storage systems using spherically encapsulated phase-change material. They also presented experimental results for such a system. Saitoh and Morrison and Abdel-Khalik (1978) developed a theoretical model for studying the transient behavior of phase-change energy storage unit and studied the performance of solar heating systems using air and liquid as the working fluid. Humphries and Griggs (1977) have studied latent thermal energy storage system suitable for spacecraft thermal control. Their work also contains a comprehensive listing of thermodynamics properties for paraffin. Jurinak and Abdel-Khalik (1979) presented a simple empirical method for sizing phase-change energy storage units for air-based solar heating systems. Saxena, Subrahmiyam, and Sarkar (1982) developed a preliminary model to study phase change process within a shell and tube heat exchanger. Yimer (1982) analyzed the heat transfer inside PCM thermal energy systems with internal longitudinal fins. Prusa, Maxwell and Timmer (1988) developed a design criteria for thermal energy storage which consists of rectangular PCM containers and discussed the effects of key

parameters to discharging periods. Analysis to heat transfer was only based on heat conduction mechanisms. Additional works examining the dynamics of latent thermal energy storage systems may be found in (Asgarpoor et al. 1982; Meron et al. 1983; Yanadori et al. 1986; and Delaunay et al. 1986).

The goal of the current study is to develop a model for an ice thermal energy storage system which is used to shift peak-load for air conditioning systems. In the storage system considered, water is filled in flat rectangular containers and the heat transfer fluid flows horizontally in the channels between the containers. The emphasis is on the phase change process (melting) occurring in containers. The mathematical formulation is based on one-dimensional heat transfer for a cartesian coordinate system. Effects of conduction and convection are included in the analysis. The convection correlation used in the analysis was obtained from previous studies. An asymmetric case due to ice floating during the melting process is incorporated in the model. The position of ice in the container is determined by a force balance on the ice. The solutions are obtained numerically by a finite-difference method. The influences of different factors, such as, inlet temperature of heat transfer fluid, initial system temperature, and geometric parameters of the storage system, etc, on heat transfer rate and discharging time (or melting time), have been evaluated and discussed. The results from this model provide a basis to design this type of thermal energy storage systems.

ANALYSIS

Fig. 1 illustrates the thermal energy storage system simulated in the present work. The thermal storage system consists of rectangular containers in a big tank. Phase-change material (water) fills in the containers. The containers are arranged side by side and stacked horizontally. Heat transfer fluid flows through the channels which are between the containers. A detailed geometry of a container is illustrated in Fig. 2.

A mathematical model, which is capable of predicting heat transfer process for the thermal energy storage system, must be in response to different situations occurring in the system. Consequently, the whole process of the heat transfer for the melting in the system have been subdivided into three major processes according to the type of the heat transfer processes which are occurring.

1. Pre-Melting process includes three sub-cases:

- Case 1. Sensible heating of the container wall occurs. and the thermal layer extends in the region of the container wall.
- Case 2. Sensible heating of the ice occurs, and the thermal layer extends in the ice region.
- Case 3. Sensible heating of the ice also occurs. the thermal layer has reached

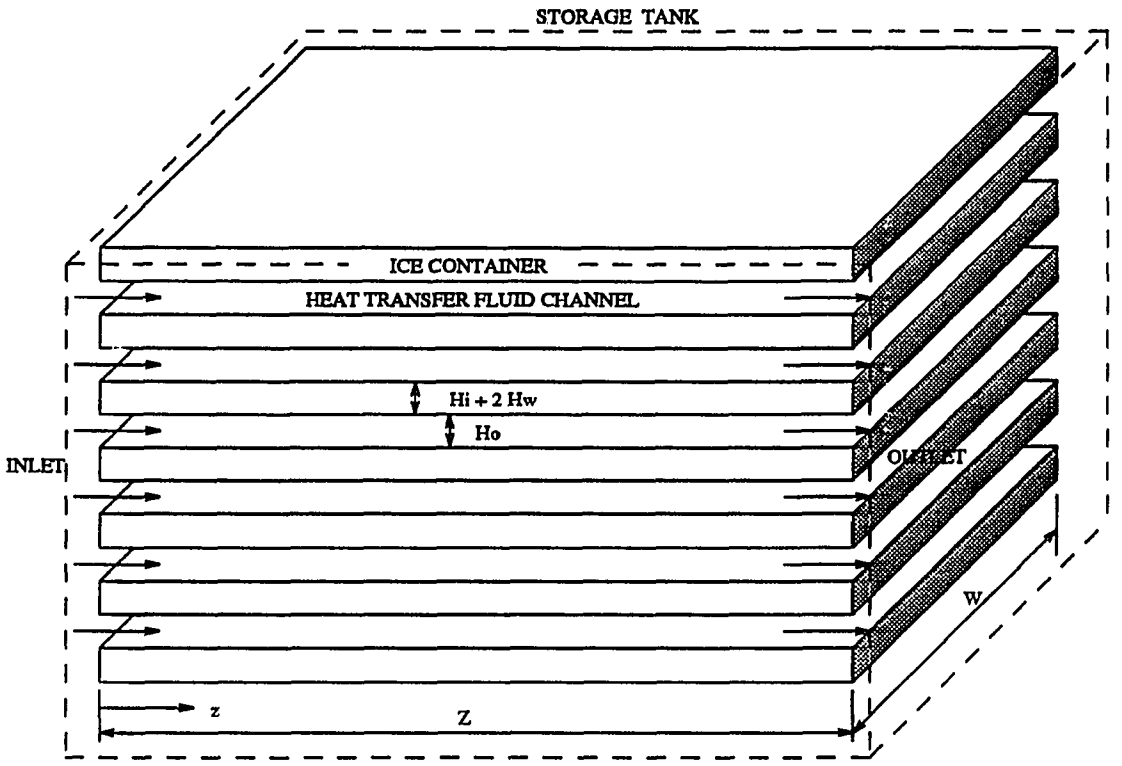

Figure 1: Schematic diagram of thermal storage system

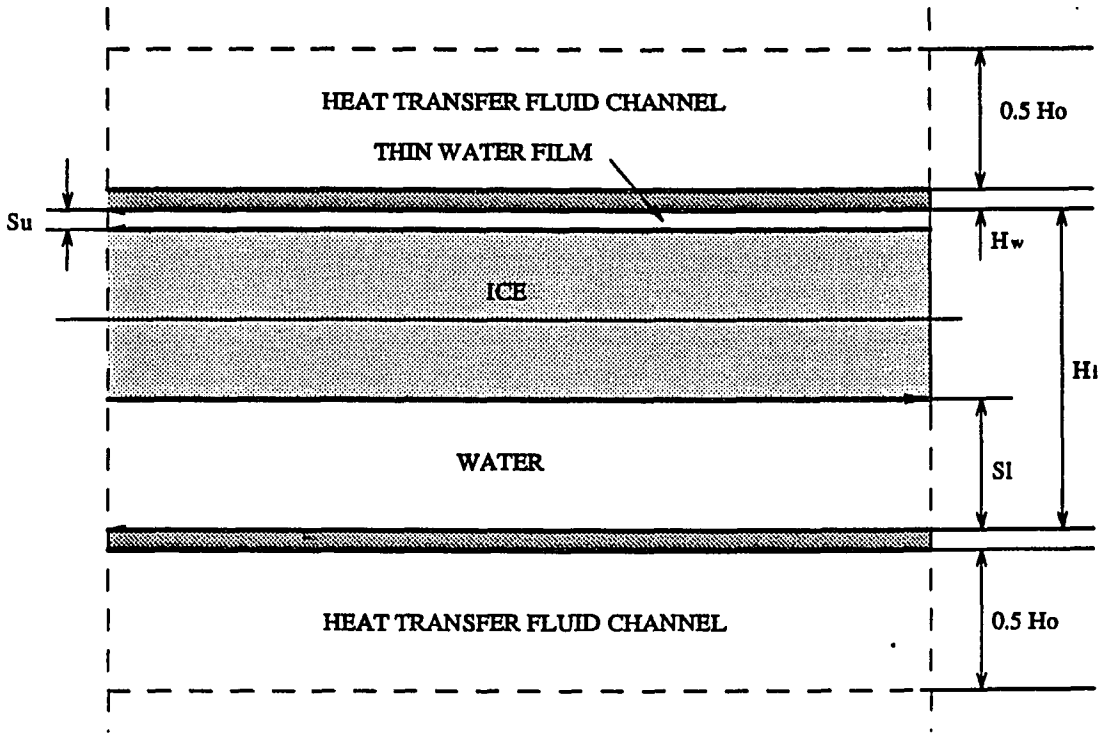

Figure 2: Rectangular container geometry detail

the horizontal symmetric line of the container. but the temperature at the inside wall of the container is still lower than the melting point; therefore, no melting occurs.

2. Melting process includes two sub-cases:

   - Case 4. The thermal layer does not reach the symmetric line of the container. The temperature at the inside wall of the container has reached or accessed the melting point, and melting occurs.

   - Case 5. The melting occurs continually. The thermal layer has reached the symmetric line of the container and the temperature at the symmetric line increases and closes to the melting point quickly. The ice floats up due to the difference of density between the ice and water. This results in an asymmetric case.

3. Post-Melting process:

   - Case 6. Melting is complete and only sensible heating of the liquid PCM and container wall occurs.

Detailed illustrations of the six cases are shown in Fig. 3.

Although considerable effort has been taken to realistically model the latent energy storage system, a number of assumptions are still necessary. The assumptions are as follows:

- Initially the system is at a uniform temperature which may be at or below the melting point.

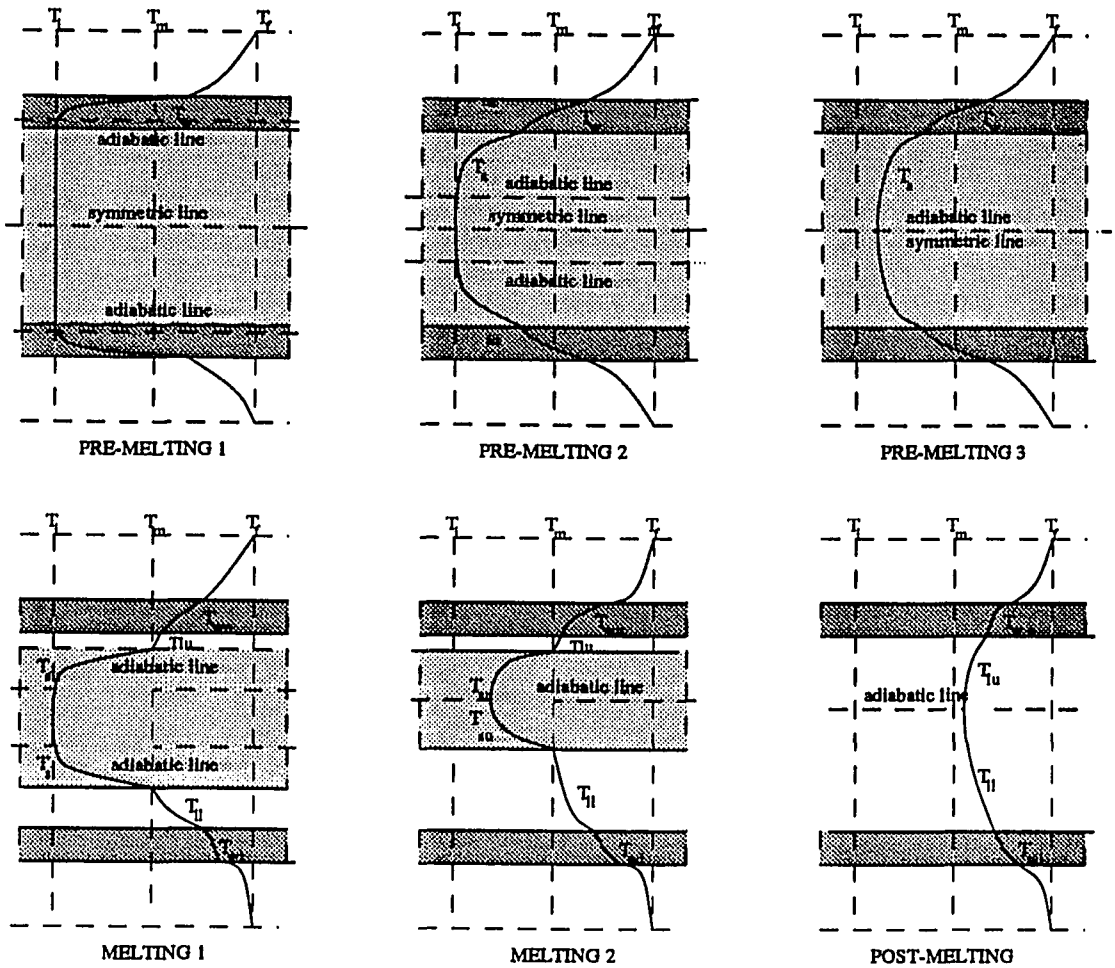

Figure 3: Sub-cases in melting process

- Heat transfer in the enclosure is one-dimensional. Heat transfer in the axial direction (the direction of the heat transfer flow) is assumed to be negligible compared to the heat transfer in the transverse direction (perpendicular to the flow direction).

- The critical Rayleigh number is $1,700$. Before the Rayleigh Number Ra reaches the critical point, conduction plays a control role in heat transfer. Otherwise, natural convection dominates the heat transfer when the Rayleigh number exceeds the critical point.

- The temperature distribution in the ice is considered to be symmetric about the horizontal center line of the ice slab. This is based on the fact that sensible heat plays only a minor part and the subcooling does not have big influence on the overall melting process.

- The flow of the heat transfer fluid in the channels is fully developed; therefore, heat transfer correlations for the internal flow can be used in the model.

Dimensionless Governing Equations

In order to reduce the number of variables and render the design problem more tractable, the problem is formulated, and subsequent design information is given in dimensionless form. This provides a tremendous simplification, even though the number of dependent and independent variables remain unaltered. Even more important is the fact that by nondimensionalizing the problem, dynamic similitude is revealed, which increases the physical understanding of the problem. The dimensionless terms are defined as follows:

$\Theta_k = (T_k - T_m)/(T_{fi} - T_m), \quad k = w,\ or\ l,\ or\ s,\ or\ a$

$y_k^* = y_k/H_i, \quad k = w,\ or\ l,\ or\ s,\ or\ a,$

$H_o^* = H_o/H_i;\ \ H_w^* = H_w/H_i;\ \ H_i^* = 1,\ \ s_u^* = s_u/H_i;\ \ s_d^* = s_d/H_i;$

$W^* = W/H_i,$

$z^* = z/Z; \quad \Delta z^* = \Delta z/Z,$

$V^* = VH^2/\alpha Z,$

$t^* = \alpha t/H^2, \quad \Delta t^* = \alpha \Delta t/H^2.$

Governing equations used in the different regions and at the boundaries are based on energy conservation. In the solid regions, only heat conduction occurs. but in the liquid region, the effects of heat convection are considered. The situations are described for the different cases respectively.

For case 1, the heat transfer is symmetric about the horizontal center line, there are only two regions to be considered.

In the heat transfer fluid channel, the balance of energy yields

$$\frac{\partial \Theta_f}{\partial t^*} + V^* \frac{\partial \Theta_f}{\partial z^*} = \frac{h_o H_i}{\alpha_l \rho_f c_f H_o^*}(\Theta_{w1} - \Theta_f), \tag{1}$$

and in the container wall, the conduction equation is given by

$$\frac{\partial \Theta_w}{\partial t^*} = \frac{\alpha_w}{\alpha_l} \frac{\partial^2 \Theta_w}{\partial y_w^{*2}}, \quad 0 \le y_w^* \le y_t^*, \tag{2}$$

subject to initial condition and boundary conditions

$$\Theta_f = \Theta_w = \Theta_i, \quad for\ all\ y^* \quad at\ t^* = 0, \tag{3}$$

$$\frac{\partial \Theta_w}{\partial t^*} = -\frac{h_o H_i}{k_w}(\Theta_f - \Theta_{w1}), \quad at\ y_w^* = 0, \tag{4}$$

$$\frac{\partial \Theta_w}{\partial y_w^*} = 0, \quad at\ y_w^* = y_t^*. \tag{5}$$

For case 2 and case 3, the governing equations in the flow channel as well as the container wall remain the same as those in case 1. Additional equations in the ice are as follows:

$$\frac{\partial \Theta_s}{\partial t^*} = \frac{\alpha_s}{\alpha_l}\frac{\partial^2 \Theta_w}{\partial y_s^{*2}}, \qquad 0 < y_s^* \leq y_t^*, \tag{6}$$

where, $y_t^* \leq 0.5$ for case 2, and $y_t^* = 0.5$ for case 3.

and Eq. (6) subjects to the boundary conditions:

$$\frac{\partial \Theta_w}{\partial y_w^*} = -\frac{h_o H_i}{k_w}(\Theta_f - \Theta_{w1}), \qquad at\ y_w^* = 0, \tag{7}$$

$$\Theta_w = \Theta_s, \qquad \frac{\partial \Theta_w}{\partial y_w^*} = \frac{k_s}{k_w}\frac{\partial \Theta_s}{\partial y_s^*}, \qquad at\ y_s^* = 0, \tag{8}$$

$$\Theta_s = \Theta_t, \qquad \frac{\partial \Theta_s}{\partial y_s^*} = 0, \qquad at\ y_s^* = y_t^*. \tag{9}$$

In the melting process (case 4 and case 5), the heat transfer is asymmetric about the center line due to the ice floating after melting has occurred. The governing equations are more complicated than those in the pre-melting process.

In the flow channel, the outside temperature of the top container wall is different as that of the bottom container wall. Eq. (1) can be replaced by

$$\frac{\partial \Theta_f}{\partial t^*} + V^*\frac{\partial \Theta_f}{\partial z^*} = \frac{h_o H_i}{2\alpha_l \rho_f c_f H_o^*}(\Theta_{w1_u} + \Theta_{w1_d} - 2\Theta_f). \tag{10}$$

At the outside of the top container wall and outside of the bottom container wall, the governing equations have the same form as that used in the pre-melting.

for the top wall

$$\frac{\partial \Theta_{w_u}}{\partial t^*} = \frac{\alpha_w}{\alpha_l}\frac{\partial^2 \Theta_{w_u}}{\partial y_{w_u}^{*\,2}}, \qquad 0 \leq y_{wu}^* \leq H_w^*, \tag{11}$$

for the bottom wall

$$\frac{\partial \Theta_{w_d}}{\partial t^*} = \frac{\alpha_w}{\alpha_l}\frac{\partial^2 \Theta_{w_d}}{\partial y_{w_d}^{*\,2}}, \qquad 0 \leq y_{wd}^* \leq H_w^*. \tag{12}$$

Above the ice, water film is very thin, and the inside surface temperature of the top container wall is closed to the melting point. The natural convection effect is weak, and the forced convection caused by the melting flow in horizontal direction could also be neglected; therefore, heat transfer occurs only in a conduction mechanism. The governing equations are following :

$$\frac{\partial \Theta_{lu}}{\partial t^*} = \frac{\partial^2 \Theta_{lu}}{\partial y_{l\,u}^{*2}}, \quad 0 < y_{l\,u}^* \leq s_u^*, \tag{13}$$

subject to:

$$\Theta_{w_u} = \Theta_{w2_u} \quad and \quad k_w \frac{\partial \Theta_{w_u}}{\partial y_{w_u}^*} = k_l \frac{\partial \Theta_{l_u}}{\partial y_{l_u}^*}, \quad at\ y_{w_u}^* = H_w^*. \tag{14}$$

The thickness of the thin water film above the ice can be determined by the balance of the pressure existing in the thin water film and buoyancy force on the ice. The detailed description and derivation can be found in (Yong and Maxwell, 1993 b). Result is

$$\frac{2}{3}\left[(\frac{ds_u^*}{dt^*})^2 + 24\frac{\nu}{\alpha_l s_u^*}\frac{ds_u^*}{dt^*}\right]\frac{w^{*3}}{s_u^{*2}} = \frac{gH_i^4}{\alpha_l^2} W^*(1 - s_u^* - s_d^*)(1 - \frac{\rho_s}{\rho_l}). \tag{15}$$

where the left hand side represents the total pressure caused by the melting flow in the thin water film above the ice, and the right hand side represents the buoyancy force acting on the ice.

At the upper ice-water interface, the energy balance equation is

$$\frac{ds_u}{dt^*} = Ste\left(-\frac{\partial \Theta_{l_u}}{\partial y_{l_u}^*} + \frac{k_s}{k_l}\frac{\partial \Theta_s}{\partial y_{s_u}^*}\right), \quad \Theta_{l_u} = \Theta_s = \Theta_m = 0 \quad at\ y_{l_u}^* = s_u \tag{16}$$

In the water below the ice slab, the governing equation has the same form as that in the thin water layer if only heat conduction occurs.

$$\frac{\partial \Theta_{ld}}{\partial t^*} = \frac{\partial^2 \Theta_{ld}}{\partial y_{l\,d}^{*2}}, \quad 0 \leq y_{l\,d}^* \leq s_d^* \tag{17}$$

which subjects to the boundary conditions:

$$\Theta_{w_d} = \Theta_{w2_d} \quad and \quad k_w \frac{\partial \Theta_{w_d}}{\partial y^*_{w_d}} = k_l \frac{\partial \Theta_{l_d}}{\partial y^*_{l_d}}, \quad at\ y^*_{w_d} = H^*_w. \tag{18}$$

At the solid-liquid interface,

$$\frac{ds_d}{dt^*} = Ste \left(-\frac{\partial \Theta_{l_d}}{\partial y^*_{l_d}} + \frac{k_s}{k_l} \frac{\partial \Theta_s}{\partial y^*_{s_d}} \right), \quad \Theta_{l_d}, \Theta_s = \Theta_m = 0 \quad at\ y^*_{l_d} = s^*_d. \tag{19}$$

When convection heat transfer occurs in the liquid region below the ice, Eq. (19) can be replaced by

$$\frac{\partial \Theta_{w_d}}{\partial y_{w_d}} = \frac{h_w H_i}{k_w} (\Theta_m - \Theta_{w2_d}), \quad at \quad y^*_{w_d} = H^*_w, \tag{20}$$

here, h_w is the natural convection heat transfer coefficient at the inside surface of the lower container wall. Correspondingly, on the solid-liquid interface

$$\frac{ds^*_d}{dt^*} = Ste \left[\frac{h_{int} H_i}{k_l} (\Theta_{w2_d} - \Theta_m) + \frac{k_s}{k_l} \frac{\partial \Theta_s}{\partial y^*_{s_d}} \right], \quad \Theta_{l_d} = \Theta_s = \Theta_m = 0 \quad at\ y^*_{l_d} = s^*_d, \tag{21}$$

where, h_{int} is natural convection heat transfer coefficient on the interface.

In the ice, it was assumed the adiabatic lines are either symmetric about the horizontal center line of the container(for case 4) or the same as that (for case 5). The energy equations in both the upper side and lower side of the ice are

$$\frac{\partial \Theta_{s_u}}{\partial t^*} = \frac{\alpha_s}{\alpha_l} \frac{\partial^2 \Theta_{s_u}}{\partial {y^*_{s_u}}^2}, \quad 0 < y^*_{s_u} \leq 0.5(1 - s^*_u - s^*_d), \tag{22}$$

$$\frac{\partial \Theta_{s_d}}{\partial t^*} = \frac{\alpha_s}{\alpha_l} \frac{\partial^2 \Theta_{s_d}}{\partial {y^*_{s_d}}^2}, \quad 0 < y^*_{s_d} \leq 0.5(1 - s^*_u - s^*_d), \tag{23}$$

and at the thermal layer (or the symmetric line), the boundary condition is

$$\Theta_{s_u} = \Theta_{s_d} = \Theta_t, \quad \frac{\partial \Theta_s}{\partial y^*_s} = 0, \quad at\ y^*_s = y^*_t, \tag{24}$$

Θ_t will be determined by averaging the values obtained from two sides.

When the post-melting process (case 6) begins, the entire of the container is occupied by water, and no further latent heat exists in the container. The temperature distribution are not necessary to be symmetric to the horizontal center line of the container because temperatures on the upside and downside are different when melting completed. But the adiabatic line is not easily located after the post-melting starts. This case will not be discussed in the current study.

Application of Integral Method

The formulation given previously has resulted in a mathematical model which consists of several systems of coupled partial differential equations with appropriate initial and boundary conditions. The integral method is employed in the current work to reduce the number of independent variables. Quadratic polynomial approximations are used for the temperature distributions in the different regions of cases 1-5. The assumptions for the temperature profiles must satisfy the initial and boundary conditions in each case. This section will follow the precedent set in the preceding one.

For the case 1, the temperature profile in the container wall is assumed as:

$$\Theta_w = \Theta_{w1} - 2\frac{(\Theta_{w1} - \Theta_t)}{y_t^*} y_w^* + \frac{(\Theta_{w1} - \Theta a)}{y_t^{*2}} y_w^*, \quad 0 \le y_w^* \le y_t^* < H_w^*, \tag{25}$$

and $\Theta_t = \Theta_i$.

Substituting Eq. (25) in the governing equation (2) allows it to be integrated as follows:

$$\frac{d}{dt^*}\int_0^{y_t^*} \Theta_w dy_s^* - \Theta_t \frac{dy_w^*}{dt^*} \Big|_0^{y_t^*} = \frac{\alpha_w}{\alpha_l} \frac{\partial \Theta_w}{\partial y_w^*} \Big|_0^{y_t^*} \tag{26}$$

which yields

$$y_t^*\dot{\Theta}_{w1}/3 + (\Theta_{w1} - \Theta_t)\dot{y}_t^*/3 = 2(\Theta_{w1} - \Theta_t)/y_t^*, \tag{27}$$

where, Θ_{w1} is a unknown variable, and y_t^* is given by Prusa et al. (1989) as

$$y_t^* = \sqrt{6\frac{\alpha_w}{\alpha_l}t^*}. \tag{28}$$

For case 2, the assumptions of the temperature in the wall and solid region are as follows:

$$\Theta_w = \Theta_{w1} + \frac{h_o H_i(\Theta_{w1} - \Theta_f)}{k_w} y_w^* + \left[\frac{(\Theta_{w2} - \Theta_{w1})}{H_w^*} + \frac{h_o H_i(\Theta_f - \Theta_{w1})}{k_w H_w^*}\right] y_w^{*2}, \tag{29}$$

$$\Theta_s = \Theta_{w2} - \frac{2(\Theta_{w2} - \Theta_t)}{y_t^*} y_s^* + \frac{(\Theta_{w2} - \Theta_t)}{y_t^{*2}} y_s^{*2}, \tag{30}$$

where $0 \leq y_t^* \leq 0.5$ and $\Theta_t = \Theta_i$. The above equations are substituted into the following integral equations with respect to y_w^* in the interval $(0 - H_W^*)$ and Y_s^* in the interval $(0 - y_t^*)$ respectively, This gives

$$\frac{d}{dt^*}\int_0^{H_w^*} \Theta_w dy_w^* = \frac{\alpha_w}{\alpha_l}\frac{\partial \Theta_w}{\partial y_w^*}\Big|_0^{H_W^*} \tag{31}$$

$$\frac{d}{dt^*}\int_0^{y_t^*} \Theta_s dy_s^* - \Theta_t \frac{dy_s^*}{dt^*}\Big|_0^{y_t^*} = \frac{\alpha_s}{\alpha_l}\frac{\partial \Theta_s}{\partial y_s^*}\Big|_0^{y_t^*} \tag{32}$$

which yields

$$\frac{h_0 H_i H_w^{*2}}{6k_w}\dot{\Theta}_f - \left[\frac{2H_w^*}{3} - \frac{h_o H_i H_w^{*2}}{6k_w}\right]\dot{\Theta}_{w1} + \frac{H_w^*}{3}\dot{\Theta}_{w2} = \frac{2\alpha_w h_o H_i}{\alpha_l k_w}\Theta_f - \frac{2\alpha_w}{\alpha_l}\left(\frac{1}{H_w^*} + \frac{h_o H_i}{k_w}\right)\Theta_{w1} + \frac{2\alpha_w}{\alpha_l H_w^*}\Theta_{w2}, \tag{33}$$

and

$$y_t^*\dot{\Theta}_{w2}/3 + (\Theta_{w2} - \Theta_t)\dot{y}_t^*/3 = 2(\Theta_{w2} - \Theta_t)/y_t^*, \tag{34}$$

where, Θ_f, Θ_{w1}, and Θ_{w2} are unknown variables, y_t^* is also given in (Prusa et al. 1989) as

$$y_t^* = \sqrt{6\frac{\alpha_s}{\alpha_l}t^*}. \tag{35}$$

In case 3, the temperature distribution in the wall is the same as that in case 2. The thermal layer has reached the centerline of the container, and the temperature at the centerline increases with time. The temperature distribution in the solid region is assumed to be as follows:

$$\Theta_s = \Theta_{w2} - 4(\Theta_{w2} - \Theta_t)y_s^* + 4(\Theta_{w2} - \Theta_t)y_s^{*2}. \tag{36}$$

After the substitutions and the integrations, there are

$$\begin{aligned}&\frac{h_0 H_i H_w^{*2}}{6k_w}\dot{\Theta}_f + \left(\frac{2H_w^*}{3} + \frac{h_o H_i H_w^{*2}}{6k_w}\right)\dot{\Theta}_{w1} + \frac{H_w^*}{3}\dot{\Theta}_{w2} \\ &= \frac{2\alpha_w h_o H_i}{\alpha_l k_w}\Theta_f - \frac{2\alpha_w}{\alpha_l}\left(\frac{1}{H_w^*} + \frac{h_o H_i}{k_w}\right)\Theta_{w1} + \frac{2\alpha_w}{\alpha_l H_w^*}\Theta_{w2},\end{aligned} \tag{37}$$

and

$$\frac{1}{3}\dot{\Theta}_{w2} + \frac{2}{3}\dot{\Theta}_t = 2(\Theta_{w2} - \Theta_t), \tag{38}$$

where, $\Theta_f, \Theta_{w1}, \Theta_{w2}$ and Θ_t are unknowns in the above equations.

In the melting processes (case 4 and 5), the temperature profiles in both of the up-side wall and downside wall and the solid region have the same form as those used in case 3. The temperature profile in the thin water film is also assumed to be:

$$\begin{aligned}\Theta_{l_u} &= \Theta_{w2_u} + \frac{k_w}{k_l}\left[\frac{2(\Theta_{w2_u} - \Theta_{w1_u})}{H_w^*} + \frac{h_o H_i(\Theta_f - \Theta_{w1})}{k_w}\right] y_{l_u}^* \\ &+ \left\{\frac{\Theta_{w2_u} - \Theta_{w1_u}}{H_w^* s_u^*} - \frac{k_w}{k_l}\left[\frac{2(\Theta_{w2_u} - \Theta_{w1_u})}{H_w^* s_u^*} + \frac{h_o H_i(\Theta_f - \Theta_{w1_u})}{k_w s_u^*}\right]\right\} y_{l_u}^*.\end{aligned} \tag{39}$$

If only heat conduction occurs in the water below the ice, the temperature in this region has similar form as that in the water film, that is

$$\Theta_{l_d} = \Theta_{w2_d} + \frac{k_w}{k_l}\left[\frac{2(\Theta_{w2_d} - \Theta_{w1_d})}{H_w^*} + \frac{h_o H_i(\Theta_f - \Theta_{w1_d})}{k_w}\right] y_{l_d}^* + \left\{\frac{\Theta_{w2_d} - \Theta_{w1_d}}{H_w^* s_d^*} - \frac{k_w}{k_l}\left[\frac{2(\Theta_{w2} - \Theta_{w1})}{H_w^* s_u^*} + h_o H_i(\Theta_f - \Theta_{w1_d})k_w s_d^*\right]\right\} y_{l_d}^{*\,2}. \quad (40)$$

Through similar procedure of substitution and integration, the following expressions for these liquid regions are obtained:

$$\frac{h_o H_i s_u^{*2}}{6k_l}\dot{\Theta}_f - \left(\frac{k_w s_u^{*2}}{3k_2 H_w^*} + \frac{h_o H_i s_u^{*2}}{6k_l}\right)\dot{\Theta}_{w1_u} + \left(\frac{2s_u^*}{3} + \frac{k_w s_u^{*2}}{3k_2 H_w^*}\right)\dot{\Theta}_{w2_u} = -\frac{h_o H_i}{k_l}\Theta_f + 2\left(\frac{h_o H_i}{k_l} + \frac{2k_w}{k_l H_w^*}\right)\Theta_{wi_u} - 2\left(\frac{1}{s_u^*} + \frac{2k_w}{k_l H_w^*}\right)\Theta_{w2_u}, \quad (41)$$

and

$$\frac{h_o H_i s_d^{*2}}{6k_l}\dot{\Theta}_f - \left(\frac{k_w s_d^{*2}}{3k_2 H_w^*} + \frac{h_o H_i s_d^{*2}}{6k_l}\right)\dot{\Theta}_{w1_d} + \left(\frac{2s_d^*}{3} + \frac{k_w s_d^{*2}}{3k_2 H_d^*}\right)\dot{\Theta}_{w2_d} + \left[\frac{h_o H_i s_d^{*2}}{3k_l}(\Theta_{w1_d} - \Theta_f) + \frac{2}{3}\Theta_{w2_d} + \frac{2k_w s_d^*}{3k_l H_w^*}(\Theta_{w2_d}\Theta_{w1})\right]\dot{s}_d^* = -\frac{h_o H_i}{k_l}\Theta_f + 2\left(\frac{h_o H_i}{k_l} + \frac{2k_w}{k_l H_w^*}\right)\Theta_{w1_d} - 2\left(\frac{1}{s_d^*} + \frac{2k_w}{k_l H_w^*}\right)\Theta_{w2_d}. \quad (42)$$

On both the upper interface and lower interface, substituting the assumptions of temperature distributions and applying appreciate boundary conditions to Eq. (16) and Eq. (19) yields

$$\dot{s}_u^* = Ste\left[\frac{h_o H_i}{k_w}\Theta_f - \frac{k_w}{k_l}\left(\frac{2}{H_w^*} + \frac{2k_w}{H_w^* k_l}\right)\Theta_{w1_u} + \left(\frac{2}{s_u^*} + \frac{2k_w}{k_l H_w^*}\right)\Theta_{w2_u} + \frac{2k_s}{k_l s_u^*}\Theta_t\right] \quad (43)$$

$$\dot{s}_d^* = Ste\left[\frac{h_o H_i}{k_w}\Theta_f - \frac{k_w}{k_l}\left(\frac{2}{H_w^*} + \frac{2k_w}{H_w^* k_l}\right)\Theta_{w1_d} + \left(\frac{2}{s_d^*} + \frac{2k_w}{k_l H_w^*}\right)\Theta_{w2_d} + \frac{2k_s}{k_l s_d^*}\Theta_t\right]. \quad (44)$$

Additionally, the transcendental Eq. (15) is needed here.

In the solid region, the similar equation of temperature distribution used in case 2 is employed for case 4, and that used in case 3 for case 5. After integration and arrangement, they are

$$y_t^* \dot{y}_t^* = 6\frac{\alpha_s}{\alpha_l} \tag{45}$$

$$\frac{1}{3}\Theta_t \dot{s}_u^* + \frac{2}{3}(1 - s_u^*)\dot{\Theta}_t + \frac{2\alpha_s \Theta_t}{\alpha_l(1 - s_u^*)} = 0, \quad for\ case\ 5. \tag{46}$$

As the temperature of the down-inside wall and distance of the down-interface to the down-side wall increase, convection heat transfer becomes stronger. The energy balances for the liquid region below the ice slab and interface can be expressed as

$$\frac{h_o H_i}{k_w}\Theta_f - (\frac{h_o H_i}{k_w} + \frac{2}{H_w^*})\Theta_{w1_d} + (\frac{2}{H_w^*} + \frac{h_w H_i}{k_w})\Theta_{w2_d} = 0 \tag{47}$$

and

$$\dot{s}_d^* = Ste\left[\frac{Nu}{s_d^*} - \frac{2k_s\Theta_t}{k_l(1 - s_d^*)}\right]. \tag{48}$$

In case 4, $\Theta_f, \Theta_{w1_u}, \Theta_{w2_u}, \Theta_{w1_d}, \Theta_{w1_d}, s_u^*, s_d^*$, and y_t^* are unknowns. But in case 5, only y_t^* is replaced by Θ_t as an unknown.

So far, all terms with $\frac{\partial}{\partial y_k^*}$ in the partial differential equations for case (1-5) have been eliminated by applying the integral method. The systems of partial differential equations have become the systems of ordinary differential equations respecting to dimensionless time.

Numerical Method and Computational Procedure

Although the systems of partial differential equations have become the systems of ordinary differential equations, the new systems are still highly nonlinear and coupled, and formulations are still analytically intractable. At the present time, the

method used to solve the wide range of the relevant dimensionless groups is the finite difference method.

Since finite differencing is relatively straight forward, only the details for case 5, which is the most important and complicated process in the overall melting, is presented.

In the flow channel, the governing equation is in a form of partial differential equation. Consequently, Θ_f must be made a discrete variable spatially as well as temporally. A one-dimensional computational grid consisting of M nodes is introduced along the axis of the flow channel (see Fig.4), with the first node located precisely at the inlet of the channel. Forward time differencing coupled with upward space differencing of equation results in the following finite difference equation for Θ_f:

$$(\frac{1}{\Delta t^*} + \frac{V^*}{\Delta z} + \frac{2h_oH_i}{\rho_f c_f \alpha_l H_o^*})\Theta_{fj}^n - \frac{h_oH_i}{\rho_f c_f \alpha_l H_o^*}\Theta_{w1_uj}^n - \frac{h_oH_i}{\rho_f c_f \alpha_l H_o^*}\Theta_{w1_dj}^n = \frac{1}{\Delta t^*}\Theta_{f_j}^{n-1} + \frac{V^*}{\Delta z^*}\Theta_{f_{j-1}}^n. \quad (49)$$

In the other regions, all the ordinary differential equations have to be changed into finite difference equations. A differential term is transferred into the finite difference expression as:

$$\dot{x} = \frac{x^n - x^{n-1}}{\Delta t^*}, \quad (50)$$

where, x presents a unknown dependent variable, such as Θ_f, Θ_{w1_u}, Θ_{w2_u} , Θ_{w1_d}, Θ_{w2_d}, Θ_t, s_u^*, or s_d^*; n refers to time level, and Δt^*, the time step.

The system of finite difference equations can be rearranged and expressed as the following explicit form:

$$[A][X] = [C], \quad (51)$$

where $[A]$ is a matrix of nonlinear coefficients, $[X]$ is a matrix of unknown variables, and $[C]$ is a matrix of nonlinear sources. For case 5, Eq. (51) is presented as:

$$\begin{bmatrix} a_{11} & a_{12} & a_{13} & a_{14} & a_{15} & a_{16} & a_{17} \\ a_{21} & a_{22} & a_{23} & a_{24} & a_{25} & a_{26} & a_{27} \\ a_{31} & a_{32} & a_{33} & a_{34} & a_{35} & a_{36} & a_{37} \\ a_{41} & a_{42} & a_{43} & a_{44} & a_{45} & a_{46} & a_{47} \\ a_{51} & a_{52} & a_{53} & a_{54} & a_{55} & a_{56} & a_{57} \\ a_{61} & a_{62} & a_{63} & a_{64} & a_{65} & a_{66} & a_{67} \\ a_{71} & a_{72} & a_{73} & a_{74} & a_{75} & a_{76} & a_{77} \end{bmatrix} \begin{bmatrix} \Theta_f \\ \Theta_{w1_u} \\ \Theta_{w2_u} \\ \Theta_{w1_d} \\ \Theta_{w2_d} \\ \Theta_t \\ s_d^* \end{bmatrix} = \begin{bmatrix} c_1 \\ c_2 \\ c_3 \\ c_4 \\ c_5 \\ c_6 \\ c_7 \end{bmatrix}. \tag{52}$$

where

$$a_{11} = \frac{h_o H_i}{\rho_f c_f \alpha_l H_o^*} + \frac{1}{\Delta t^*} + \frac{V^*}{\Delta z^*},$$

$$a_{12} = -\frac{h_o H_i}{\rho_f c_f \alpha_l H_o^*},$$

$$a_{13} = 0,$$

$$a_{14} = -\frac{h_o H_i}{\rho_f c_f \alpha_l H_o^*},$$

$$a_{15} = a_{16} = a_{17} = 0$$

$$a_{21} = -\frac{h_o H_i H_w^{*2}}{6 k_w \Delta t^*} - \frac{2\alpha_w h_o H_i}{\alpha_l k_w},$$

$$a_{22} = -\left(\frac{2H_w^*}{3\Delta t^*} + \frac{h_o H_i H_w^{*2}}{6\Delta t^* k_w} + \frac{2\alpha_w}{\alpha_l k_w} + \frac{h_o H_i \alpha_w}{\alpha_l k_w}\right),$$

$$a_{23} = -\frac{2\alpha_w}{\alpha_l H_w^*} + \frac{H_w^*}{3\Delta t^*},$$

$$a_{24} = a_{25} = a_{26} = a_{27} = 0,$$

$$a_{31} = \frac{h_o H_i H_w^{*2}}{6k_l \Delta t^*} + \frac{2h_o H_i}{k_l},$$

$$a_{32} = -\left(\frac{k_w s_u^{*2}}{3k_l H_w^*} + \frac{h_o H_i s_u^{*2}}{6k_l}\right)/\Delta t^* + 2\left(\frac{h_o H_i}{k_l} + \frac{2k_w}{k_l H_w^*}\right),$$

$$a_{33} = (\frac{2s_u^*}{3} + \frac{k_w s_u^{*2}}{3k_i H_w^{*2}})/\Delta t^* - 2(\frac{1}{s_u^*} + \frac{2k_w}{k_l H_w^{*2}}),$$

$$a_{34} = a_{35} = a_{36} = 0,$$

$$a_{37} = \left[\frac{h_o H_i s_u^*}{3k_l}\Theta_f - \left(\frac{h_o H_i s_u^*}{3k_i} + \frac{2k_w s_u^*}{3k_l H_w^*}\right)\Theta_{w1_u} + \left(\frac{2k_w s_u^*}{k_l H_w^*} + \frac{2}{3}\right)\Theta_{w2_u}\right]/\Delta t^*,$$

$$a_{41} = -\frac{h_o H_i H_w^{*2}}{6k_w \Delta t^*} - \frac{2\alpha_w h_o H_i}{\alpha_l k_w},$$

$$a_{42} = a_{43} = a_{46} = a_{47} = 0,$$

$$a_{44} = -\left(\frac{2H_w^*}{3\Delta t^*} + \frac{h_o H_i H_w^{*2}}{6\Delta t^* k_w} + \frac{2\alpha_w}{\alpha_l k_w} + \frac{h_o H_i \alpha_w}{\alpha_l k_w}\right),$$

$$a_{45} = -\frac{2\alpha_w}{\alpha_l H_w^*} + \frac{H^*}{3\Delta t^*},$$

$$a_{51} = \frac{h_o H_i H_w^{*2}}{6k_l \Delta t^*} + \frac{2h_o H_i}{k_l},$$

$$a_{52} = a_{53} = a_{56} = 0,$$

$$a_{54} = -\left(\frac{k_w s_d^{*2}}{3k_l H_w^*} + \frac{h_o H_i s_d^{*2}}{6k_l}\right)/\Delta t^* + 2\left(\frac{h_o H_i}{k_l} + \frac{2k_w}{k_l H_w^*}\right),$$

$$a_{55} = (\frac{2s_d^*}{3} + \frac{k_w s_d^{*2}}{3k_i H_w^{*2}})/\Delta t^* - 2(\frac{1}{s_d^*} + \frac{2k_w}{k_l H_w^{*2}}),$$

$$a_{57} = \left[\frac{h_o H - i s_d^*}{3k_l}\Theta_f - \left(\frac{h_o H_i s_d^*}{3k_i} + \frac{2k_w s_d^*}{3k_l H_w^*}\right)\Theta_{w1_d} + \left(\frac{2k_w s_d^*}{k_l H_w^*} + \frac{2}{3}\right)\Theta_{w2_d}\right]/\Delta t^*,$$

$$a_{61} = a_{62} = a_{63} = a_{64} = a_{65} = 0,$$

$$a_{66} = \frac{2(1 - s_u^*)}{3\Delta t^*} + \frac{2}{1 - s_u^*},$$

$$a_{67} = \frac{\Theta_t}{3\Delta t^*},$$

$$a_{71} = -\frac{h_o H_i Ste}{k_l},$$

$$a_{72} = a_{73},$$

$$a_{74} = Ste\left(\frac{2k_w}{k_l H_w^*} + \frac{h_o H_i}{k_l}\right),$$

$$a_{75} = -Ste\left(\frac{1}{s_d^*} + \frac{2k_w}{H_w^* k_l}\right),$$

$$a_{76} = -2Ste\frac{k_s}{k_l 91 - s_d^*)},$$

$$a_{77} = \frac{1}{\Delta t^*},$$

$$c_1 = \frac{1}{\Delta t^*}\Theta_f^{n-1} + \frac{V^*}{\Delta z^*}(\Theta_{w1_u}^{n-1} + \Theta_{w1_d}^{n-1}),$$

$$c_2 = -\frac{h_o H_i H_w^{*2}}{6k_w \Delta t^*}\Theta_f^{n-1} + \left(\frac{2H_w^*}{3} + \frac{h_o H_i H_w^*}{6k_w}\right)\Theta_{w1_u}^{n-1}/\Delta t^* + \frac{H_w^*}{3\Delta t^*}\Theta_{w2_u}^{n-1},$$

$$c_3 = \frac{h_o H_i s_u^{*2}}{6k_l \Delta t^*}\Theta_f^{n-1} - \left(\frac{2k_w s_u^{*2}}{3k_l H_w^*} + \frac{h_o H_i s_u^{*2}}{6k_l}\right)\Theta_{w1_u}^{n-1}\Delta t^* + \left(\frac{2s_u^*}{3} + \frac{k_w s_u^{*2}}{3k_l H_w^*}\right)\Theta_{w2_u}^{n-1}/\Delta t^*,$$

$$c_4 = -\frac{h_o H_i H_w^{*2}}{6k_w \Delta t^*}\Theta_f^{n-1} + \left(\frac{2H_w^*}{3} + \frac{h_o H_i H_w^*}{6k_w}\right)\Theta_{w1_d}^{n-1}/\Delta t^* + \frac{H_w^*}{3\Delta t^*}\Theta_{w2_d}^{n-1},$$

$$c_5 = \frac{h_o H_i s_d^{*2}}{6k_l \Delta t^*}\Theta_f^{n-1} - \left(\frac{2k_w s_d^{*2}}{3k_l H_w^*} + \frac{h_o H_i s_d^{*2}}{6k_l}\right)\Theta_{w1_d}^{n-1}\Delta t^* + \left(\frac{2s_d^*}{3} + \frac{k_w s_d^{*2}}{3k_l H_w^*}\right)\Theta_{w2_d}^{n-1}/\Delta t^*,$$

$$+ \left[\frac{h_o H_i s_d^*}{3k_l}\Theta_f - \left(\frac{h_o H_i s_d^*}{3k_l} + \frac{2k_w s^*}{3k_l H_w^*}\right)\Theta_{w1_d} + \left(\frac{2k_w s_d^*}{3_l H_w^*} + \frac{2}{3}\right)\right] s_d^{*n-1}/\Delta t^*,$$

$$c_6 = \frac{2(1-s^*)}{3\Delta t^*}\Theta_t^{n-1} + \frac{\Theta_t}{3\Delta t^*}s^{*n-1},$$

$$c_7 = s_d^{*n-1}/\Delta t^*.$$

The variables involved in [A] and [C], such as Θ_f, Θ_{w1_u}, Θ_{w2_u}, Θ_{w1_d}, Θ_{w2_d}, Θ_t and s_d^* are considered as knowns. The values from the previous time step $(n-1)$ are used as the first set of guess values in the current step (n). Another unknown variable of s_u^* is determined by solving the transcendental equation (15) with the Newton-Raphson method, and can be substituted into the above matrix systems as a known value. Therefore, Eq. (52) can be treated as a linear system, and solved by the Gauss method. Iterations are necessary to update the variables in A and C until the differences between two closed iterations for a specified variables satisfy the requirement of the error.

In the axial direction, M nodes are divided uniformly (see Fig. 4). The dependent variables $\Theta_f, \Theta_{w1}, \Theta_{w2}, s_u^*, s_d^*$, etc, must be considered to be functions of position z^*. That is, the numerical model must be simultaneously applied at every node in the flow channel, and the downstream temperature of the previous node $j-1$ is used as the upstream temperature of the node j. The starting time at node j is counted as

$$t_{j_0}^* = j\Delta z^*/V^*. \tag{53}$$

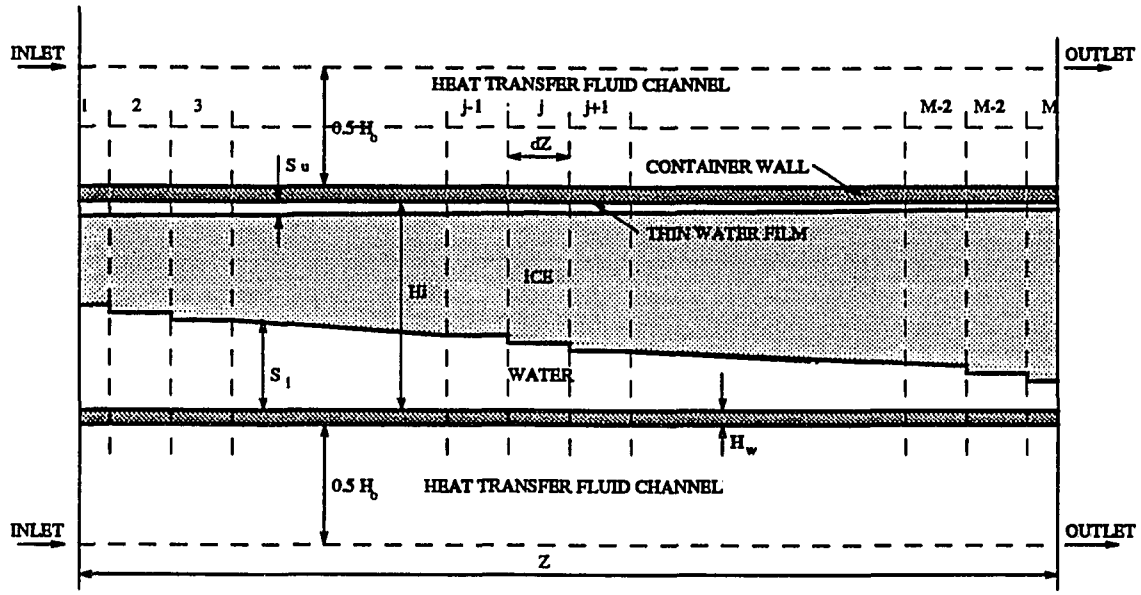

Figure 4: Diagram of computational grid for overall storage system

The algorithm consists of a main program which sweeps down the whole channel from the inlet to outlet and five subroutines that correspond to five appropriate cases. The flow chart of the main program is shown in Fig. 5, and that for the subroutine of case 5 in Fig. 6.

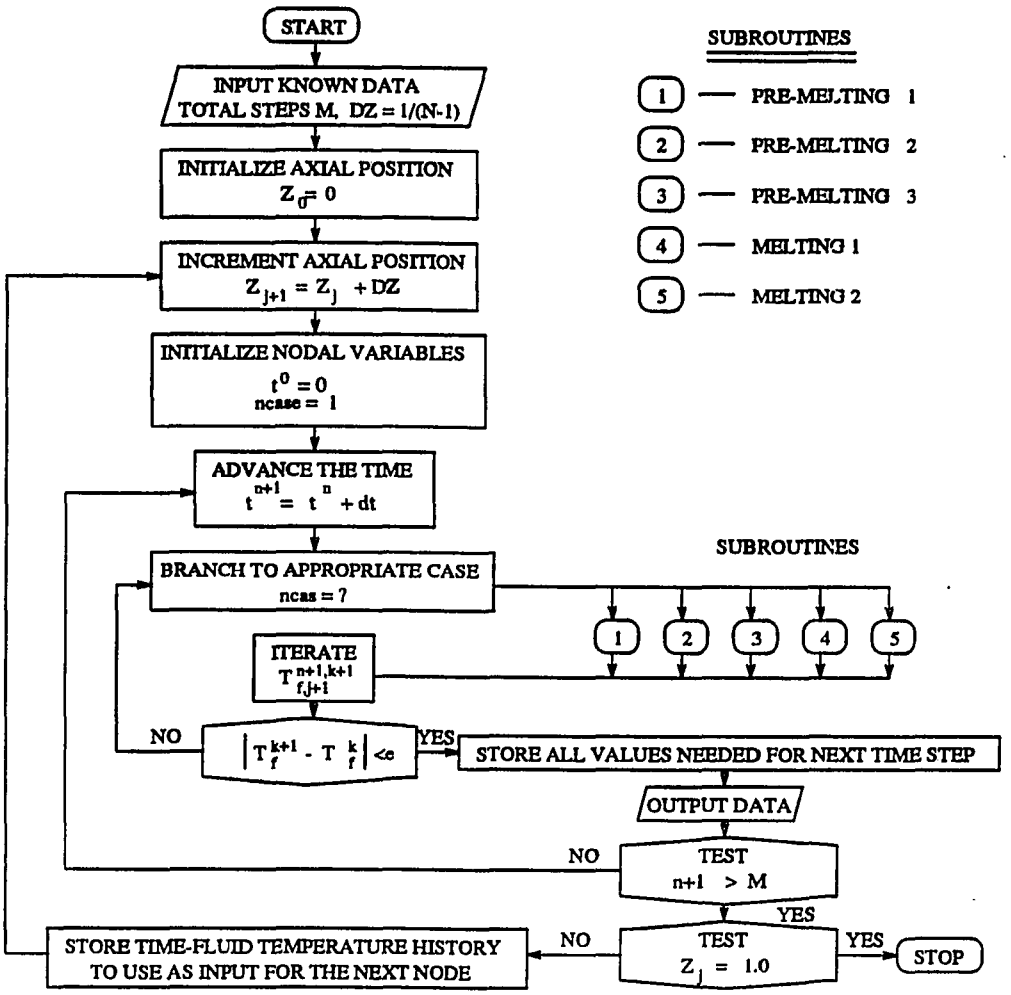

Figure 5: Main program flow chart

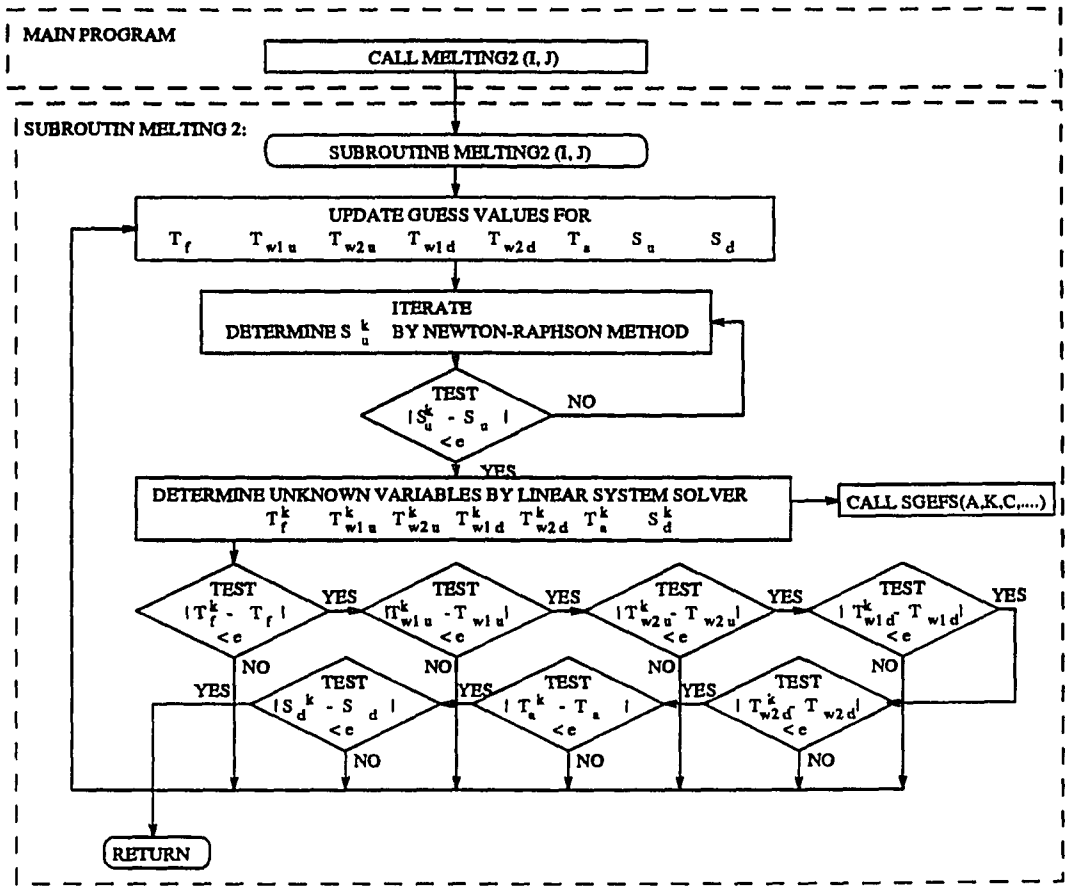

Figure 6: Flow chart of subroutine 5 (case 5)

RESULTS AND DISCUSSION

For the most popular cooling thermal storage system used for commercial air conditioning, material combinations are selected as:

Phase-Change Material	Container	Heat Transfer Fluid
water-ice	polyethylene	ethylene glycol-water

The thermodynamic properties of the above materials are obtained from Beaton et al (1989). The thermodynamic properties regarding the ice, container, and heat transfer fluid are assumed to be constant. The properties of the water are considered to vary with temperature, since some properties of water, for example, thermal expansion coefficient β, are sensible to temperature. A subroutine is used in the model to evaluate the thermodynamic properties of the liquid water.

The heat transfer coefficient for the internal flow in the flow channel h_o, which varies with the Reynolds number Re, is selected from Incropera and De Witt (1990). The natural convection heat transfer occurs on the water below the ice when the Ra reaches or excesses 1700. Nu_w and Nu_{int} are given in (Yong and Maxwell, 1993 a).

The performance of a thermal energy storage system can not be represented by a single quantity, and depends on several independent variables. The computer model have been run under varying conditions, which are regarding to inlet temperature of

the heat transfer fluid, initial temperature of the system, and geometric parameters of the container and flow channel. The range of the independent variables are listed as

$T_{fi}(^{o}c)$	$T_i(^{o}c)$	$H_i(mm)$	$H_o(mm)$	$H_w(mm)$	$V(m/s)$
$5-15$	$-5-0$	$30-60$	$10-40$	$1-4$	$0.02-0.2$

Correspondingly, the dimensionless terms of the above ranges are

Ste	Θ_i	$H_i^*(H_i/40)$	H_o^*	H_w^*	V^*
$0.062-0.187$	$-1-0$	$0.5-1.5$	$0.25-1.0$	$0.025-0.1$	$11.6-116$

The results of the system response are presented in graphical form. Fig. 7 shows the temperature distribution for overall storage at a specified time. We can observe that the temperature near the inlet of the storage is higher than that near the outlet because the heat energy in the heating fluid is used to melt ice in the container along the axial direction. Another phenomena is that temperature distribution is asymmetric the upside and downside, which is caused by ice floating up. The upper interface of the ice slab almost contacts to the up-inside wall of the container, and the up-inside wall temperature is close to the melting point during the melting. Also, it is shown in Fig. 8 that the distance of the ice-water interface to the bottom wall increases more near the inlet than that happens near the outlet, because the temperature difference between the heating fluid and ice slab in the container is greater and the heat transfer is stronger in the region close to the inlet.

In order to gain some insight into the effect each of the six variable on the

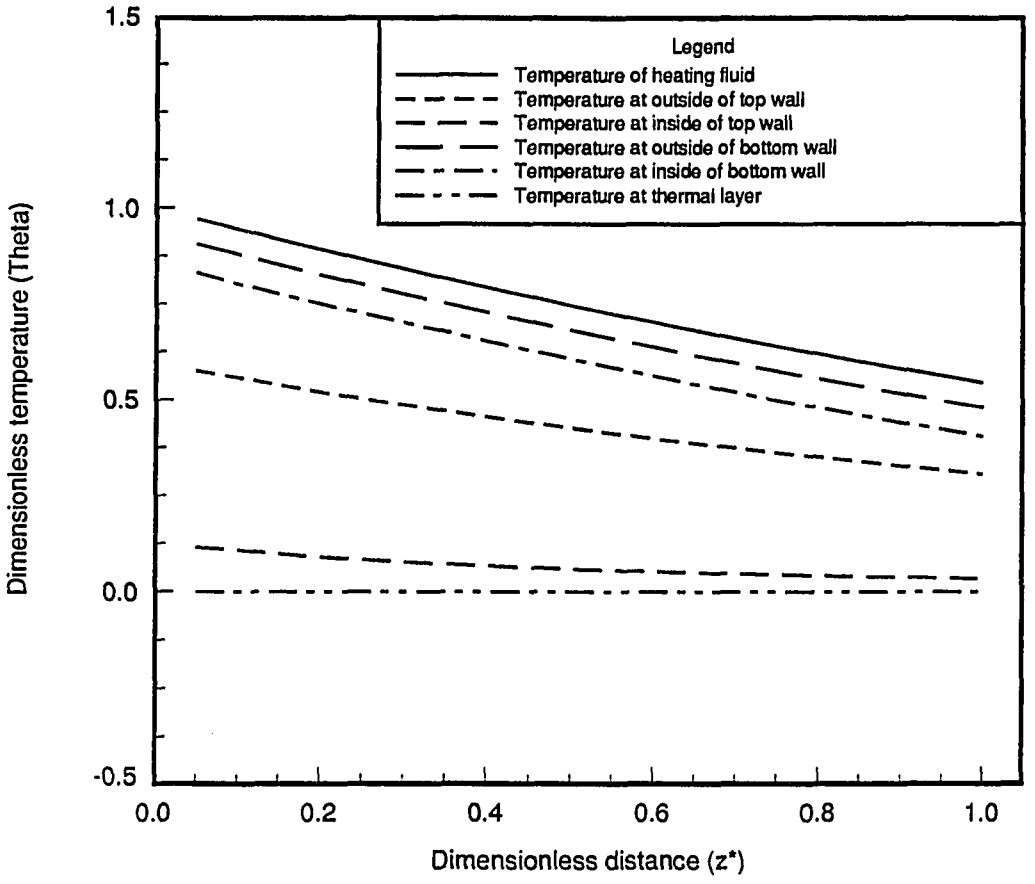

Figure 7: Temperature distribution in the storage system at a time ($t^* = 1.25$) under condition: $Ste = 0.062$, $\Theta_i = -0.6$, $H_i^* = H_i(m)/0.04(m) = 1$, $H_o^* = 1$, $H_w^* = 0.05$, $V^* = 11.6$

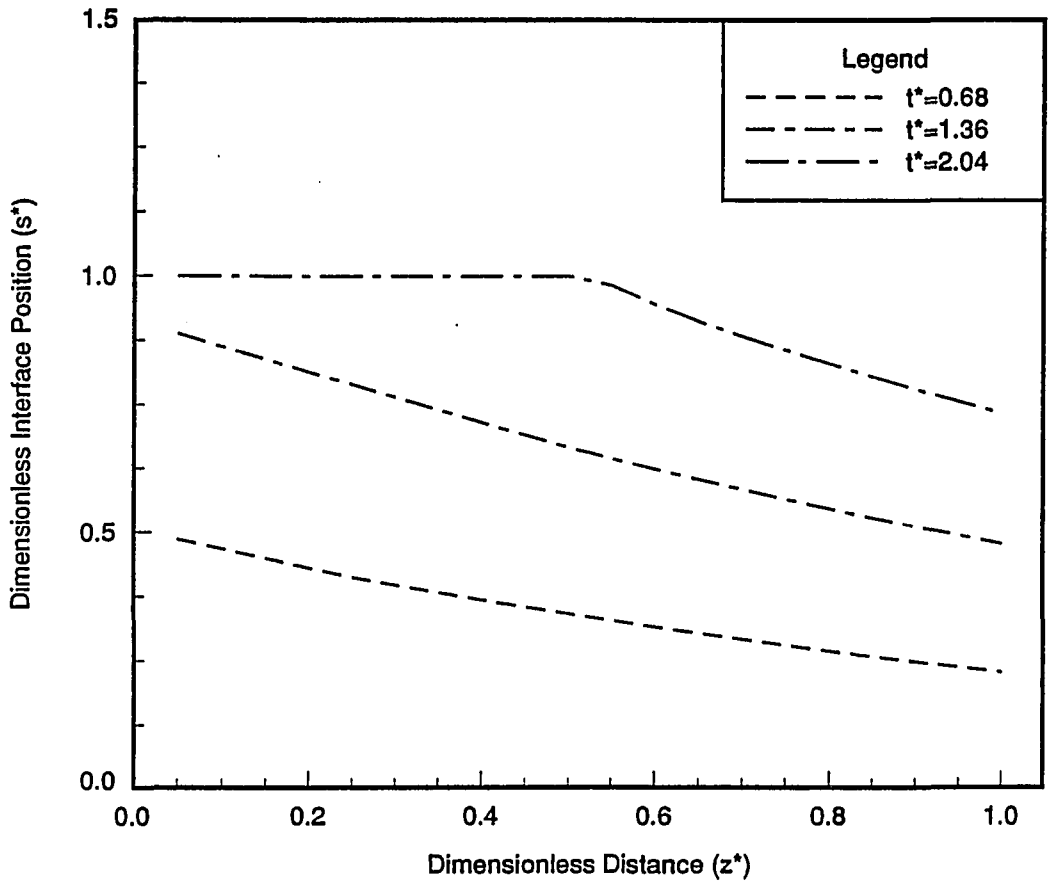

Figure 8: Interface position in the storage system with variation of time under condition: $Ste = 0.062$, $\Theta_i = -0.6$, $H_i^* = H_i(m)/0.04(m) = 1$, $H_o^* = 1$, $H_w^* = 0.05$, $V^* = 11.6$

performance, a parametric study has been conducted where only one variable varies for a situation. The effects of variation of the variables, $\Theta_i, Ste, H_i^*, H_0^*, H_w^*$, and V^*, are illustrated in Fig. 9 through Fig. 14 respectively. Each plot shows the dimensionless outlet temperature as a function of dimensionless time as a single parameter varies. With refers to the outlet temperature and the discharge time (melting period), the conclusions shown in Table 1 can be made:

Table 1. Influences of Variables

Independent Variable	Outlet Temperature	Discharge Time
Increasing Θ_i	No significant change	No significant change
Increasing Ste	Higher	Decreases
Increasing H_i^*	No significant change	Increases
Increasing H_o^*	Higher	Decreases
Increasing H_w^*	Higher	Increases
Increasing V^*	Higher	Decreases

From this study, it is found that the initial temperature Θ_i (or subcooling degree) has little effect on the system performance (see Fig. 9). This results in that only five variables, Ste, H_i^*, H_0^*, H_w^*, and V^*, are needed to be considered in the engineering analysis. Generally, that the outlet temperature of the heat transfer fluid remains low for as long as possible is desired for an application of the cooling energy storage system. The Ste (or inlet temperature of the heating fluid) has a greater effect on the system (see Fig. 10), but this factor is usually kept nearly constant (such as $5°C$) in practice. The container's thickness H_i^* doesn't affect the outlet temperature significantly, but changes the discharge time (see Fig. 11); therefore H_i can be

selected according to the needed discharge time. From Fig. 12, it is shown that the outlet temperature is proportional to the flow channel thickness, and the discharge time. The reduction of the flow channel thickness can reduce the outlet temperature and extend the discharge time, as well as make the system more compact (see Fig. 13). Also, the thin container wall is preferred in the design of the storage system because it reduces heat transfer resistance and cost of the container (see Fig. 14). The velocity of the heat transfer flow in the channel is a key factor. The lower velocity will cause lower heat transfer between the heat transfer fluid and the container's wall and need more heat transfer surfaces to meet the requirement of cooling load, but the higher velocity causes the higher outlet temperature and reduces the discharge time. Therefore this variable must be carefully chosen according to the requirement in an application.

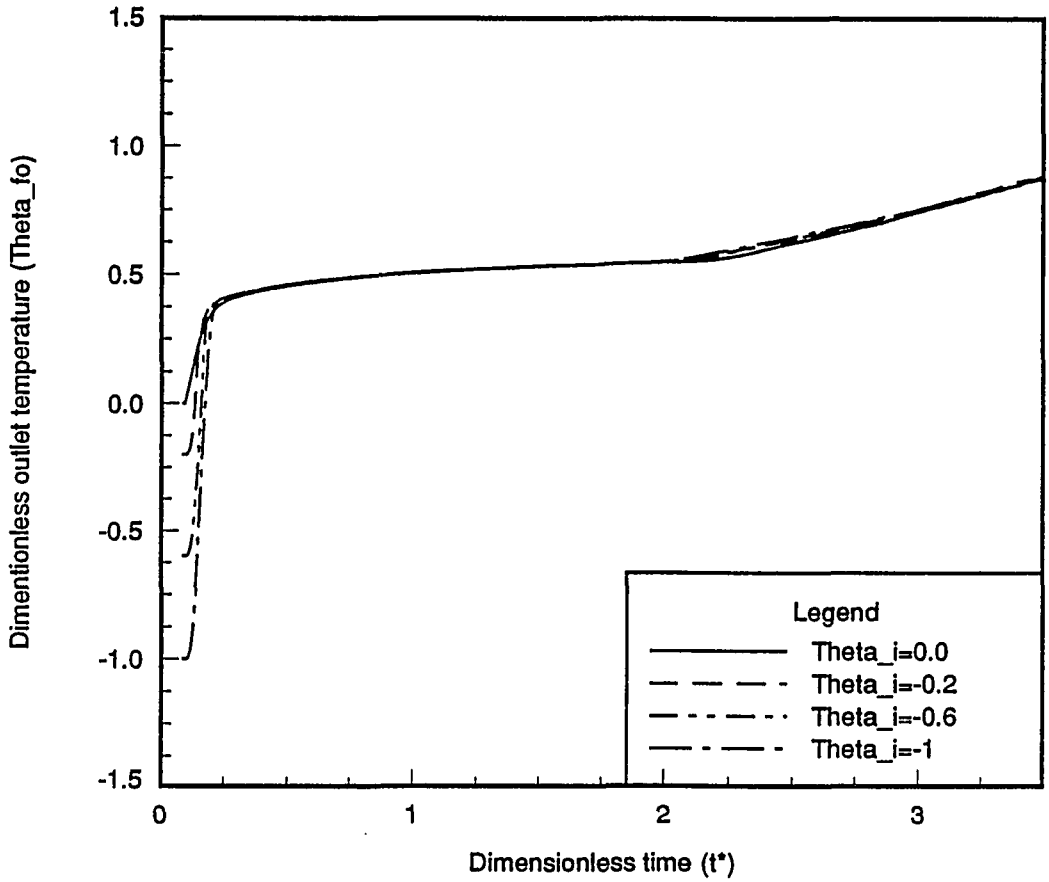

Figure 9: Outlet temperature vs time for variation of Θ_i (referring to initial subcooling temperature) under condition: $Ste = 0.062$, $H_i^* = H_i(m)/0.04(m) = 1$, $H_o^* = 1$, $H_w^* = 0.05$, $V^* = 11.6$

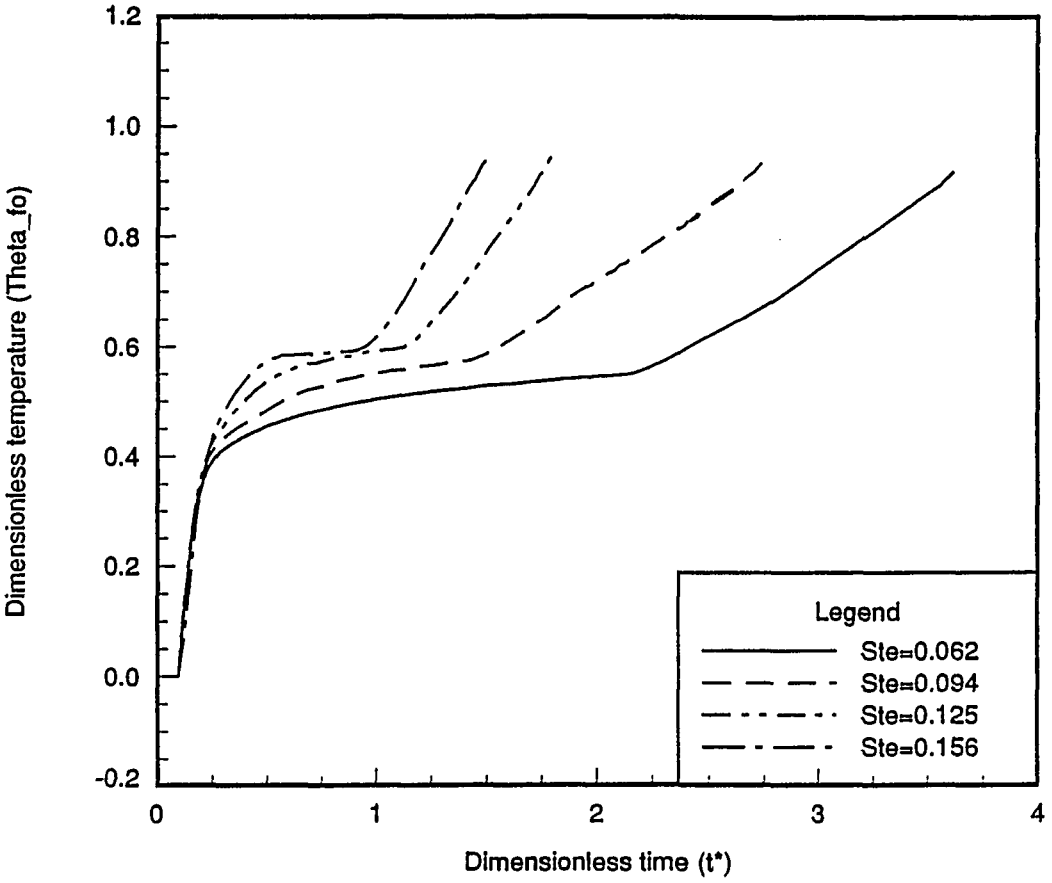

Figure 10: Outlet temperature vs time for variation of Ste (referring to inlet temperature of heat transfer fluid) under condition: $\Theta_i = 0.0$, $H_i^* = H_i(m)/0.04(m) = 1$, $H_o^* = 1$, $H_w^* = 0.05$, $V^* = 11.6$

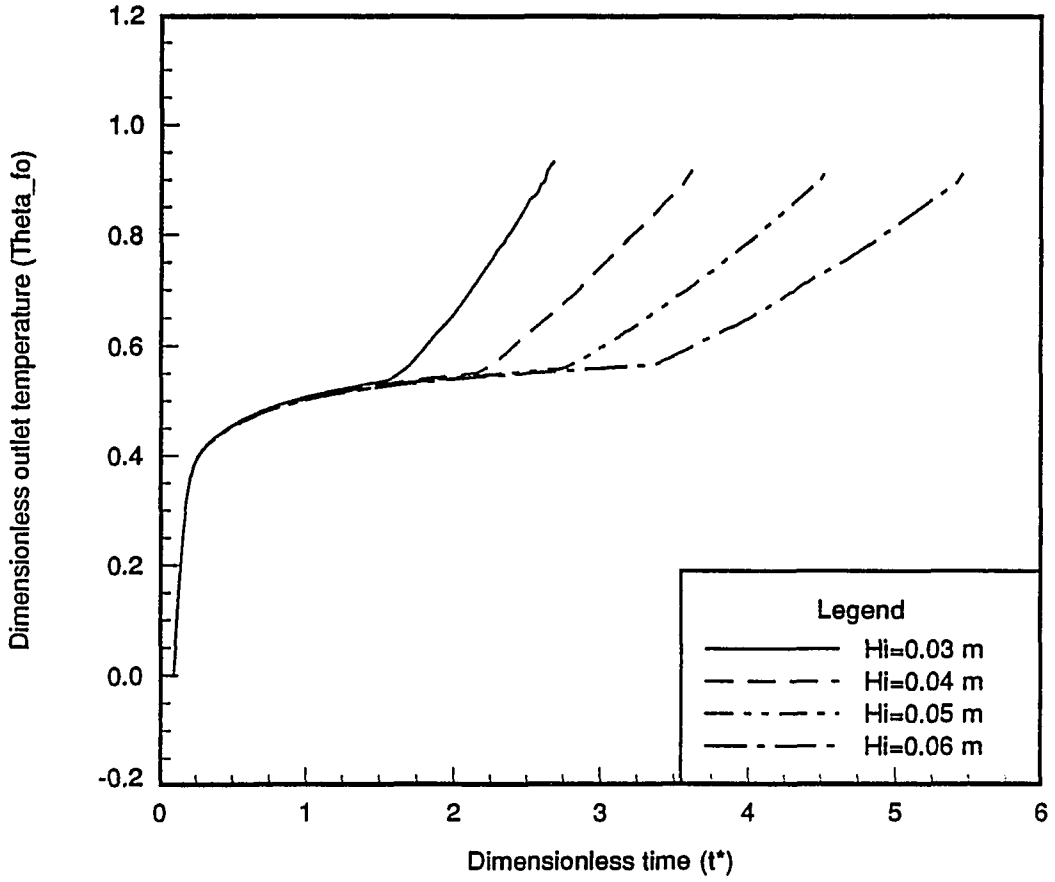

Figure 11: Outlet temperature vs time for variation of H_i^* (referring to thickness of the container) under condition: $Ste = 0.062$, $\Theta_i = 0.0$, $H_i^* = H_i(m)/0.04(m)$, $H_o^* = 1$, $H_w^* = 0.05$, $V^* = 11.6$

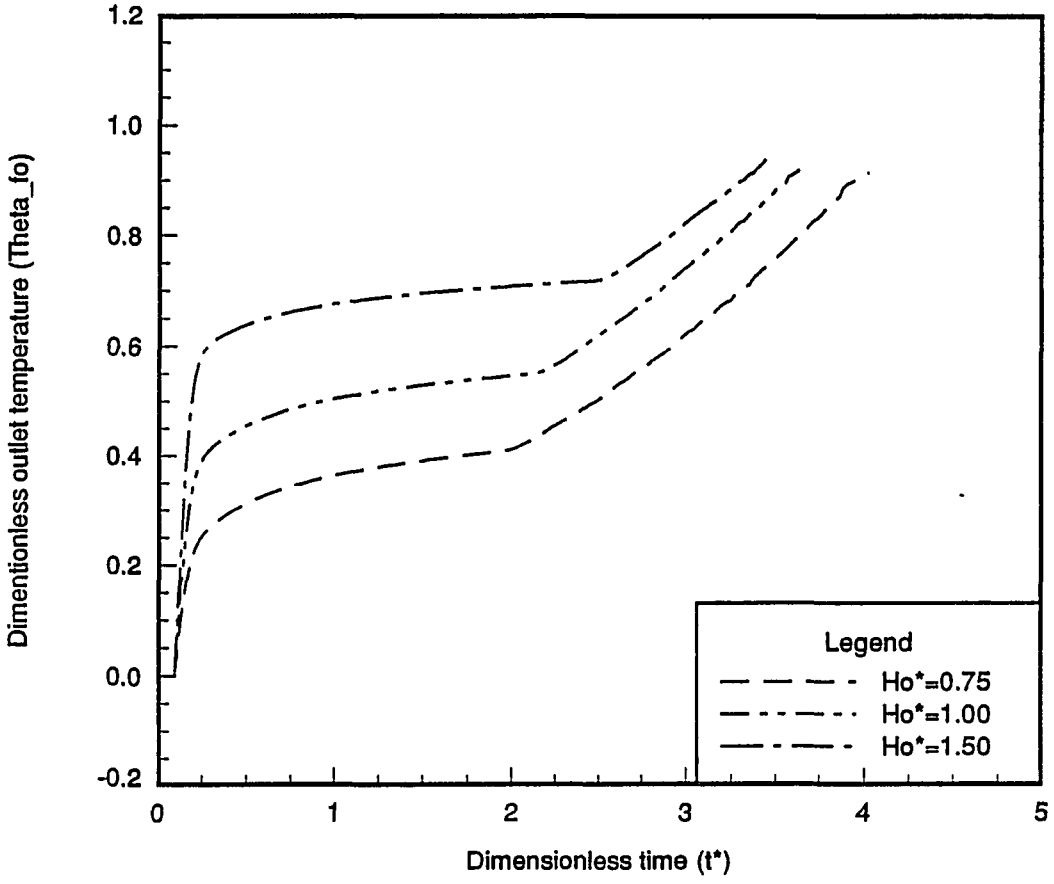

Figure 12: Outlet temperature vs time for variation of H_o^* (referring to thickness of the flow channel) under condition: $Ste = 0.062$, $\Theta_i = 0.0$, $H_i^* = H_i(m)/0.04(m) = 1$, $H_w^* = 0.05$, $V^* = 11.6$

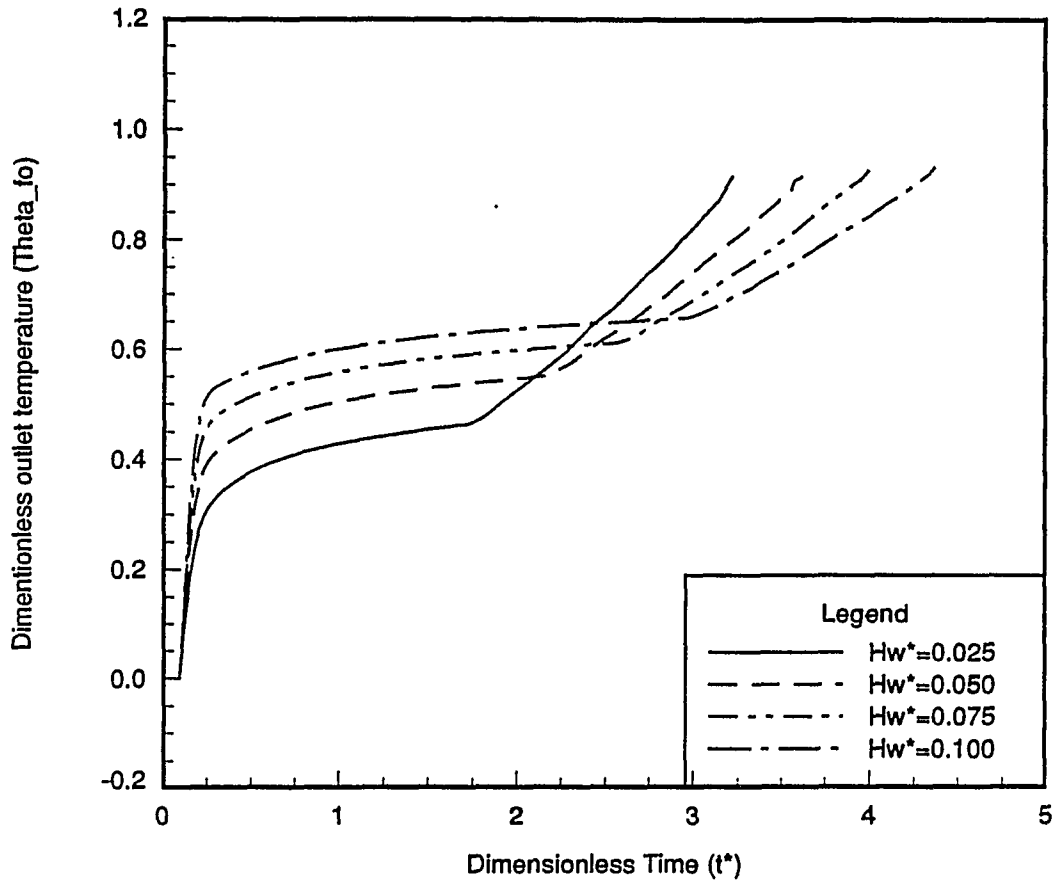

Figure 13: Outlet temperature vs time for variation of H_w^* (referring to thickness of the container wall) under condition: $Ste = 0.062$, $\Theta_i = 0.0$, $H_i^* = H_i(m)/0.04(m) = 1$, $H_o^* = 1$, $V^* = 11.6$

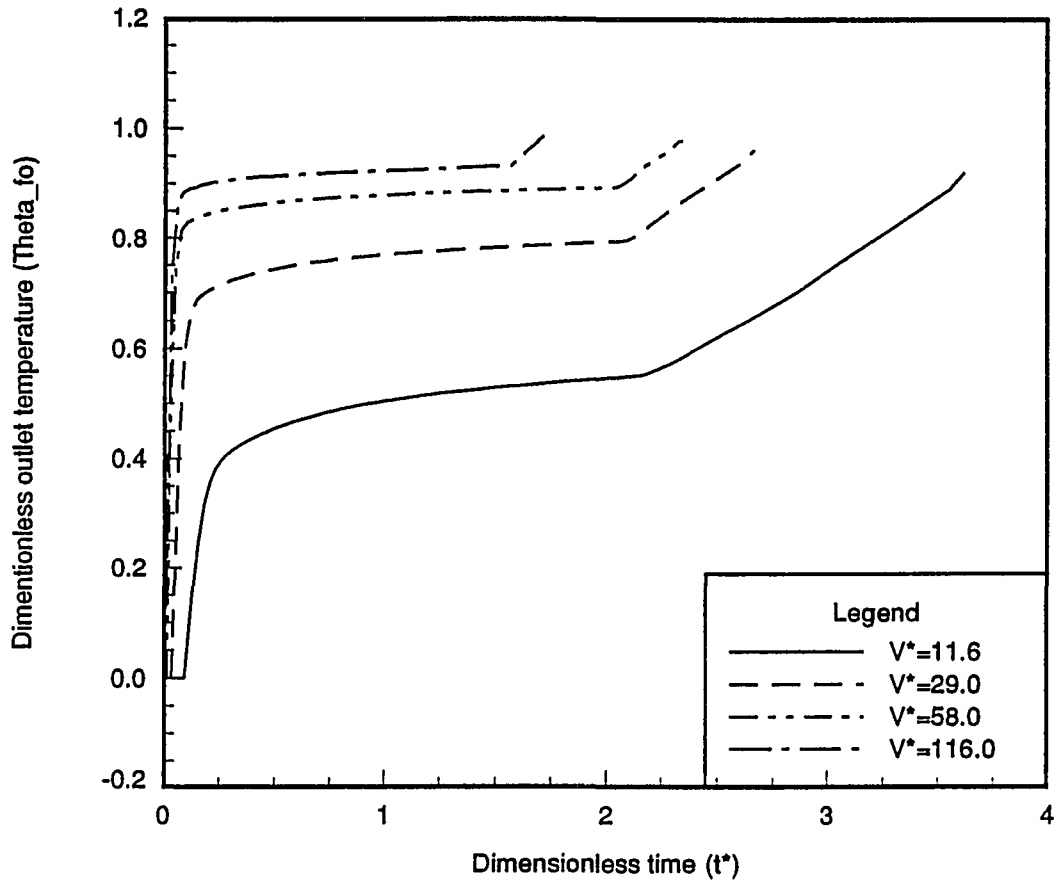

Figure 14: Outlet temperature vs time for variation of V_i^* (referring to velocity of the fluid flow) under condition: $Ste = 0.062$, $\Theta_i = 0.0$, $H_i^* = H_i(m)/0.04(m) = 1$, $H_o^* = 1$, $H_w^* = 0.05$

CONCLUSION

The preliminary model for the thermal energy storage system which consists of rectangular PCM containers has been developed. The integral method was employed to transfer the governing equations from the partial differential equations to the ordinary differential equations; then the systems of the ordinary equations were solved by the finite difference method. The model was run to evaluate the performance of the overall system for several melting cases. The effects of the independent variables on the system performance were analyzed and discussed. The results from this study could provide a valuable basis to engineering design for the thermal energy storage used in air conditioning systems.

REFERENCES

Asgarpoor, S., and Bayazitoglu, C. L. F., "Heat Transfer in Laminar Flow with a Phase Change Boundary," *Journal of Heat Transfer*, Vol. 104, pp. 678-682, 1982

Beaton, C. F., and Hewitt, G. F.,*Physical Property Data for the Design Engineer*, Hemisphere Publishing Corporation, New York, 1989

Delaunay, D., Bransier, J., and Bardon, J. F., "Modeling of Cylindrical Latent Heat Storage," *Int. J. Chemical Eng.*, Vol. 26, pp. 82-89, 1986

Humphries, W. R., and Griggs, E. I., "Adesigm Handbook for Phase Change Thermal Control and Energy Storage Devices," NASA Technical Paper 1074, 1977

Incropera, F. P., and De Witt, D. P., *Introduction to Heat Transfer* (Second Edition), John, Wiley and Sons, New York, 1990

Jurinak, J. J., and Abdel-Khalik, S. I., "Sizing Phase Change Energy Storage Units for Air-Based Solar Heating Systems," *Solar Energy*, Vol. 22, pp. 355-359, 1979

Meron, A. S., Weber, M. E., and Mujumdai, A. S., "The Dynamics of Energy Storage for Paraffin Wax in Cylindrical Containers," *Can. J. Chem. Eng.*, Vol. 61, pp. 647-653, 1983

Morrison, D. J., and Abdel-Khalik, S. I. "Effects of Phase-Change Energy Storage on the Performance of Air-Based and Liquid-Based Solar Heating Systems," *Solar Energy*, Vol. 20, pp. 57-67, 1978

Prusa, J. M., Maxwell, G. M., and Timmer, K. J., "Design Criteria for

Thermal-Energy Storage Systems of Contained Phase-Change Material," Technical Report, ISU-ERI-Ames-89144 HTL-49, 1988

Saitoh, T., and Hirose, K. "High- Performance Phase-Change Thermal Energy Storage Using Spherical Capsules," *ASME paper*, 84-HT-8, 1984

Saxena, S., Subrahmaniyam, S., and Sarkar, M. K., "A preliminary Model for Phase Change Thermal Energy Storage in a Shell and Tube Heat Exchanger," *Solar Energy*, Vol. 29, pp. 257-263, 1982

Yanadori, M., and Masuda, T., " Heat Transferential Study on a Heat Storage Container with Phase Change Material," *Solar Energy,* Vol. 36, pp. 169-177, 1986

Yimer, B., "Transient Thermal Analysis of phase Change Materials Thermal Energy Systems with Internal Longitudinal Fins of Different Geometries," *ASME paper*, 81-WA/HT-9, 1981

Yong, L., and Maxwell, G. M., "An Experimental Investigation to Ice Melting in Rectangular Enclosure," to be submitted, 1993a

Yong, L., and Maxwell, G. M., "Melting of Unfixed Ice in Horizontal Rectangular Enclosure Heated Isothermally," to be submitted, 1993b

GENERAL CONCLUSION

Various experiments have been performed, and several analytical models have been developed for melting and freezing of the encapsulated phase change materials used in thermal energy storage systems.

The findings of this study demonstrated the importance of natural convection in solid-liquid phase change processes. The Nusselt number for convection-dominated ice melting was found lower than that in single phase heat transfer. When ice in the enclosure floated up due to buoyancy, a conduction controlled heat transfer occurred through the thin liquid layer above the ice slab, and a convection controlled heat transfer happened on the bottom. Subcooling tended to delay the onset of convection heat transfer, but had no significant effect to overall melting process; superheating had similar effect on the freezing process. The operation parameters, e.g., inlet temperature and flow velocity of the heat transfer fluid in the flow channel, had important influences on the performance of the thermal storage system. The geometric factors, such as, the ratio of the container height to the flow channel height, also effected the overall performance of the system.

The integral method was employed in the analysis to simplify partial differential equations into ordinary differential equations, and the finite difference method was used to solve problems numerically. The results obtained by the models had satis-

factory agreement with the experimental data. It appears that an effective computer model would be of great value to a designer of the system.

REFERENCES

Viskanta, R., "Natural Convection Melting and Solidification", *Natural Convection: Fundamental and Applications* (edited by S. Kakac, W. Aung and R. Viskanta), Hemisphere, Washington, D. C.. 1985, pp. 845-877

Yao, L. S. and Prusa, J., "Melting and Freezing", *Advance in Heat Transfer*, Vol. 19, 1989, pp. 1-83

ACKNOWLEDGMENTS

I would like to express my sincere appreciation to my major professors, Dr. Gregory M. Maxwell. His advice, guidance, and support made the completion of this work not only possible, but also enjoyable.

I would like to thank the members of my program of study committee, Dr. Bruce R. Munson, Dr. Ron Nelson, Dr. Michael B. Pate, and Dr. John C. Tannehill, for their great teaching and valuable advice.

I would like to thank my wife Feng and my family for their constant love, help and encouragement.

I gratefully acknowledge the financial support received from the Electric Power Research Center, under the direction of Dr. John W. Lamont, and from the Department of Mechanical Engineering at Iowa State University.